



MOTORVEHICLE UNIVERSITY OF EMILIA-ROMAGNA
UNIVERSITY OF BOLOGNA

Advanced Automotive Engineering
Advanced Sportscar Manufacturing

Automatic control of a throttle valve system

Automatic control

Professor:
Nicola Mimmo

Students:
Lorenzo Catellani
Giorgio Gori
Franco Pistellato

Contents

ABSTRACT	
1 Introduction	1
1.1 Throttle valve system structure	2
1.1.1 Architectures of Throttle Valve Systems	2
1.2 Motivations	2
1.3 State of the Art	4
1.4 Contributions	5
1.5 Position Sensors	6
1.5.1 Rotary Encoders	6
1.5.2 Rotary Potentiometers	7
1.5.3 MA600 Rotary Position Sensor	8
2 Throttle valve	10
2.1 Model and Problem Formulation	10
2.1.1 Assumptions for Control Problem	11
2.2 System Equations and Parameters	11
2.2.1 Circuit and Motor Dynamics	12
2.2.2 Torque and Motion Equations	13
2.2.3 Modeling of the Airflow Torque	14
2.2.4 List of Symbols	19
2.3 Linearisation	20
2.3.1 Linearisation Conditions	22
2.4 Linear System Analysis	24
2.4.1 Eigenvalues and Eigenvectors	24
2.5 Reachability	30
2.6 Integral Action	32
2.7 Observability	34
2.8 Reference Signal	36
2.8.1 Transfer Function	37

2.8.2	Filter Description	37
2.8.3	Resulting Signal	38
2.8.4	Signal Definitions and Transformations	41
2.8.5	Filtered Reference Signal and Derivatives	41
3	Proposed solutions	44
3.1	Control Architecture	44
3.2	Optimal Control for the Feedback	45
3.2.1	Cost Function	46
3.2.2	Solution of the Optimal Control Problem	47
3.2.3	Tuning of \mathbf{K}_S and \mathbf{K}_I	50
3.2.4	Selection of \mathbf{Q} and \mathbf{R}	51
3.3	Observer	55
3.3.1	Observer Dynamics	55
3.3.2	Dual System	55
3.3.3	Optimal Control for the Observer	57
3.3.4	Tuning of \mathbf{Q}_d and \mathbf{R}_d	59
3.4	Noise	62
3.5	Linear Feed-Forward Control	67
3.5.1	System Dynamics	67
3.5.2	Change of Coordinates	68
4	Case studies	75
4.1	References	75
4.2	Fast Transitions	76
4.3	Faster Transitions	81
4.4	Sharp Peaks and Cusps Test	85
4.5	Complex Driving Cycle	90
4.5.1	Validation of the Updated Tuning Strategy	98
4.6	Highway Entrance Maneuver	100
4.7	Overtaking Maneuver	104
5	APPLICATION	109
5.1	Simulink blocks description	109
5.2	Non-linear Plant	109
5.3	Reference and Feed-forward block	111
5.4	Control block for non-linear system	111
5.4.1	Integral Action and State Feedback for non-linear . .	112
5.4.2	Observer for non-linear system	113
5.5	Linear Plant	113

5.6	Control block for linear system	114
5.6.1	State Feedback and Integral Action for linear system .	114
5.6.2	Observer for linear system	115
5.7	Measurement block	115
6	Conclusions and Further Improvements	117
6.1	General Improvements	117
6.2	Improvement of the Rotational Speed	119
6.3	Improvement of the Volumetric Efficiency	120
6.4	Conclusions	120

ABSTRACT

In recent years, the automotive industry has faced stricter regulations related to emissions, drivability, and vehicle safety, which require the development of increasingly efficient engine control systems. The advent of advanced control units has enabled the use of more sophisticated control strategies. One significant technological development is Drive-by-Wire (DbW) technology, which includes the electronic throttle control system (ETCS). This report presents the modeling of a throttle valve control system and discusses its components, the motivations for precisely controlling it, and the state-of-the-art in current control strategies.

Chapter 1

Introduction

The throttle valve is a critical component of internal combustion engines, responsible for controlling the amount of air that enters the intake manifold. This process directly impacts the air-fuel mixture, essential for efficient combustion.



Figure 1.1: Throttle valve

1.1 Throttle valve system structure

The structure of a typical throttle valve system includes the following elements.

- **Throttle Body:** The main housing that holds the butterfly plate.
- **Butterfly Plate:** A rotating disk that adjusts the airflow based on its angular position.
- **Actuator:** The mechanism that moves the butterfly plate; this can be mechanical or electronic.
- **Sensors:** Devices that measure the valve's position and provide feedback to the engine control unit (ECU).

1.1.1 Architectures of Throttle Valve Systems

Throttle valve systems have evolved from simple mechanical linkages to sophisticated electronic configurations.

- **Mechanical Throttle Control:** This traditional system uses a cable connected to the accelerator pedal. Pressing the pedal rotates the butterfly plate via the cable.
- **Electronic Throttle Control (ETC):** In modern vehicles, ETC systems use an electric motor to control the valve's position. The accelerator pedal's input is detected by sensors and processed by the ECU, which sends signals to the actuator to achieve the desired valve position. This architecture enables precise control and integration with other vehicle systems, such as stability and cruise control.

1.2 Motivations

Accurate control of the throttle valve is essential for several reasons.

- **Performance and Fuel Efficiency for Everyday Vehicles:** The position of the throttle valve determines the air intake and consequently the air-fuel ratio, which is crucial for achieving efficient combustion. Optimal control ensures that the engine operates at an ideal performance level, maximizing power output, and improving fuel economy. This leads to a more responsive driving experience, smoother

acceleration, and better fuel efficiency, which is especially beneficial for daily use and city vehicles.

- **Emissions Reduction:** With stricter environmental regulations, reducing emissions is a priority in engine management. Proper throttle control helps maintain the correct air-fuel mixture, minimizing emissions such as carbon monoxide (CO), hydrocarbons (HC), and nitrogen oxides (NOx). By adapting to different engine loads and conditions, modern throttle control can keep emissions low while complying with regulatory standards.
- **Engine Durability:** Precise control of the throttle valve can extend the engine life. Avoiding extreme air-fuel mixtures prevents harmful phenomena such as knocking and incomplete combustion, which can cause wear and tear to engine components. In addition, controlled throttle transitions help maintain consistent engine performance, reducing mechanical stress.
- **Drivability and Comfort in Urban Settings:** For urban and city vehicles, a smooth throttle response is essential for comfortable driving and easy maneuvering in stop-and-go traffic. Accurate throttle control minimizes abrupt movements, resulting in a more refined and predictable driving experience. This contributes to reduced driver fatigue and improved comfort during everyday commutes.
- **High-Performance Response for Sports Cars:** In sports and high-performance cars, throttle control is crucial for delivering rapid and precise power response. Advanced control systems ensure that the engine reacts instantly to driver inputs, enhancing driving dynamics and providing an exhilarating experience. This allows for better handling during rapid acceleration, cornering, and high-speed maneuvers, making the car more agile and responsive.
- **Integration with Advanced Systems:** Modern vehicles feature systems like ADAS (Advanced Driver Assistance Systems) and hybrid powertrains that require seamless communication between different control units. The precise control of the throttle valve enables better integration with these systems, supporting features such as adaptive cruise control and regenerative braking in hybrid vehicles.

1.3 State of the Art

Internal combustion engines require precise regulation of airflow to manage engine speed, torque, spark timing, and air-fuel ratio. Until the late 1980s, drivers directly controlled engine speed and power through a mechanical cable connected to the accelerator pedal. Cruise control systems also used this cable linkage, relying on a vacuum or an electric motor to adjust engine speed.

However, in 1998, electronic throttle control (ETC) systems using wire technology were introduced, with the BMW Series 7 being the first to incorporate electronic throttle body (ETB) technology.

Recent advancements have enabled the operation of throttle valves using electric actuators and advanced control systems. Automotive manufacturers are increasingly developing electronic control systems for throttle bodies, as replacing traditional cables with electronic systems improves response time and overall throttle performance.

In modern vehicles, the engine control unit (ECU) calculates the optimal angle for the throttle plate, considering factors such as accelerator pedal position, engine speed, and cruise control settings. This calculation aims to maintain the ideal stoichiometric air-fuel mixture, reducing emissions and enhancing energy efficiency. For high energy performance, the throttle valve must respond rapidly when switching between stoichiometric and lean mixtures, necessitating actuators with faster response times and higher precision.

Significant developments in throttle valve control include the following.

- **Traditional Control Methods:** The Proportional-Integral-Derivative (PID) controller has long been a staple for throttle control due to its simplicity and effectiveness. PID controllers regulate the valve position by minimizing the error between the desired and actual positions. Although effective for basic control tasks, PID controllers face challenges in adapting to changing conditions without retuning.
- **Advanced Control Techniques:** More recent advancements have introduced Model Predictive Control (MPC), which utilizes a predictive model of the throttle system to optimize control actions over a future time horizon. MPC is capable of handling multivariable interactions and constraints, making it particularly suitable for systems with complex dynamics. Adaptive control strategies are also implemented to allow real-time parameter adjustments, ensuring stable performance under varying engine conditions.

- **Integration of Machine Learning:** The role of machine learning in throttle control has grown, enabling more adaptive and predictive systems. Machine learning algorithms leverage historical data to refine throttle response and improve fuel efficiency over time. Hybrid approaches that integrate traditional methods such as PID or MPC with machine learning provide enhanced robustness and adaptability, allowing the system to maintain efficiency across various operating conditions.
- **Current Challenges and Future Trends:** Despite these advancements, challenges remain, such as optimizing control algorithms for real-time execution and ensuring seamless integration with other vehicle subsystems. Future research is anticipated to further incorporate AI-driven models and enhance computational efficiency, supporting the development of next-generation automotive throttle control systems.

1.4 Contributions

This project addresses the challenge of achieving optimal control of an automotive throttle valve, focusing on improving performance and drivability. The throttle valve regulates the engine's air intake, which directly impacts the air-fuel ratio, combustion efficiency, and ultimately, vehicle performance. The main objectives are to ensure smooth and responsive throttle action, precise control of air intake for fuel efficiency, and enhanced engine longevity through minimized mechanical stress.

To solve this problem, a control system is designed with three primary blocks: an Observer, a Feedback Path, and a Feed-Forward Path.

The Observer processes sensor measurements to estimate key state variables, including the electrical current through the circuit, throttle position θ , and angular velocity $\dot{\theta}$. This estimation provides essential feedback for the control system, enabling real-time adjustments.

The Feedback Path utilizes matrices \mathbf{K}_S and \mathbf{K}_I to generate a control signal \mathbf{u}_{FB} that corrects deviations from desired values, ensuring stability and accuracy.

Additionally, the Feed-Forward Path improves response by applying control signals \mathbf{u}_{FF} when reference inputs or their derivatives are known, allowing the system to anticipate and adapt to dynamic changes effectively.

This control structure enhances performance by optimizing throttle response, which is critical in everyday vehicles for fuel efficiency and smooth

acceleration, as well as in high-performance sports cars where immediate and precise power delivery is essential. Additionally, the system improves drivability and comfort, especially in urban environments where consistent and smooth throttle response contributes to a more refined driving experience.

Depending on the tuning of specific parameters during the control design phase, the system can be adjusted to prioritize either performance or comfort and drivability, or to find an optimal balance between the two.

1.5 Position Sensors

In order to effectively control the throttle and other critical aspects of the engine, sensors are required to monitor key parameters and provide real-time feedback. These sensors enable precise adjustments in response to dynamic conditions, ensuring optimal performance, efficiency, and safety. This section provides an overview of the sensor used in our system, a position sensor that has been carefully selected for its reliability, precision, and suitability for harsh automotive environments.

In control theory, the control action depends on the error between the actual value of a variable (e.g., throttle valve position) and its reference value.

Since the actual state is unknown a priori, the error e must be obtained from the output \mathbf{y} of the measurement sensors:

$$e = y - \theta_{\text{ref}} \quad (1.1)$$

Thus, the measurement vector \mathbf{y} must accurately reflect the actual angular position:

$$y = \theta + \nu_{\text{pos}} \quad (1.2)$$

Position sensors provide crucial feedback on the angular position of the throttle valve, allowing for precise control and adjustment. Accurate position sensing is essential to ensure that the throttle responds correctly to the driver's input and to maintain optimal air-fuel mixtures for efficient combustion. There are two main types of position sensors commonly used for throttle control: rotary encoders and rotary potentiometers.

1.5.1 Rotary Encoders

Rotary encoders convert the angular position or motion of a shaft into an electrical signal. They are known for their precision and are widely used

in applications requiring accurate position feedback. Key characteristics of rotary encoders include.

Rotary encoders can accurately measure the position of a shaft, which is essential for precise control in applications like throttle and motor control. The resolution specifies the granularity of measurement, typically indicated in pulses per revolution (PPR). Higher resolution allows for finer position adjustments.

The produced outputs can be digital or analog: digital encoders offer discrete signals, while analog ones provide a continuous output. Many encoders can determine the direction of rotation, which is beneficial for applications requiring bidirectional control.

There are several types of rotary encoders, each suitable for specific use cases:

- incremental encoders generate pulses as the shaft rotates, tracking movement relative to a starting position. They typically require additional circuitry to maintain an absolute position;
- absolute encoders provide a unique code for each shaft position, enabling exact position tracking without the need for a reference point;
- optical encoders use light to detect position changes, offering high accuracy, making them ideal for precision applications;
- magnetic encoders utilize magnetic fields to detect position changes, providing robustness in harsh environments.

1.5.2 Rotary Potentiometers

Rotary potentiometers are simpler position sensors that convert angular displacement into a proportional voltage signal. They are widely used in applications that require straightforward position feedback without the complexity of an encoder. A rotary potentiometer consists of a resistive track and a movable contact (wiper) that slides along the track as the shaft rotates. The output voltage changes according to the wiper's position, producing an analog signal proportional to the shaft's angle.

The advantages of rotary potentiometers are several.

- **Simplicity:** They produce an analog signal that is easy to process and integrate into control systems without the need for complex electronics;

- **Compatibility with Analog Systems:** Their analog output makes them suitable for use in systems that do not require digital signals, providing a straightforward integration solution;
- **Cost-Effectiveness:** Potentiometers are generally more affordable than rotary encoders, making them a cost-efficient choice for applications that do not require high precision.

However, rotary potentiometers are subject to wear over time due to the physical contact between the wiper and the resistive track, which can reduce accuracy and lifespan in high-usage applications. Additionally, the analog output may be affected by noise and interference, especially in harsh conditions with high vibration or extreme temperatures.

1.5.3 MA600 Rotary Position Sensor

The Monolithic Power Systems MA600 is a high-precision magnetic rotary position sensor with advanced Tunneling Magnetoresistive (TMR) technology, making it suitable for demanding applications such as automotive throttle position control. Its high resolution and low noise ensure exceptional accuracy, even in harsh automotive environments.

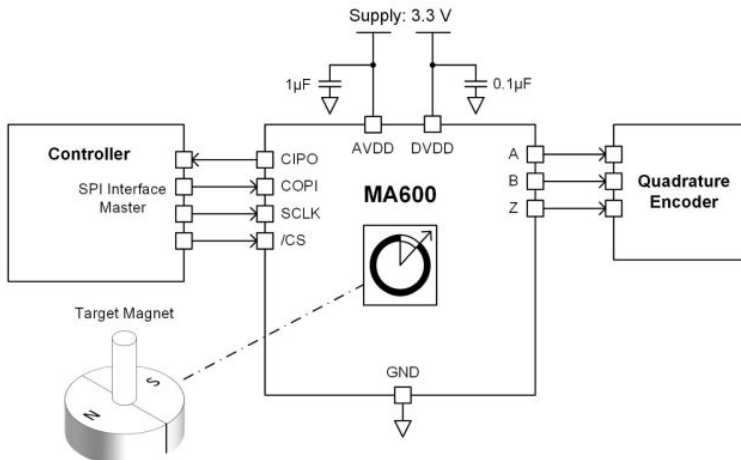


Figure 1.2: Monolithic Power Systems MA600

The MA600 sensor, with a noise RMS ranging from 0.002° to 0.015° , depending on the digital filter configuration, delivers reliable angle measurements for throttle valve control. This level of accuracy provides a smooth

and predictable throttle response, enabling optimal performance and fuel efficiency. For standard road vehicles, its precision ensures comfortable and efficient operation, while its configurability allows adaptation to high-performance requirements through filter optimization.

The MA600 operates on TMR sensing technology, offering superior sensitivity and immunity to environmental contaminants such as dust and dirt. The sensor is designed to work with a simple two-pole magnet, ensuring easy integration into throttle body assemblies. Additionally, its wide operating temperature range and robustness make it ideal for harsh automotive conditions.

Like many sensors, the MA600 is powered at a typical 5 V, regulated down from higher system voltages. Automotive ECUs typically include built-in voltage regulators to ensure stable operation of sensors and other electronics.

Parameter	Value
Resolution	14 bits (16,384 steps per revolution)
Measurement Range	0° to 360° (full rotational angle)
Noise RMS	0.002° to 0.015° (configurable)
Interface	Digital output (SPI, ABI, UVW, PWM)
Supply Voltage	3.3 V or 5 V typical
Operating T Range	-40°C to 125°C
Magnetic Technology	TMR, resilient to dust and contaminants
Integration Requirements	Requires a two-pole magnet
Power Compatibility	Compatible with automotive power systems

Table 1.1: Summary of MA600 sensor parameters.

Chapter 2

Throttle valve

2.1 Model and Problem Formulation

The system can be described by the following mathematical equations, which represent its state evolution, output, and error dynamics:

$$\dot{\mathbf{x}} = \mathbf{f}(\mathbf{x}, \mathbf{u}, \mathbf{w}) \quad \mathbf{x}(t_0) = \mathbf{x}_0 \quad (2.1)$$

$$\mathbf{y} = \mathbf{h}(\mathbf{x}, \mathbf{u}, \mathbf{w}) \quad (2.2)$$

$$\mathbf{e} = \mathbf{h}_e(\mathbf{x}, \mathbf{u}, \mathbf{w}) \quad (2.3)$$

The main mathematical symbols and their definitions are as follows:

- $\mathbf{x} \in \mathbb{R}^n$: **Plant state**, representing the internal states of the system.
- $\mathbf{d} \in \mathbb{R}^d$: **Disturbances**, external inputs that can affect the system's behavior.
- $\mathbf{r} \in \mathbb{R}^r$: **References**, the desired set points that the system aims to follow.
- $\mathbf{u} \in \mathbb{R}^p$: **Control inputs**, command signals applied to the system to influence its behavior.
- $\mathbf{y} \in \mathbb{R}^q$: **Measurements**, the observable outputs from the plant used for feedback control.
- $\mathbf{e} \in \mathbb{R}^m$: **Goals**, the objectives that the control system aims to achieve.
- $\mathbf{v} \in \mathbb{R}^q$: **Noises**, representing external disturbances or inaccuracies affecting the measurements.

The following additional details describe the physical interpretation of the main variables:

- $\mathbf{r}(t)$ is the **desired position** and is expressed in radians.
- $\mathbf{e}(t)$ is the **error signal**, defined as the difference between the desired position and the feedback position.
- $\mathbf{u}(t)$ represents the **control command voltage** for the plant, expressed in volts.
- $\mathbf{y}(t)$ is the **plant output**, which corresponds to the feedback angular position of the throttle valve, expressed in radians.

2.1.1 Assumptions for Control Problem

To approach the control problem effectively, the following assumptions are made:

1. The disturbance \mathbf{w} is not directly observable, requiring the system design to achieve control objectives despite its influence.
2. The disturbance \mathbf{d} must be bounded for a manageable system behavior.
3. The reference \mathbf{r} is fixed and predetermined, serving as the desired set point for the system.
4. For $\mathbf{u} \in \mathbb{R}^p$ and $\mathbf{e} \in \mathbb{R}^m$, it is assumed that $p \geq m$ to guarantee the existence of a solution for the control problem.
5. The error \mathbf{e} can be calculated using the measurements \mathbf{y} .

2.2 System Equations and Parameters

The first step in the design process involves formulating a set of equations to describe the system's state.

The main parameters are defined as:

- I : Current through the motor.
- θ : Actual throttle angle position.
- $\dot{\theta}$: Actual throttle angular velocity.

- p : Intake manifold pressure, that is part of the plant but will not be included as part of the state, as it is not a control variable.

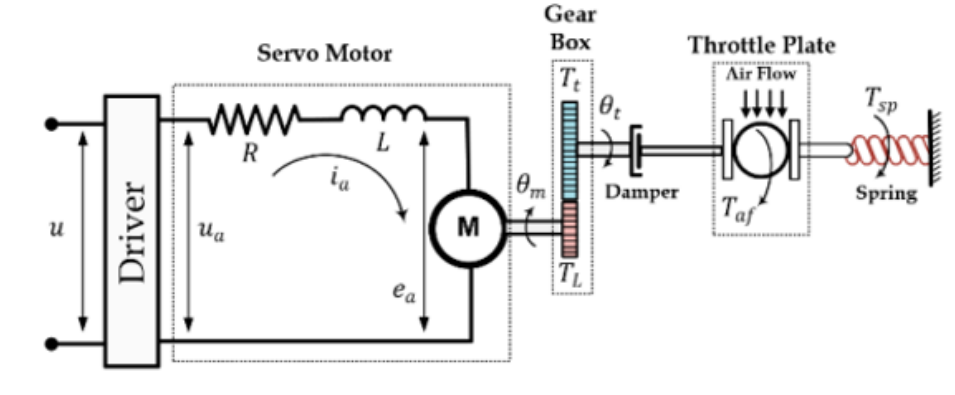


Figure 2.1: Scheme of the throttle valve system

So despite having 4 variables for the plant, the state is represented just by the first 3 ones.

$$\mathbf{x} = \begin{bmatrix} x_1 \\ x_2 \\ x_3 \end{bmatrix} = \begin{bmatrix} I \\ \theta \\ \dot{\theta} \end{bmatrix}$$

This approach is chosen because the pressure variable, while crucial as a system parameter, is not directly part of the state being controlled. Consequently, current, throttle angle, and angular velocity will be the focus of the control design, while the pressure will be monitored and analyzed as an important parameter that influences system behavior without being explicitly controlled.

2.2.1 Circuit and Motor Dynamics

Applying Kirchhoff's voltage law to the armature circuit yields:

$$u_a = R_a I + L \dot{I} + e_a \quad (2.4)$$

where:

- R_a is the armature resistance,
- L is the armature inductance,

- K_d is the drive gain,
- u_a is the applied voltage,
- I is the current through the motor winding,
- e_a is the back electromotive force (e.m.f), defined as:

$$e_a = K_b \dot{\theta}_m \quad (2.5)$$

with back e.m.f constant K_b and motor shaft's angular velocity $\dot{\theta}_m$.

2.2.2 Torque and Motion Equations

The torque generated by the DC motor is:

$$T_m = K_t I \quad (2.6)$$

The torque balances the motion of the motor shaft and load torque T_L :

$$T_m = J_m \ddot{\theta}_m + T_L \quad (2.7)$$

where K_t is the motor torque constant and J_m the motor shaft inertia.

On the gear side, the transmitted torque T_t acts against the throttle motion, spring torque and against damping:

$$T_t = J_t \ddot{\theta} + B \dot{\theta} + T_{sp} + T_{af} \quad (2.8)$$

where:

- J_t is the throttle inertia,
- B represents damping coefficient,
- T_{af} is the torque due to airflow,
- T_{sp} is the return spring torque, defined by:

$$T_{sp} = K_{sp}(\theta + \theta_o) \quad (2.9)$$

with spring's elastic coefficient K_{sp} and preload angle θ_o set to 10°.

This last torque contribution is due to the fact that, in order to ensure a return to the "limp-home" position (fully closed, given the system is an Electronic Throttle Control for gasoline applications), the actuator's return spring is preloaded.

The connection between the two sides, the motor and the gear ones, is done throughout a transmission with ratio N equal to 4, so that:

$$T_t = N T_L \quad (2.10)$$

2.2.3 Modeling of the Airflow Torque

When considering the torque equations, it is crucial to include and analyze the effect of the air passing through the throttle plate during engine operation. This airflow actively generates a torque that opposes the transmitted torque, regulating and controlling the throttle plate angle. The airflow pulses longitudinally within the intake manifold, with its behavior depending on the longitudinal position in the manifold and time. Additionally, the airflow varies across different cross-sections of the intake manifold. Therefore, modeling the air intake process presents significant challenges.

To address this issue, the Mean Value ICE (Internal Combustion Engine) Model is used. This model captures the dynamics of the main engine variables, both measurable and unmeasurable, without considering cycle-to-cycle variations. The Mean Value Model (MVM) is derived from a physical analysis of the primary phenomena occurring inside the engine, with the model parameters determined through empirical fitting. The MVM is widely recognized for its good predictive capabilities while maintaining simplicity.

An acceptable simplification made in this analysis assumes that the temperature and pressure values within the intake manifold are equal to the ambient conditions. This assumption helps reduce the complexity of the model while still providing reliable results for practical applications.

According to the MVM, the variation in intake manifold pressure over time is influenced by several factors:

$$\dot{p} = -\frac{nV_d\eta_V}{120V} p + \frac{RT_{\text{amb}}}{V} \dot{m}(t), \quad (2.11)$$

where:

- $V_d = 0.003 \text{ m}^3$ is the engine displacement, representing the total volume swept by all the pistons during a single cycle,
- $V = 0.0016 \text{ m}^3$ is the manifold-port passage volume, indicating the volume within the intake manifold,
- $R = 8.314 \frac{\text{J}}{\text{kg}\cdot\text{K}}$ is the gas constant, a physical quantity used in thermodynamic equations,
- η_V is the volumetric efficiency, representing the effectiveness of the engine in filling its cylinders with air during the intake process,
- $\dot{m}(t)$ is the air mass flow rate,

- $n = 1900 + 3000 \cdot \theta$ is the rotational speed of the engine [rpm], defined in function of the reference value in order to have an appropriate correlation between the opening angle of the valve and the engine speed.
- $T_{\text{amb}} = 288 \text{ K}$ is the ambient temperature, representing the temperature of the surrounding air.

The intake flow $\dot{m}(t)$ can be expressed as:

$$\dot{m}(t) = C_f \frac{\pi}{4} D^2 \frac{p_{\text{amb}}}{\sqrt{RT_{\text{amb}}}} \beta_1(\theta) \beta_2[p(t)], \quad (2.12)$$

where:

- $C_f = 0.83$ is the flow coefficient of the throttle body throat,
- $D = 0.04 \text{ m}$ is the throttle bore diameter, which is the internal diameter of the throttle,
- $p_{\text{amb}} = 101325 \text{ Pa}$ is the ambient pressure, representing the pressure of the surrounding air,
- $\beta_1(\theta)$ is a flow correction factor that accounts for the geometry and position of the throttle plate,
- $\beta_2[p(t)]$ is a flow correction factor that depends on the intake manifold pressure and adjusts for changes in airflow dynamics.

The term $\beta_1(\theta)$ is modeled as:

$$\begin{aligned} \beta_1 = & \left(1 - \frac{\cos(\theta)}{\cos(\theta_o)} \right) \frac{2}{\pi} \left(\frac{0.14}{\cos(\theta)} \sqrt{\cos^2(\theta) - 0.14^2 \cos^2(\theta_o)} + \right) \\ & + \frac{2}{\pi} \left(\frac{\cos(\theta)}{\cos(\theta_o)} \arcsin \left(\frac{0.14 \cos(\theta_o)}{\cos(\theta)} \right) - 0.14 \sqrt{1 - 0.14^2} - \arcsin(0.14) \right) \end{aligned} \quad (2.13)$$

The correction factor $\beta_2[p(t)]$ is defined as:

$$\beta_2[p(t)] = \begin{cases} \sqrt{\frac{2k}{k-1} \left[\left(\frac{p(t)}{p_{\text{amb}}} \right)^{\frac{k-1}{k}} - \left(\frac{p(t)}{p_{\text{amb}}} \right)^{\frac{k+1}{k}} \right]} & \text{if } \frac{p(t)}{p_{\text{amb}}} \geq \left(\frac{2}{k+1} \right)^{\frac{k}{k-1}} \\ \sqrt{\frac{k+1}{2(k-1)}} & \text{otherwise} \end{cases} \quad (2.14)$$

where $k = 1.4$ is the specific heat ratio.

When β_2 becomes constant, the system reaches the sonic block condition, as shown in figure 2.2.

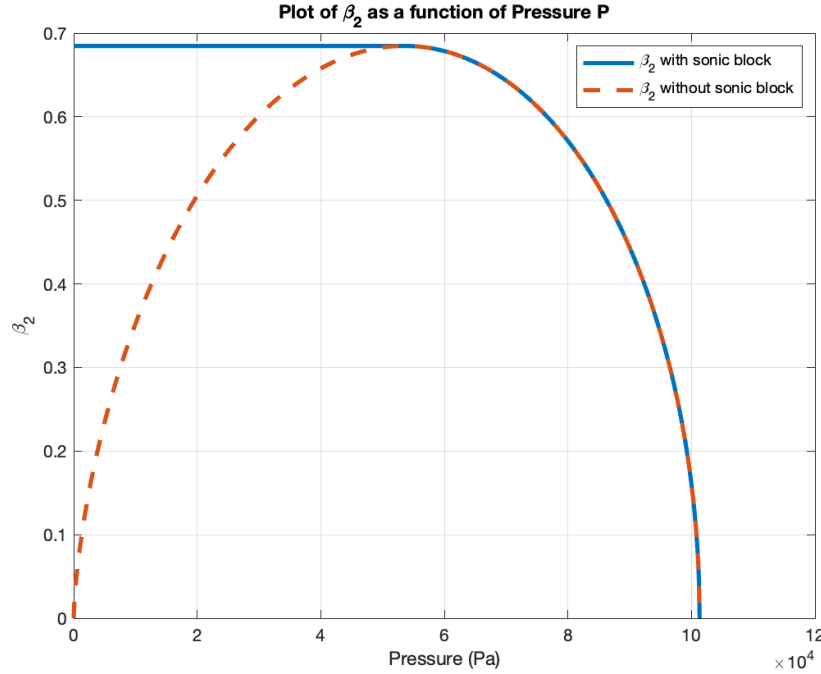


Figure 2.2: Curve of β_2 in function of the pressure

In this state, the air mass flow no longer increases despite differences in pressure between the throttle plate's entrance and exit, since the airflow has reached the speed of sound. This condition, known as choked flow, limits the air intake performance, as any further pressure increase becomes ineffective in altering the flow characteristics.

The theoretical aerodynamic torque due to drag in a butterfly valve is expressed as:

$$T_{af,th} = \frac{1}{2}\rho C_d A V^2 \frac{D}{2} \quad (2.15)$$

where:

- $T_{af,th}$ is the aerodynamic torque due to drag;
- C_d is the drag coefficient (typically assumed to be $C_d = 1$ for simplicity),
- ρ is the fluid density (assumed constant for incompressible flow);

- $A = \pi(\frac{D}{2})^2$ is the reference area of the valve;
- V is the flow velocity.

The relationship between the flow velocity and the pressure difference can be approximated using Bernoulli's principle.

$$V^2 \propto \Delta p$$

This approximation holds well under the assumption of incompressible flow, which is strong but acceptable and coherent with the mean value model used to define the pressure in the manifold. Substituting V^2 into the torque equation yields:

$$T_{af,th} = \frac{D}{2} C_d A (p_{amb} - p) \quad (2.16)$$

where:

- p_{amb} is the ambient pressure upstream of the valve;
- p is the downstream equilibrium pressure.

In this form, the aerodynamic torque is directly proportional to the pressure difference across the valve. This formulation simplifies the computation of $T_{af,th}$ by avoiding explicit dependence on the velocity V while maintaining the physical relationship between flow dynamics and the drag-induced torque.

The drag coefficient C_d can be acceptably assumed to have a value of 1, providing a reasonable and practical approximation for the aerodynamic behavior of the valve within its angular range.

In reality this equation of the torque needs to be adjusted through a correction factor K_c taking into account several dynamic factors.

$$T_{af} = K_c T_{af,th} = \frac{D}{2} K_c C_d A (p_{amb} - p) \quad (2.17)$$

In the context of aerodynamic torque modeling for a throttle valve, the introduction of a corrective coefficient, $K_c = 0.25$ in our case, is justified by the need to account for various sources of loss and simplifications inherent in the model. These losses and inaccuracies arise from multiple factors that deviate the model from real-world conditions, necessitating a reduction in the estimated torque to achieve greater realism.

Firstly, pressure losses within the intake manifold play a significant role. The pressure upstream of the valve is often lower than the ambient pressure

p_{amb} due to frictional losses and turbulence within the manifold, especially in automotive applications where complex geometries and bends are common. Typical pressure losses in the manifold before the valve range around 1000 Pa, depending on engine speed and flow conditions. These losses reduce the effective pressure difference driving the flow and directly influence the aerodynamic torque, necessitating the penalization introduced by the corrective coefficient.

Secondly, the model assumes incompressible flow, which is a simplification that neglects the compressibility effects of air under high-pressure differences (greater or equal than 30000 Pa). In reality, a portion of the energy from the pressure difference is absorbed by density changes in the air, rather than being fully converted into flow velocity. This introduces an overestimation in the torque that the coefficient helps to correct.

Thirdly, the drag coefficient C_d is assumed to be 1 for simplicity in the base model, but in practice, it varies with the geometry of the valve and the angle of opening. For typical automotive throttle valve applications, C_d is closer to 0.6. This value is consistent with experimental observations and reflects the aerodynamic efficiency of a butterfly valve in such conditions. Using $C_d = 0.6$ instead of 1 reduces the estimated aerodynamic torque by approximately 40%, aligning better with realistic conditions.

Additionally, the Mean Value Model (MVM), used for pressure predictions, introduces inaccuracies at low throttle angles. For instance, at the throttle opening of 12° chosen for the linearisation, the MVM predicts a downstream pressure of 778.7876 Pa, which is significantly lower than typical experimental values for this condition, often around 25000 Pa. This underestimation of pressure results in an exaggerated pressure difference and, consequently, an overestimation of the aerodynamic torque. The corrective coefficient compensates for this systematic error, bridging the gap between theoretical and practical values.

Finally, geometrical and aerodynamic effects within the valve itself contribute to non-uniform flow distributions and turbulence that reduce the effective force on the valve plate. For example, flow separation and viscous losses near the edges of the valve dissipate a portion of the dynamic pressure energy, further reducing the torque below the idealized estimate.

In summary, the corrective coefficient $K_c = 0.25$ aggregates the effects of manifold pressure losses, compressibility corrections, realistic C_d values, inaccuracies in the MVM and internal aerodynamic losses. This value provides a reasonable and empirically supported correction to align the torque predictions with real-world behavior in automotive throttle valve applications.

2.2.4 List of Symbols

All the parameters used, comprehending their definition, value and measurement unit, are grouped in the following list.

Symbol	Meaning	Value + Unit
\mathbf{x}	Plant state	-
\mathbf{d}	Disturbances	-
\mathbf{r}	References	-
\mathbf{u}	Control inputs	-
\mathbf{y}	Measurements	-
\mathbf{e}	Goals	-
I_a	Current through the circuit	-
θ	Angular position of the throttle valve	-
$\dot{\theta}$	Angular velocity of the throttle valve	-
p	Pressure in the intake manifold	-
ν	Noises	-
R_a	Circuit electrical resistance	2Ω
L	Circuit inductance	0.0017 H
K_b	Back-electromotive force constant	$0.025 \frac{\text{V}\cdot\text{s}}{\text{rad}}$
K_d	Control gain	3
N	Reduction ratio	4
K_t	Torque constant	$0.075 \frac{\text{Nm}}{\text{A}}$
J_m	Motor inertia	$0.02 \text{ kg} \cdot \text{m}^2$
J_t	Total inertia	$0.01 \text{ kg} \cdot \text{m}^2$
K_{sp}	Return spring stiffness	$0.32 \frac{\text{Nm}}{\text{rad}}$
B	Viscous damping coefficient	$0.05 \frac{\text{Nm}\cdot\text{s}}{\text{rad}}$
T_{af}	Torque due to aerodynamic load	-
V_d	Displacement volume of the engine	0.003 m^3
η_V	Volumetric efficiency	0.75
n	Rotational speed	-
V	Total volume of the combustion chamber	0.0016 m^3
R	Gas constant	$8.314 \frac{\text{J}}{\text{mol}\cdot\text{K}}$ 288 K
T_{amb}	Ambient temperature	288 K
p_{amb}	Ambient pressure	101325 Pa
θ_o	Preload angle of the throttle valve	0.175 rad
ρ	Air density at ambient conditions	$1.225 \frac{\text{kg}}{\text{m}^3}$
C_d	Drag coefficient	1
K_c	Aerodynamic torque correction coefficient	0.25

2.3 Linearisation

The behavior of the plant is represented through a mathematical model described by a set of nonlinear ordinary differential equations. Considering the inputs \mathbf{u} , the exogenous variables \mathbf{w} , the outputs \mathbf{y} , and the error \mathbf{e} , the dynamics of the plant are given by:

$$\dot{\mathbf{x}} = f(\mathbf{x}, \mathbf{u}, \mathbf{w}) \quad \mathbf{x}(t_0) = \mathbf{x}_0 \quad (2.18)$$

$$\mathbf{y} = h(\mathbf{x}, \mathbf{u}, \mathbf{w}) \quad (2.19)$$

$$\mathbf{e} = h_e(\mathbf{x}, \mathbf{u}, \mathbf{w}) \quad (2.20)$$

The state vector $\mathbf{x} \in \mathbb{R}^n$, where $n \in \mathbb{N}$, is crucial for describing the system. Given that the plant exhibits nonlinear dynamics, it is necessary to linearize it to facilitate control system design. Linearising a nonlinear system involves approximating it by a linear system in a small neighborhood around a specific stationary operating point where the system operates. This approximation enables simpler control strategies.

The stationary operating point, used as the basis for linearisation, is derived from the reference triplet $(\mathbf{x}^*, \mathbf{u}^*, \mathbf{w}^*)$ and is expressed as:

$$\dot{\mathbf{x}}^* = f(\mathbf{x}^*, \mathbf{u}^*, \mathbf{w}^*) \quad \mathbf{x}^*(t_0) = \mathbf{x}_0^* \quad (2.21)$$

$$\mathbf{y}^* = h(\mathbf{x}^*, \mathbf{u}^*, \mathbf{w}^*) \quad (2.22)$$

$$\tilde{\mathbf{e}}^* = h_e(\mathbf{x}^*, \mathbf{u}^*, \mathbf{w}^*) \quad (2.23)$$

An equilibrium triplet $(\mathbf{x}^*, \mathbf{u}^*, \mathbf{w}^*)$ satisfies the following condition:

$$\exists \mathbf{x}^*, \mathbf{u}^*, \mathbf{w}^* : \dot{\mathbf{x}}^* = f(\mathbf{x}^*, \mathbf{u}^*, \mathbf{w}^*) = 0 \quad (2.24)$$

This condition indicates the existence of an equilibrium state where the state derivative $\dot{\mathbf{x}}^*$ is zero, meaning the system has reached a steady state.

It is important to assess the perturbations around this operating point. The perturbations can be determined as follows:

$$\tilde{\mathbf{x}} = \dot{\mathbf{x}} - \dot{\mathbf{x}}^* = f(\mathbf{x}, \mathbf{u}, \mathbf{w}) - f(\mathbf{x}^*, \mathbf{u}^*, \mathbf{w}^*) \quad \tilde{\mathbf{x}}(t_0) = \mathbf{x}_0 - \mathbf{x}_0^* \quad (2.25)$$

$$\tilde{\mathbf{y}} = \mathbf{y} - \mathbf{y}^* = h(\mathbf{x}, \mathbf{u}, \mathbf{w}) - h(\mathbf{x}^*, \mathbf{u}^*, \mathbf{w}^*) \quad (2.26)$$

$$\tilde{\mathbf{e}} = \mathbf{e} - \mathbf{e}^* = h_e(\mathbf{x}, \mathbf{u}, \mathbf{w}) - h_e(\mathbf{x}^*, \mathbf{u}^*, \mathbf{w}^*) \quad (2.27)$$

By defining $\tilde{\mathbf{u}} = \mathbf{u} - \mathbf{u}^*$ and $\tilde{\mathbf{w}} = \mathbf{w} - \mathbf{w}^*$, the expression for $\tilde{\mathbf{x}}$ becomes:

$$\begin{aligned} \tilde{\mathbf{x}} &= f(\tilde{\mathbf{x}} + \mathbf{x}^*, \tilde{\mathbf{u}} + \mathbf{u}^*, \tilde{\mathbf{w}} + \mathbf{w}^*) - f(\mathbf{x}^*, \mathbf{u}^*, \mathbf{w}^*) \\ &= \frac{\partial f}{\partial \mathbf{x}} \Big|_{\substack{\mathbf{x}=\mathbf{x}^* \\ \mathbf{u}=\mathbf{u}^* \\ \mathbf{w}=\mathbf{w}^*}} \cdot \tilde{\mathbf{x}} + \frac{\partial f}{\partial \mathbf{u}} \Big|_{\substack{\mathbf{x}=\mathbf{x}^* \\ \mathbf{u}=\mathbf{u}^* \\ \mathbf{w}=\mathbf{w}^*}} \cdot \tilde{\mathbf{u}} + \frac{\partial f}{\partial \mathbf{w}} \Big|_{\substack{\mathbf{x}=\mathbf{x}^* \\ \mathbf{u}=\mathbf{u}^* \\ \mathbf{w}=\mathbf{w}^*}} \cdot \tilde{\mathbf{w}} + o(\|\tilde{\mathbf{x}}\|^2, \|\tilde{\mathbf{u}}\|^2, \|\tilde{\mathbf{w}}\|^2) \end{aligned} \quad (2.28)$$

This result is derived using Taylor series expansion:

$$\begin{aligned} f(\mathbf{x}, \mathbf{u}, \mathbf{w}) &= f(\mathbf{x}^*, \mathbf{u}^*, \mathbf{w}^*) + \frac{\partial f}{\partial \mathbf{x}} \cdot (\mathbf{x} - \mathbf{x}^*) + \frac{\partial f}{\partial \mathbf{u}} \cdot (\mathbf{u} - \mathbf{u}^*) + \frac{\partial f}{\partial \mathbf{w}} \cdot (\mathbf{w} - \mathbf{w}^*) \\ &\quad + \frac{\partial^2 f}{\partial \mathbf{x}^2} \cdot (\mathbf{x} - \mathbf{x}^*)^2 + \frac{\partial^2 f}{\partial \mathbf{u}^2} \cdot (\mathbf{u} - \mathbf{u}^*)^2 + \frac{\partial^2 f}{\partial \mathbf{w}^2} \cdot (\mathbf{w} - \mathbf{w}^*)^2 + \dots \end{aligned} \quad (2.29)$$

By neglecting terms of second order and higher, we can substitute this expansion into the expressions for $\tilde{\mathbf{y}}$ and $\tilde{\mathbf{e}}$:

$$\tilde{\mathbf{y}} = \frac{\partial h}{\partial \mathbf{x}} \cdot \tilde{\mathbf{x}} + \frac{\partial h}{\partial \mathbf{u}} \cdot \tilde{\mathbf{u}} + \frac{\partial h}{\partial \mathbf{w}} \cdot \tilde{\mathbf{w}} + o(\|\tilde{\mathbf{x}}^2\|, \|\tilde{\mathbf{u}}^2\|, \|\tilde{\mathbf{w}}^2\|) \quad (2.30)$$

$$\tilde{\mathbf{e}} = \frac{\partial h_e}{\partial \mathbf{x}} \cdot \tilde{\mathbf{x}} + \frac{\partial h_e}{\partial \mathbf{u}} \cdot \tilde{\mathbf{u}} + \frac{\partial h_e}{\partial \mathbf{w}} \cdot \tilde{\mathbf{w}} + o(\|\tilde{\mathbf{x}}^2\|, \|\tilde{\mathbf{u}}^2\|, \|\tilde{\mathbf{w}}^2\|) \quad (2.31)$$

Defining the following matrices allows for a more compact representation:

$$\left(\begin{array}{lll} \mathbf{A} = \frac{\partial f}{\partial \mathbf{x}} \Big|_{\substack{\mathbf{x}=\mathbf{x}^* \\ \mathbf{u}=\mathbf{u}^* \\ \mathbf{w}=\mathbf{w}^*}} & \mathbf{B}_1 = \frac{\partial f}{\partial \mathbf{u}} \Big|_{\substack{\mathbf{x}=\mathbf{x}^* \\ \mathbf{u}=\mathbf{u}^* \\ \mathbf{w}=\mathbf{w}^*}} & \mathbf{B}_2 = \frac{\partial f}{\partial \mathbf{w}} \Big|_{\substack{\mathbf{x}=\mathbf{x}^* \\ \mathbf{u}=\mathbf{u}^* \\ \mathbf{w}=\mathbf{w}^*}} \\ \mathbf{C} = \frac{\partial h}{\partial \mathbf{x}} \Big|_{\substack{\mathbf{x}=\mathbf{x}^* \\ \mathbf{u}=\mathbf{u}^* \\ \mathbf{w}=\mathbf{w}^*}} & \mathbf{D}_1 = \frac{\partial h}{\partial \mathbf{u}} \Big|_{\substack{\mathbf{x}=\mathbf{x}^* \\ \mathbf{u}=\mathbf{u}^* \\ \mathbf{w}=\mathbf{w}^*}} & \mathbf{D}_2 = \frac{\partial h}{\partial \mathbf{w}} \Big|_{\substack{\mathbf{x}=\mathbf{x}^* \\ \mathbf{u}=\mathbf{u}^* \\ \mathbf{w}=\mathbf{w}^*}} \\ \mathbf{C}_e = \frac{\partial h_e}{\partial \mathbf{x}} \Big|_{\substack{\mathbf{x}=\mathbf{x}^* \\ \mathbf{u}=\mathbf{u}^* \\ \mathbf{w}=\mathbf{w}^*}} & \mathbf{D}_{1e} = \frac{\partial h_e}{\partial \mathbf{u}} \Big|_{\substack{\mathbf{x}=\mathbf{x}^* \\ \mathbf{u}=\mathbf{u}^* \\ \mathbf{w}=\mathbf{w}^*}} & \mathbf{D}_{2e} = \frac{\partial h_e}{\partial \mathbf{w}} \Big|_{\substack{\mathbf{x}=\mathbf{x}^* \\ \mathbf{u}=\mathbf{u}^* \\ \mathbf{w}=\mathbf{w}^*}} \end{array} \right)$$

Neglecting higher-order terms, we obtain the linear model:

$$\begin{cases} \dot{\mathbf{x}} = \mathbf{A} \cdot \mathbf{x} + \mathbf{B}_1 \cdot \mathbf{u} + \mathbf{B}_2 \cdot \mathbf{w} \\ \mathbf{y} = \mathbf{C} \cdot \mathbf{x} + \mathbf{D}_1 \cdot \mathbf{u} + \mathbf{D}_2 \cdot \mathbf{w} \\ \mathbf{e} = \mathbf{C}_e \cdot \mathbf{x} + \mathbf{D}_{1e} \cdot \mathbf{u} + \mathbf{D}_{2e} \cdot \mathbf{w} \end{cases}$$

The evolution of the state $\dot{\mathbf{x}}$ is expressed through the following equations.

$$\dot{x}_1 = -\frac{R_a}{L} I - \frac{N K_b}{L} \dot{\theta} + \frac{K_d}{L} u \quad (2.32)$$

$$\dot{x}_2 = \dot{\theta} = x_3 \quad (2.33)$$

$$\dot{x}_3 = \frac{N K_t}{N^2 J_m + J_t} I - \frac{K_{sp}}{N^2 J_m + J_t} \theta - \frac{B}{N^2 J_m + J_t} \dot{\theta} - \frac{T_{af} + K_{sp} \theta_o}{N^2 J_m + J_t} \quad (2.34)$$

$$\dot{x}_4 = -\frac{V_d \eta V n}{120 V} p + \frac{R T_{amb} \dot{m}}{V} \quad (2.35)$$

In this analysis, the matrices that represent the state are first expressed in a parametric form, capturing the system's dynamics in terms of general

parameters. Once the equilibrium point is defined, these matrices are then evaluated and represented in numerical form. This approach allows for a more flexible model that can be adapted to specific operating conditions before being resolved into concrete numerical values.

$$\mathbf{A} = \begin{bmatrix} -\frac{R_a}{L} & 0 & -\frac{NK_b}{L} \\ 0 & 0 & 1 \\ \frac{NK_t}{N^2 J_m + J_t} & -\frac{K_{sp}}{N^2 J_m + J_t} & -\frac{B}{N^2 J_m + J_t} \end{bmatrix} \quad (2.36)$$

$$\mathbf{B}_1 = \begin{bmatrix} \frac{K_d}{L} \\ 0 \\ 0 \end{bmatrix} \quad (2.37)$$

$$\mathbf{B}_2 = \begin{bmatrix} 0 & 0 & 0 \\ 0 & 0 & 0 \\ 0 & 0 & 0 \end{bmatrix} \quad (2.38)$$

2.3.1 Linearisation Conditions

The linearisation is performed with the following conditions:

$$\begin{aligned} \theta^* &= 12^\circ = 0.2094 \text{ rad} \\ \dot{\theta}^* &= 0 \frac{\text{rad}}{\text{s}} \\ p^* &= 778.7876 \text{ Pa} \\ I^* &= \frac{K_{sp}(\theta^* + \theta_o) + T_{af}}{K_t N} = 4.5320 \text{ A} \\ u^* &= 3.0154 \text{ V} \\ d^* &= 0 \\ v^* &= 0 \\ r^* &= 0.2094 \text{ rad} \end{aligned}$$

Linearising the system around 12° offers significant advantages. This operating point is frequently traversed and exhibits notable instabilities, making it critical for ensuring local stability and control precision. Optimizing the control strategy at this point reduces sensitivity to perturbations and enhances performance where it is most needed.

The main drawback of this approach is that focusing on 12° may degrade the system's overall stability if it frequently operates across a wider range of angles. This trade-off is a natural limitation of local linearisation.

However, the planned implementation of a feedback stabilizer with integral action and feed-forward control mitigates this limitation. The feedback stabilizer will address local stability, the integral action will correct steady-state errors, and the feed-forward control will handle predictable disturbances. This combination ensures robust performance across the operating range, making 12° a logical and effective choice for linearisation.

Having defined the equilibrium triplet, the matrices characterizing the dynamics of the system are reported below. It is important to remind the fact that the pressure is just part of the plant so the state dimension, and so the matrix \mathbf{A} dimension, is $n = 3$ and not $n = 4$.

$$\mathbf{A} = \begin{bmatrix} -1176.5 & 0 & -58.8235 \\ 0 & 0 & 1 \\ 0.9091 & -0.9697 & -0.1515 \end{bmatrix}$$

$$\mathbf{B}_1 = \begin{bmatrix} 1764.7 \\ 0 \\ 0 \end{bmatrix}$$

$$\mathbf{B}_2 = \begin{bmatrix} 0 & 0 & 0 \\ 0 & 0 & 0 \\ 0 & 0 & 0 \end{bmatrix}$$

The matrices vary according to the chosen equilibrium triplet, meaning the linearized state dynamics are influenced by these equilibrium conditions. Since our original system is non-linear, the resulting linearized system inherently depends on these specific equilibrium values.

The other matrices are the ones related to the measurements and to the error.

$$\mathbf{C} = [0 \ 1 \ 0]$$

$$\mathbf{D}_1 = 0$$

$$\mathbf{D}_2 = [0 \ 1 \ 0]$$

$$\mathbf{C}_e = [0 \ 1 \ 0]$$

$$\mathbf{D}_{1e} = 0$$

$$\mathbf{D}_{2e} = [0 \ 1 \ -1]$$

An important observation is that $\mathbf{C}_e = \mathbf{C}$, and likewise, $\mathbf{D}_{1e} = \mathbf{D}_1$ while \mathbf{D}_{2e} differs from \mathbf{D}_2^* only for the last column. This result is expected, since the error represents the difference between the measured values and their respective reference points.

2.4 Linear System Analysis

Following the linearisation process, two key stability definitions are established to assess the system's robustness and boundedness.

1. For any initial condition $\tilde{\mathbf{x}}(t_0)$, the variables $\tilde{\mathbf{x}}$, $\tilde{\mathbf{u}}$, $\tilde{\mathbf{y}}$, and $\tilde{\mathbf{e}}$ remain bounded for all $t \geq 0$. This ensures that the system's errors are contained within limits for any initial state, indicating a robust and stable response.
2. When $\dot{\mathbf{d}} = 0$ and $\nu = 0$, it can be inferred that $\limsup_{t \rightarrow \infty} \|\tilde{\mathbf{e}}(t)\| = 0$. This condition implies that disturbances are constant and noise effects are negligible, enabling the system to reach a steady state without persistent error.

In this section, the system's natural response is analyzed in absence of control inputs.

A central part of this analysis is examining the eigenvalues and eigenvectors of the system matrix \mathbf{A} , as they are fundamentally connected to the system's inherent dynamics. Specifically, the ability of trajectories to remain bounded is directly influenced by the eigenvalues of \mathbf{A} , as will be detailed in the following section.

2.4.1 Eigenvalues and Eigenvectors

In order to assess the asymptotic behavior of the linearized system and determine whether it remains stable or diverges from the equilibrium condition, an analysis of self-stability is conducted on the system represented by:

$$\dot{\mathbf{x}} = \mathbf{Ax}$$

From this point forward, we will simplify the notation by omitting the "tilde" symbol for linearized coordinates. The goal is to perform a coordinate transformation that simplifies the system's representation, ideally by

converting it into its Jordan canonical form. This transformation facilitates understanding the fundamental dynamics of the system, allowing us to analyze it in terms of its elementary components.

To begin with, we calculate the eigenvalues of the system's \mathbf{A} matrix. This involves solving for non-trivial solutions, λ , that satisfy:

$$\begin{aligned}\det(\mathbf{A} - \lambda\mathbf{I}) &= 0 \\ (\mathbf{A} - \lambda\mathbf{I})\mathbf{v} &= 0\end{aligned}$$

Once the eigenvalues λ_i are obtained, we can find the corresponding eigenvectors \mathbf{v}_i , which help describe the direction and behavior of the system's trajectories.

In this specific analysis, the system has three eigenvalues λ_i , which depend on the \mathbf{A} matrix derived from the linearization process around a specific operating point, defined by the equilibrium triplet $(\mathbf{x}^*, \mathbf{u}^*, \mathbf{w}^*)$. Changes in these equilibrium conditions lead to modifications in the \mathbf{A} matrix and, consequently, in the eigenvalues. It has been observed that the choice of parameters for the linearization point significantly affects the eigenvalues and therefore the stability of the system.

For this study, the linearization point was selected to reflect a common operating condition, accepting some approximation errors inherent to the linearization. Analyzing the eigenvalues of \mathbf{A} is crucial for understanding the system's asymptotic stability. The calculated eigenvalues provide insights into the stability characteristics of the linearized model.

$$\begin{aligned}\lambda_1 &= -1176.4 + 0.0000i \\ \lambda_2 &= -0.0985 + 0.9798i \\ \lambda_3 &= -0.0985 - 0.9798i\end{aligned}\tag{2.39}$$

The related eigenvectors are also computed and reported below.

$$\mathbf{v}_1 = \begin{bmatrix} 1.0000 \\ 6.5695 \times 10^{-7} \\ -7.7286 \times 10^{-4} \end{bmatrix}\tag{2.40}$$

$$\mathbf{v}_2 = \begin{bmatrix} 0.0035 - 0.0349i \\ 0.7121 \\ -0.0701 + 0.6977i \end{bmatrix}\tag{2.41}$$

$$\mathbf{v}_3 = \begin{bmatrix} 0.0035 + 0.0349i \\ 0.7121 \\ -0.0701 - 0.6977i \end{bmatrix}\tag{2.42}$$

Since the number of unique eigenvalues matches the rank of matrix \mathbf{A} , each eigenvalue has an algebraic multiplicity of 1, which also implies a geometric multiplicity of 1. It can also be seen that all the eigenvalues have negative real parts, allowing us to conclude that the system is BIBS (Bounded Input Bounded State) stable and the matrix \mathbf{A} is Hurwitz. The imaginary parts of the eigenvalues are related to the oscillatory behavior of the system's modes.

The Jordan transformation serves as the mathematical tool that facilitates the transition to a new coordinate system. This transformation relies on constructing a sequence of generalized eigenvectors, which form a chain of linearly independent eigenvectors. The transformation is expressed as:

$$\mathbf{J} = \mathbf{V}^{-1} \mathbf{A} \mathbf{V}.$$

where:

- \mathbf{J} is the matrix in Jordan form;
- \mathbf{V} is the matrix consisting of a chain of generalized eigenvectors associated with \mathbf{A} . From a physical perspective, these vectors correspond to the shape of the system modes during free evolution.

The Jordan block \mathbf{J} obtained through the transformation is an alternative representation of the matrix \mathbf{A} . In particular, it is a diagonal matrix containing the eigenvalues of \mathbf{A} :

$$\mathbf{J} = \begin{bmatrix} -1176.4 + 0.0000i & 0 & 0 \\ 0 & -0.0985 + 0.9798i & 0 \\ 0 & 0 & -0.0985 - 0.9798i \end{bmatrix}$$

It's also possible to reduce the matrix \mathbf{J} to pure real values isolating the real and the imaginary parts and then collecting them in columns, deriving a matrix form that is more appropriate to the requirements of the project:

$$\mathbf{J}_{real} = \begin{bmatrix} -1176.4 & 0 & 0 \\ 0 & -0.0985 & 0.9798 \\ 0 & -0.9798 & -0.0985 \end{bmatrix}$$

All the eigenvectors can be consolidated in a single matrix \mathbf{V} , containing only real values by isolating the real from the imaginary components and arranging them in columns.

The matrix \mathbf{V} represents the composition of eigenvectors associated with each eigenvalue.

$$\mathbf{V} = \begin{bmatrix} 1.0000 & 0.0035 & -0.0349 \\ 6.5695 \times 10^{-7} & 0.7121 & 0 \\ -7.7286 \times 10^{-4} & -0.0701 & 0.6977 \end{bmatrix} \quad (2.43)$$

To analyze the system's dynamics, we leverage the eigenvalues and eigenvectors to perform a coordinate transformation.

This allows to create a representation of the system comprising independent sub-systems. By using the eigenvector matrix \mathbf{V} , it is possible to rewrite the system in its Jordan canonical form by applying the transformation matrix $\mathbf{T} = \mathbf{V}^{-1}$.

Thus, the system in the transformed coordinates can be expressed as:

$$\dot{\mathbf{z}} = \mathbf{J}\mathbf{z}, \quad \text{with } \mathbf{z}(t_0) = \mathbf{z}_0; \quad (2.44)$$

where

$$\mathbf{z}(t) = e^{\mathbf{J}t}\mathbf{z}(0). \quad (2.45)$$

In the original coordinates, this relationship is represented by:

$$\mathbf{x} = \mathbf{V}\mathbf{z}. \quad (2.46)$$

This transformation enables a clearer understanding of the system's dynamics by analyzing the behavior of the eigenvalues and eigenvectors of matrix \mathbf{A} . Each eigenvalue provides insight into the stability and oscillatory nature of the system's modes.

Specifically, the real part of each eigenvalue indicates the rate of convergence or divergence: a negative real part suggests that the system's state will eventually converge to zero, indicating stability, while a positive real part would indicate instability, causing the state to grow over time. The imaginary part of each eigenvalue, on the other hand, represents the frequency of oscillation associated with that mode.

Thus, by examining both the real and imaginary components of the eigenvalues, one can assess not only whether the system is stable but also whether it exhibits oscillatory behavior, and at what frequency these oscillations occur. This analysis provides a comprehensive view of the dynamic characteristics and response tendencies of the system.

Finally, each state variable's dynamic influence from each eigenvector can be represented through the matrix \mathbf{V}_n that contains all the elements v_{ij} of the matrix \mathbf{V} weighted over each row \mathbf{V}_i .

$$\mathbf{V}_n = \begin{bmatrix} 96.3049 & 0.3349 & 3.3602 \\ 0.0001 & 99.9999 & 0 \\ 0.1006 & 9.1245 & 90.7750 \end{bmatrix} \quad (2.47)$$

To better understand each mode's impact on each state variable radar charts are useful.

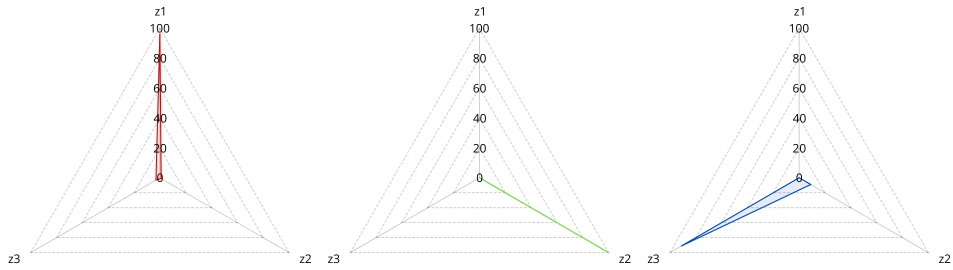


Figure 2.3: Impact of the modes on the state variables

Figure 2.3 can be described as follows:

- x_1 : is the current. It is mainly affected by the first 2 components. Specifically, 96.3049% of x_1 is influenced by z_1 , while 3.3602% is due to z_3 , with a minimal contribution from z_2 . Since the component z_1 has a negative real part, the current will converge quickly with almost no oscillations;
- x_2 : is the angular position of the throttle valve. It is primarily influenced by the component z_2 for 99.9999%. The remaining 0.0001% of x_2 is affected by z_1 while no contribute is given by z_3 . The component z_2 has a low negative real part and an imaginary contribution, which means that the angular position will converge very slowly and with some oscillations;
- x_3 : is the angular velocity of the throttle valve. It is mainly influenced by z_3 and z_2 . 90.7750% of x_3 is influenced by z_3 , 9.1245% is due to z_2 while z_1 is responsible for just the 1.0006%. As in the case of the angular position, also the angular velocity will converge slowly and oscillate due the presence of small negative real part and imaginary part of z_2 and z_3 .

It is worth noting that, since all the eigenvalues listed in equation (2.39) are complex numbers with negative real parts, our system exhibits BIBS

stability. So each state initially oscillates but ultimately converges to a stable value.

This behavior will be shown in two different cases, firstly starting from equilibrium conditions, then beginning the simulation from a different point.

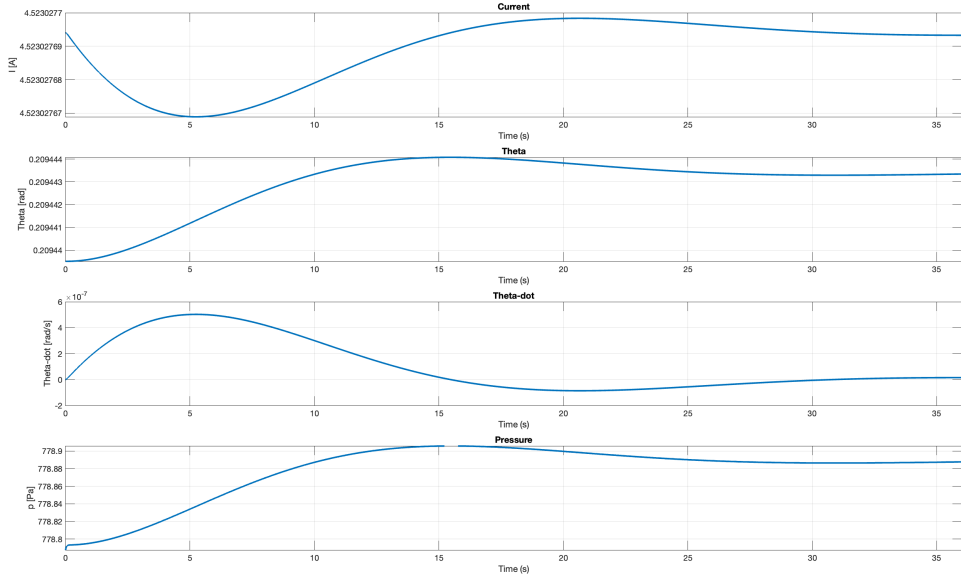


Figure 2.4: State plots starting from equilibrium conditions

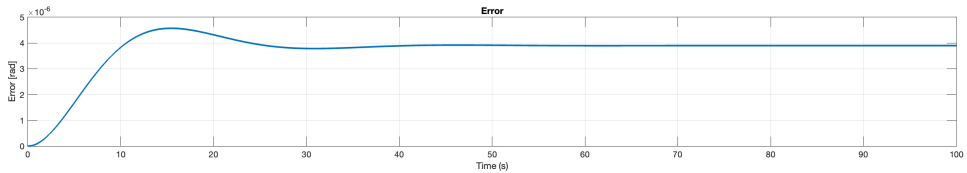


Figure 2.5: Error signal starting from equilibrium conditions

All the states, after an oscillating transient, go back to the equilibrium conditions. The plot of the error is also going to be shown and, as expected, after the oscillatory transient it goes back to zero. In this specific case it remains constant at $4 \times 10^{-6} \text{ rad}$ but this order of magnitude is so small that can be considered null.

The pressure, the final angular position, and so the error, slightly deviate from the equilibrium values due to negligibly small numerical discrepancies.

In the second scenario, illustrated below, the system's inherent stabil-

ity is evident, as each state variable gradually settles back to the desired equilibrium values.

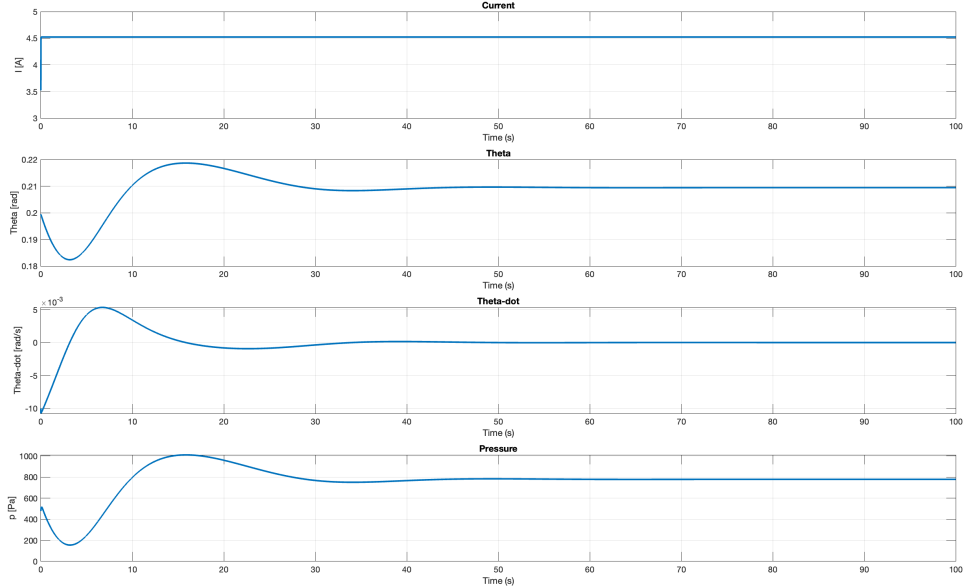


Figure 2.6: State plots starting from different conditions

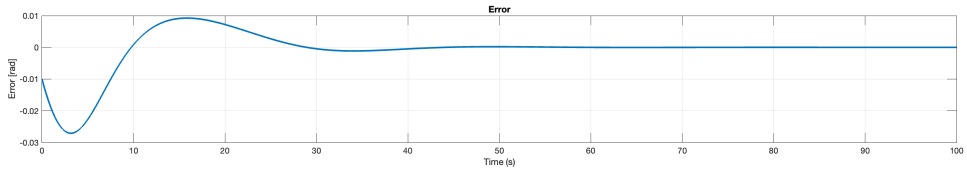


Figure 2.7: Error signal starting from different conditions

2.5 Reachability

The reachability study is performed to understand which parts of \mathbf{A} can be modified by the control and which have limitations in the control's ability to steer certain states back to equilibrium. The objective is to identify the set of states, called the reachability set \mathbf{R} , that represents states that can be reached starting from the origin.

The dimensions of this matrix are $n \times n \cdot p$, where $n = 3$ is the dimension of the state vector and $p = 1$ is the dimension of the control, so $\mathbf{R} \in \mathbb{R}^{3 \times 3}$.

The matrix \mathbf{R} is constructed as:

$$\mathbf{R} = [\mathbf{B}_1 \quad \mathbf{AB}_1 \quad \mathbf{A}^2\mathbf{B}_1]$$

The system is said to be fully reachable if $\text{rank}(\mathbf{R}) = n = 3$, which means that the matrix has full rank.

In cases where the system is not fully reachable, it is necessary to distinguish between the reachable and non-reachable states.

The number of reachable states, denoted by n_r , is given by:

$$n_r = \text{rank}(\mathbf{R}) \quad (2.48)$$

and the number of non-reachable states is determined by $n - n_r$.

To proceed, we define the transformation matrix \mathbf{T}_R^{-1} as:

$$\mathbf{T}_R^{-1} = [\text{im}(\mathbf{R}) \quad \ker(\mathbf{R}^T)] \quad (2.49)$$

Using this transformation matrix, the following transformed matrices are derived:

$$\bar{\mathbf{A}} = \mathbf{T}_R \mathbf{A} \mathbf{T}_R^{-1}, \quad \bar{\mathbf{B}}_1 = \mathbf{T}_R \mathbf{B}_1, \quad \bar{\mathbf{B}}_2 = \mathbf{T}_R \mathbf{B}_2, \quad \bar{\mathbf{C}} = \mathbf{C} \mathbf{T}_R^{-1} \quad (2.50)$$

The linear system can be expressed as:

$$\dot{\mathbf{z}} = \bar{\mathbf{A}}\mathbf{z} + \bar{\mathbf{B}}_1\tilde{\mathbf{u}} + \bar{\mathbf{B}}_2\tilde{\mathbf{w}} \quad (2.51)$$

It is possible to divide \mathbf{z} in its reachable and non reachable part, obtaining:

$$\begin{bmatrix} \dot{\mathbf{z}}_R \\ \dot{\mathbf{z}}_{NR} \end{bmatrix} = \begin{bmatrix} \bar{\mathbf{A}}_{11} & \bar{\mathbf{A}}_{12} \\ \bar{\mathbf{A}}_{21} & \bar{\mathbf{A}}_{22} \end{bmatrix} \begin{bmatrix} \mathbf{z}_R \\ \mathbf{z}_{NR} \end{bmatrix} + \begin{bmatrix} \bar{\mathbf{B}}_{11} \\ 0 \end{bmatrix} \tilde{\mathbf{u}} + \begin{bmatrix} \bar{\mathbf{B}}_{21} \\ \bar{\mathbf{B}}_{22} \end{bmatrix} \tilde{\mathbf{w}} \quad (2.52)$$

with $\bar{\mathbf{A}}_{21} = 0$.

It can be clearly observed that control can only influence the reachable part of the system, while the non-reachable dynamics remain unaffected by both the control and the reachable state.

In such cases, all state variables remain bounded if and only if the non-reachable parts of the state, over which no control authority exists, also remain bounded.

This condition is satisfied if and only if the sub-matrix $\bar{\mathbf{A}}_{22}$ is Hurwitz. When this holds true, the system is said to be stabilisable.

Expanding further:

$$\dot{\mathbf{z}}_R = \bar{\mathbf{A}}_{11}\mathbf{z}_R + \bar{\mathbf{A}}_{12}\mathbf{z}_{NR} + \bar{\mathbf{B}}_{11}\tilde{\mathbf{u}} + \bar{\mathbf{B}}_{21}\tilde{\mathbf{w}} \quad (2.53)$$

$$\dot{\mathbf{z}}_{NR} = \bar{\mathbf{A}}_{22}\mathbf{z}_{NR} + \bar{\mathbf{B}}_{22}\tilde{\mathbf{w}} \quad (2.54)$$

To proceed, the reachability matrix \mathbf{R} is derived and its rank is computed.

$$\mathbf{R} = \begin{bmatrix} 1.7647 \times 10^3 & -2.0761 \times 10^6 & 2.4424 \times 10^9 \\ 0 & 0 & 1.6043 \times 10^3 \\ 0 & 1.6043 \times 10^3 & -1.8876 \times 10^6 \end{bmatrix} \quad (2.55)$$

$$\text{rank}(\mathbf{R}) = 3 \quad (2.56)$$

```
R=[B1 A*B1 A^2*B1];
RankR=rank(R);

if RankR==length(A)
    disp('System fully reachable')
else
    disp('System not fully reachable')
end
```

This result indicates that the matrix is of full rank, meaning that all the eigenvalues of \mathbf{A} can be controlled.

Accordingly, it is possible to assert that a matrix \mathbf{K}_S exists such that $(\mathbf{A} + \mathbf{B}_1 \mathbf{K}_S)$ is Hurwitz.

This implies that a state feedback control law can be designed to make the closed-loop system BIBS stable if the exogenous $\tilde{\mathbf{w}}$ is bounded. The equation for the state feedback stabilizer in terms of \mathbf{K}_S is:

$$\tilde{\mathbf{u}} = \mathbf{K}_S \tilde{\mathbf{x}}$$

Hence, we have:

$$\dot{\tilde{\mathbf{x}}} = (\mathbf{A} + \mathbf{B}_1 \mathbf{K}_S) \tilde{\mathbf{x}} + \mathbf{B}_2 \tilde{\mathbf{w}}$$

2.6 Integral Action

The stabilizer control $\tilde{\mathbf{u}} = \mathbf{K}_S \tilde{\mathbf{x}}$ ensures that in the absence of exogenous inputs (i.e., no disturbances), the system state will converge back to the origin, making the error $\tilde{\mathbf{e}}$ zero. However, when disturbances are present, the stabilizer alone can only limit the state and the error without fully eliminating them. To address this limitation, an integral action is added to the control structure, which helps drive the error to zero in the presence of constant disturbances while still keeping the error bounded in other cases.

The error equation can be represented as:

$$\tilde{\mathbf{e}} = \mathbf{C}_e \tilde{\mathbf{x}} + \mathbf{D}_{1e} \tilde{\mathbf{u}} + \mathbf{D}_{2e} \tilde{\mathbf{w}} \quad (2.57)$$

To incorporate the integral action, a new variable $\boldsymbol{\eta}$ is introduced.

$$\dot{\boldsymbol{\eta}} = \tilde{\mathbf{e}} \quad (2.58)$$

Expanding the system to include this integral action leads to the definition of an extended state \mathbf{x}_e as:

$$\mathbf{x}_e = \begin{bmatrix} \tilde{\mathbf{x}} \\ \boldsymbol{\eta} \end{bmatrix} \quad (2.59)$$

The dynamics of the extended system are described by:

$$\begin{bmatrix} \dot{\tilde{\mathbf{x}}} \\ \dot{\boldsymbol{\eta}} \end{bmatrix} = \begin{bmatrix} \mathbf{A} & \mathbf{0} \\ \mathbf{C}_e & \mathbf{0} \end{bmatrix} \begin{bmatrix} \tilde{\mathbf{x}} \\ \boldsymbol{\eta} \end{bmatrix} + \begin{bmatrix} \mathbf{B}_1 \\ \mathbf{D}_{1e} \end{bmatrix} \tilde{\mathbf{u}} + \begin{bmatrix} \mathbf{B}_2 \\ \mathbf{D}_{2e} \end{bmatrix} \tilde{\mathbf{w}} \quad (2.60)$$

In a more concise form it is written as:

$$\dot{\mathbf{x}}_e = \mathbf{A}_e \mathbf{x}_e + \mathbf{B}_{1e} \tilde{\mathbf{u}} + \mathbf{B}_{2e} \tilde{\mathbf{w}} \quad (2.61)$$

with:

$$\mathbf{A}_e = \begin{bmatrix} \mathbf{A} & \mathbf{0} \\ \mathbf{C}_e & \mathbf{0} \end{bmatrix} = \begin{bmatrix} -1176.5 & 0 & -58.8235 & 0 \\ 0 & 0 & 1 & 0 \\ 0.9091 & -0.9697 & -0.1515 & 0 \\ 0 & 1 & 0 & 0 \end{bmatrix} \quad (2.62)$$

$$\mathbf{B}_{1e} = \begin{bmatrix} \mathbf{B}_1 \\ \mathbf{D}_{1e} \end{bmatrix} = \begin{bmatrix} 1764.7 \\ 0 \\ 0 \\ 0 \end{bmatrix} \quad (2.63)$$

$$\mathbf{B}_{2e} = \begin{bmatrix} \mathbf{B}_2 \\ \mathbf{D}_{2e} \end{bmatrix} = \begin{bmatrix} 0 & 0 & 0 \\ 0 & 0 & 0 \\ 0 & 0 & 0 \\ 0 & 1 & -1 \end{bmatrix} \quad (2.64)$$

If the pair $(\mathbf{A}_e, \mathbf{B}_{1e})$ is stabilizable, a matrix \mathbf{K}_e exists such that $(\mathbf{A}_e + \mathbf{B}_{1e} \mathbf{K}_e)$ is Hurwitz. By defining the control as $\tilde{\mathbf{u}} = \mathbf{K}_e \mathbf{x}_e$, the extended system can be rewritten as:

$$\dot{\mathbf{x}}_e = (\mathbf{A}_e + \mathbf{B}_{1e} \mathbf{K}_e) \mathbf{x}_e + \mathbf{B}_{2e} \tilde{\mathbf{w}} \quad (2.65)$$

In scenarios where $\tilde{\mathbf{w}}$ is constant, $\dot{\mathbf{x}}_e$ will asymptotically approach zero, leading to the error $\tilde{\mathbf{e}}$ being driven to zero, as it is part of the state \mathbf{x}_e . The matrix \mathbf{K}_e is structured as:

$$\mathbf{K}_e = [\mathbf{K}_S \quad \mathbf{K}_I] \quad (2.66)$$

where \mathbf{K}_S acts on the state $\tilde{\mathbf{x}}$ (stabilizing component) and \mathbf{K}_I acts on the integral of the error (integral action). These matrices are co-designed to achieve a consistent and effective control strategy.

2.7 Observability

Previously, the control law $\tilde{\mathbf{u}} = \mathbf{K}_S \tilde{\mathbf{x}}$ has been introduced to maintain BIBS (Bounded Input, Bounded State) stability in a closed-loop system.

However, in practical scenarios, this control law cannot be directly applied if the state $\tilde{\mathbf{x}}$ is not known. To address this, it is essential to use available measurements $\tilde{\mathbf{y}}$ and inputs $\tilde{\mathbf{u}}$ to estimate $\tilde{\mathbf{x}}$. This estimation is achieved through a dynamic system called an observer.

To determine observability, the first need is to check if there are parts of the system that cannot be estimated by the observer. Assuming $\tilde{\mathbf{u}} = 0$ and $\tilde{\mathbf{w}} = 0$ for all $t \geq 0$, the system response is:

$$\dot{\tilde{\mathbf{x}}} = \mathbf{A}\tilde{\mathbf{x}} \quad (2.67)$$

$$\tilde{\mathbf{y}} = \mathbf{C}\tilde{\mathbf{x}} \quad (2.68)$$

The solution to this system is:

$$\tilde{\mathbf{x}}(t) = \exp(\mathbf{A}t)\tilde{\mathbf{x}}_0 \quad \Rightarrow \quad \tilde{\mathbf{y}}(t) = \mathbf{C}\exp(\mathbf{A}t)\tilde{\mathbf{x}}_0 \quad (2.69)$$

The non-observable state ϵ can be defined as:

$$\epsilon = \{\tilde{\mathbf{x}}_0 \in \mathbb{R}^n \mid \tilde{\mathbf{y}}(t) = 0 \quad \forall t \geq 0\} \quad (2.70)$$

This implies that the control system cannot distinguish these states $\tilde{\mathbf{x}}_0$ from the origin, leading to $\tilde{\mathbf{y}}(t) = 0$.

To evaluate system observability, we define the observability matrix \mathbf{O} :

$$\mathbf{O} = \begin{bmatrix} \mathbf{C} \\ \mathbf{CA} \\ \vdots \\ \mathbf{CA}^{n-1} \end{bmatrix} \quad (2.71)$$

For a system where $n = 3$, the observability matrix is:

$$\mathbf{O} = \begin{bmatrix} \mathbf{C} \\ \mathbf{CA} \\ \mathbf{CA}^2 \end{bmatrix} \quad (2.72)$$

with matrix $\mathbf{O} \in \mathbb{R}^{3 \times 3}$.

To determine if the system is fully observable, one can examine the kernel of the observability matrix \mathbf{O} . If the dimension of the kernel $\ker(\mathbf{O})$ is zero, it means that the only vector in the kernel is the origin. This implies that the system's state can be fully reconstructed from the outputs, confirming that the pair (\mathbf{A}, \mathbf{C}) is fully observable. Another way to verify observability is by checking the rank of \mathbf{O} . If the rank of \mathbf{O} equals the dimension n of the state space, then the system is also considered fully observable.

The observability analysis allows designing a BIBS stable observer, which estimates the transformed state \mathbf{z}_O as:

$$\begin{cases} \dot{\mathbf{z}}_O = \bar{\mathbf{A}}\mathbf{z}_O + \bar{\mathbf{B}}_1\tilde{\mathbf{u}} + \mathbf{K}_O(\tilde{\mathbf{y}} - \hat{\mathbf{y}}) \\ \hat{\mathbf{y}} = \mathbf{C}\mathbf{z}_O + \mathbf{D}_1\tilde{\mathbf{u}} \end{cases} \quad (2.73)$$

where \mathbf{z}_O is the observable part of \mathbf{z} , the transformed state vector.

$$\mathbf{T}_O^{-1} = [\ker(\mathbf{O}) \quad \text{im}(\mathbf{O}^\top)] \quad (2.74)$$

$$\mathbf{z} = \mathbf{T}_O\tilde{\mathbf{x}} \quad (2.75)$$

Using this transformation matrix, the following transformed matrices are derived:

$$\bar{\mathbf{A}} = \mathbf{T}_O \mathbf{A} \mathbf{T}_O^{-1}, \quad \bar{\mathbf{B}}_1 = \mathbf{T}_O \mathbf{B}_1, \quad \bar{\mathbf{B}}_2 = \mathbf{T}_O \mathbf{B}_2, \quad \bar{\mathbf{C}} = \mathbf{C} \mathbf{T}_O^{-1} \quad (2.76)$$

The linear system can be expressed as:

$$\dot{\mathbf{z}} = \bar{\mathbf{A}}\mathbf{z} + \bar{\mathbf{B}}_1\tilde{\mathbf{u}} + \bar{\mathbf{B}}_2\tilde{\mathbf{w}} \quad (2.77)$$

It is possible to divide \mathbf{z} in its observable and non observable part, obtaining:

$$\begin{bmatrix} \dot{\mathbf{z}}_{NO} \\ \dot{\mathbf{z}}_O \end{bmatrix} = \begin{bmatrix} \bar{\mathbf{A}}_{11} & \bar{\mathbf{A}}_{12} \\ \bar{\mathbf{A}}_{21} & \bar{\mathbf{A}}_{22} \end{bmatrix} \begin{bmatrix} \mathbf{z}_{NO} \\ \mathbf{z}_O \end{bmatrix} + \begin{bmatrix} \bar{\mathbf{B}}_{11} \\ \bar{\mathbf{B}}_{12} \end{bmatrix} \tilde{\mathbf{u}} + \begin{bmatrix} \bar{\mathbf{B}}_{21} \\ \bar{\mathbf{B}}_{22} \end{bmatrix} \tilde{\mathbf{w}} \quad (2.78)$$

with $\bar{\mathbf{A}}_{21} = 0$ as the non observable part does not affect the observable one.

It is crucial that the sub-matrix $\bar{\mathbf{A}}_{11}$ is Hurwitz. When this holds true, the system is said to be detectable.

Expanding further:

$$\dot{\mathbf{z}}_{NO} = \bar{\mathbf{A}}_{11}\mathbf{z}_{NO} + \bar{\mathbf{A}}_{12}\mathbf{z}_O + \bar{\mathbf{B}}_{11}\tilde{\mathbf{u}} + \bar{\mathbf{B}}_{21}\tilde{\mathbf{w}} \quad (2.79)$$

$$\dot{\mathbf{z}}_O = \bar{\mathbf{A}}_{22}\mathbf{z}_O + \bar{\mathbf{B}}_{12}\tilde{\mathbf{u}} + \bar{\mathbf{B}}_{22}\tilde{\mathbf{w}} \quad (2.80)$$

Let $\mathbf{e}_O = \hat{\mathbf{z}}_O - \mathbf{z}_O$ represent the estimation error. The dynamics of the estimation error are given by:

$$\dot{\mathbf{e}}_O = (\bar{\mathbf{A}} - \mathbf{K}_O\bar{\mathbf{C}})\mathbf{e}_O + (\bar{\mathbf{B}}_2 + \mathbf{K}_O\mathbf{D}_2)\tilde{\mathbf{w}} \quad (2.81)$$

If $(\bar{\mathbf{A}} - \mathbf{K}_O\bar{\mathbf{C}})$ is Hurwitz, the error \mathbf{e}_O asymptotically converges to a neighborhood of the origin ensuring that the observer maintains a stable estimation.

$$\mathbf{O} = \begin{bmatrix} 0 & 1 & 0 \\ 0 & 0 & 1 \\ 0.9091 & -0.9697 & -0.1515 \end{bmatrix} \quad (2.82)$$

$$\text{rank}(\mathbf{O}) = 3 \quad (2.83)$$

```

0=[C;
  C*A;
  C*A^2];

Rank0=rank(0);

if Rank0==length(A)
    disp('System fully observable')
else
    disp('System not fully observable')
end

```

The result implies that the system is fully observable, allowing the control system to estimate all states $\hat{\mathbf{x}}$. Furthermore, there exists a matrix \mathbf{K}_O such that $(\mathbf{A} - \mathbf{K}_O\mathbf{C})$ is Hurwitz.

2.8 Reference Signal

In the context of throttle valve control, the reference signal for the angular position of the valve plays a fundamental role in ensuring precise and efficient operation.

By definition, the reference signal must be continuous and differentiable. This requirement is crucial as it directly impacts the smoothness of the control system's response and its ability to compute higher-order derivatives for advanced control actions, such as feed-forward.

In both sporty and urban driving scenarios, the throttle valve is subjected to abrupt variations, often resulting from rapid and inconsistent inputs to the accelerator pedal. These variations introduce discontinuities in the reference signal, which, if not addressed, can compromise the performance of the control system.

For standard automotive applications, rather than focusing on high performance telemetry signals typical of sports applications, it is more appropriate to process the reference signal to achieve a smoother and more continuous profile. A common and effective approach to achieving this level of continuity is to use a low-pass filter, which attenuates high-frequency components and smooths out abrupt changes in the reference signal.

2.8.1 Transfer Function

The transfer function applied in this system is specifically designed to filter the reference signal and improve its smoothness while ensuring compatibility with the control objectives. The transfer function is defined as:

$$G(S) = \frac{1}{\tau S + 1} \cdot \frac{1}{S^2 + 2\delta\omega_n S + \omega_n^2}$$

where:

- τ is the time constant of the low-pass filter, defining the speed of the initial filtering stage;
- ω_n is the natural frequency of the second-order system, responsible for shaping the dynamic response of the filtered signal;
- δ is the damping ratio, which determines the level of oscillation in the output signal after filtering.

2.8.2 Filter Description

This transfer function combines two filtering stages to achieve a smooth and continuous reference signal.

The first stage is a first-order low-pass filter, defined by $\frac{1}{\tau s + 1}$. This filter is responsible for attenuating high-frequency noise and abrupt variations, ensuring a smoother signal that is particularly suitable for automotive applications where precision and continuity are required.

The other stage is represented by $\frac{1}{s^2 + 2\delta\omega_n s + \omega_n^2}$, a second-order low-pass filter. This stage refines the frequency response, minimizing overshoot and oscillations that could otherwise destabilize the control system. By acting as a more sophisticated filtering mechanism, it ensures robust attenuation of unwanted components while maintaining the desired dynamics of the signal.

Together, these two stages provide a reliable and well-structured approach to filtering, enabling precise and efficient control actions.

2.8.3 Resulting Signal

The result is a reference signal $r(t)$ that is compatible with automotive control requirements.

This signal and its derivatives, computed up to the third order, are essential inputs for feed-forward control, enabling precise and robust tracking of the desired throttle position while handling real-world disturbances effectively.

Different reference signals are going to be used for more in-depth analysis further in the development of the control system.

Different reference signals will be utilized for a more in-depth analysis during the next phases of control system development. These signals are critical to evaluate the system's behavior under varying conditions and to fine-tune the control strategies.

To explicitly illustrate the effects discussed in the previous paragraph, one of these reference signals will be plotted both before and after the filtering process. This comparison aims to highlight the impact of the filtering technique on the signal's characteristics, specifically its role in increasing the degree of continuity and differentiability, which are essential for achieving smooth and stable control inputs.

The reference signal $r(t)$ is defined as the following piecewise function, varying over time according to the following sequence of stabilization and linear transitions.

$$r(t) = \begin{cases} 0.2094 & t < 4 \text{ s}, \\ 0.2094 + \frac{0.8727 - 0.2094}{4}(t - 4), & 4 \text{ s} \leq t < 8 \text{ s} \\ 0.8727 & 8 \text{ s} \leq t < 12 \text{ s} \\ 0.8727 - \frac{0.8727 - 0.2094}{4}(t - 12) & 12 \text{ s} \leq t < 16 \text{ s} \\ 0.2094 & 16 \text{ s} \leq t < 20 \text{ s} \\ 0.2094 + \frac{1.3089 - 0.2094}{4}(t - 20) & 20 \text{ s} \leq t < 24 \text{ s} \\ 1.3089 & 24 \text{ s} \leq t < 28 \text{ s} \\ 1.3089 - \frac{1.3089 - 0.8727}{4}(t - 28) & 28 \text{ s} \leq t < 32 \text{ s} \\ 0.8727 & t \geq 32 \text{ s} \end{cases} \quad (2.84)$$

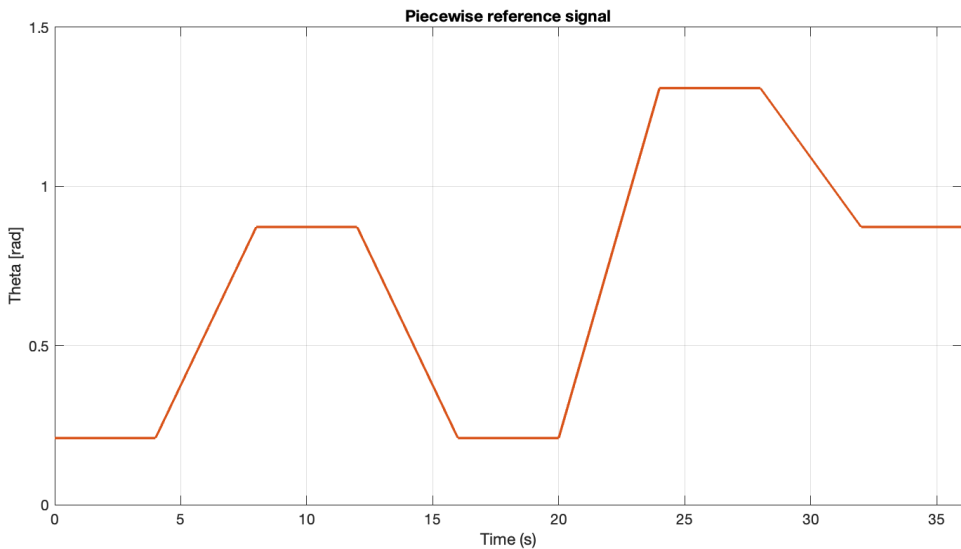


Figure 2.8: Reference signal

Each interval is described as follows:

- Interval $t < 4 \text{ s}$: stabilization at 0.2094 rad .
During this time, the signal is held constant at $r(t) = 0.2094 \text{ rad}$, which corresponds to 12° . This represents the initial stabilization phase of the system.
- Interval $4 \text{ s} \leq t < 8 \text{ s}$: linear transition from 0.2094 rad to 0.8727 rad .
During these 4 seconds, the reference signal increases linearly from

0.2094

rad (12°) to 0.8727 rad (50°). This corresponds to a controlled opening of the throttle.

- Interval $8 \text{ s} \leq t < 12 \text{ s}$: stabilization at 0.8727 rad .

The reference signal is held constant at $r(t) = 0.8727 \text{ rad}$ (50°) for 4 seconds. This represents a new stabilization phase at the larger opening angle.

- Interval $12 \text{ s} \leq t < 16 \text{ s}$: linear transition from 0.8727 rad to 0.2094 rad .

Over this interval, the reference decreases linearly from 0.8727 rad (50°) to 0.2094 rad (12°), representing a controlled closing of the throttle.

- Interval $16 \text{ s} \leq t < 20 \text{ s}$: stabilization at 0.2094 rad .

The reference signal remains constant at $r(t) = 0.2094 \text{ rad}$ (12°) for 4 seconds, entering another stabilization phase.

- Interval $20 \text{ s} \leq t < 24 \text{ s}$: linear transition from 0.2094 rad to 1.3089 rad .

During these 4 seconds, the reference signal increases linearly from 0.2094 rad (12°) to 1.3089 rad (75°), representing a wider throttle opening.

- Interval $24 \text{ s} \leq t < 28 \text{ s}$: stabilization at 1.3089 rad .

The reference signal is held constant at $r(t) = 1.3089 \text{ rad}$ (75°) for 4 seconds, maintaining the wide-open throttle.

- Interval $28 \text{ s} \leq t < 32 \text{ s}$: linear transition from 1.3089 rad to 0.8727 rad .

During this interval, the signal decreases linearly from 1.3089 rad (75°) to 0.8727 rad (50°), representing a partial throttle closing.

- interval $t \geq 32 \text{ s}$: stabilization at 0.8727 rad .

For $t \geq 32 \text{ s}$, the reference signal remains constant at $r(t) = 0.8727 \text{ rad}$ (50°), entering the final stabilization phase.

The reference used can be associated with a very calm urban scenario, characterized by intervals of acceleration, deceleration, and stabilization at certain throttle valve angles, with relatively long durations for each interval, namely 4 seconds. This signal was chosen not so much for its strict adherence to a real-world scenario, but rather because it allows for clear visualization and analysis of every aspect during each step of the control

system development. It provides the ability to examine all possible situations, including constant segments, steep slope changes, steady rises and falls, and varying throttle openings.

This reference signal is subsequently processed using a low-pass filter implemented directly in Simulink.

2.8.4 Signal Definitions and Transformations

In this section, the mathematical definitions and transformations used to process the reference signal $\mathbf{r}(t)$ and its derivatives are presented.

The variable \mathbf{m} is conventionally used to pass the state variables between blocks in the control system. It is defined as:

$$\mathbf{m} = \begin{bmatrix} m_1 \\ m_2 \\ m_3 \end{bmatrix}$$

where:

- m_1 represents the reference \mathbf{r} or its filtered version.
- m_2 is the first derivative of the signal.
- m_3 is the second derivative of the signal.

2.8.5 Filtered Reference Signal and Derivatives

The filtered reference signal and its derivatives are defined as:

- $\mathbf{b}(t) = \mathbf{r}_f(t)$ is the filtered reference signal;
- $\dot{\mathbf{b}}(t) = \frac{d\mathbf{r}_f(t)}{dt}$ is the first derivative;
- $\ddot{\mathbf{b}}(t) = \frac{d^2\mathbf{r}_f(t)}{dt^2}$ is the second derivative;
- $\dddot{\mathbf{b}}(t) = \frac{d^3\mathbf{r}_f(t)}{dt^3}$ is the third derivative.

The derivatives of the filtered signal are computed recursively using this representation of the filtering process:

$$\frac{d\mathbf{m}}{dt} = \mathbf{P}_{BE}\mathbf{m} + \mathbf{P}_{BB}\mathbf{r}$$

where:

$$\mathbf{P}_{BE} = \begin{bmatrix} -\frac{1}{\tau} & \frac{1}{\tau} & 0 \\ 0 & -\alpha & \omega \\ 0 & -\omega & -\alpha \end{bmatrix}$$

$$\mathbf{P}_{BB} = \begin{bmatrix} 0 \\ 0 \\ \frac{\omega_n}{\sqrt{1-\delta^2}} \end{bmatrix}$$

Each component of $\mathbf{b}(t)$ is derived as:

$$\begin{aligned} \mathbf{b}(t) &= \mathbf{r}_f(t) \\ \dot{\mathbf{b}}(t) &= \left[-\frac{1}{\tau} \quad \frac{1}{\tau} \quad 0 \right] \mathbf{m} \\ \ddot{\mathbf{b}}(t) &= \left[-\frac{1}{\tau} \quad \frac{1}{\tau} \quad 0 \right] \mathbf{P}_{BE} \mathbf{m} \\ \dddot{\mathbf{b}}(t) &= \left[-\frac{1}{\tau} \quad \frac{1}{\tau} \quad 0 \right] \mathbf{P}_{BE} (\mathbf{P}_{BE} \mathbf{m} + \mathbf{P}_{BB} \mathbf{r}) \end{aligned}$$

The filtering ensures that $\mathbf{b}(t)$, $\dot{\mathbf{b}}(t)$, $\ddot{\mathbf{b}}(t)$, and $\dddot{\mathbf{b}}(t)$ are smooth and continuous, which is critical for advanced control strategies.

From now on, any mention of $\mathbf{r}(t)$ will refer to the filtered signal $\mathbf{b}(t)$, unless stated otherwise.

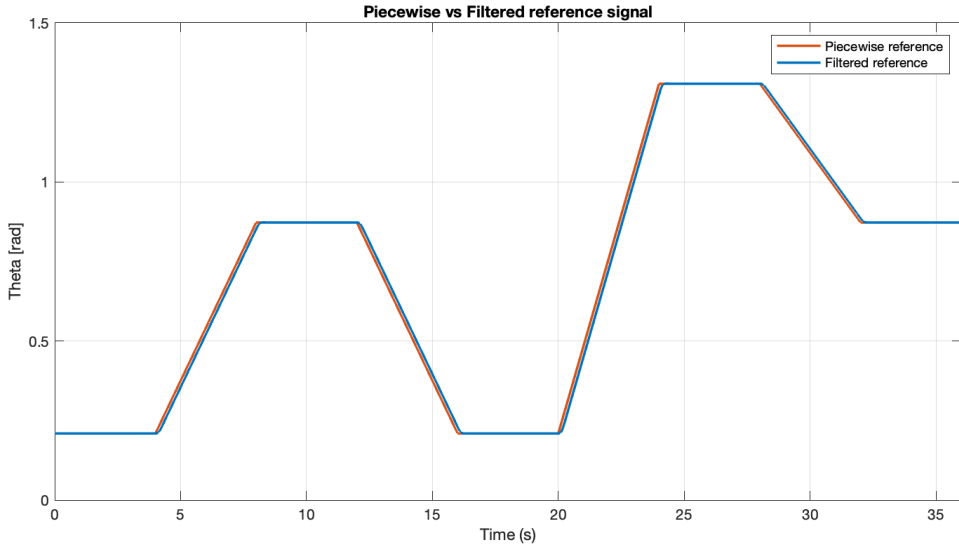


Figure 2.9: Pre and post-filtering reference signal

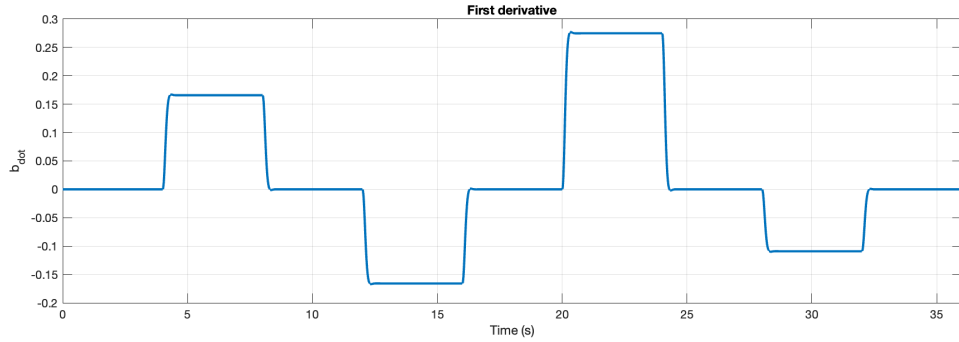


Figure 2.10: First derivative of the reference signal

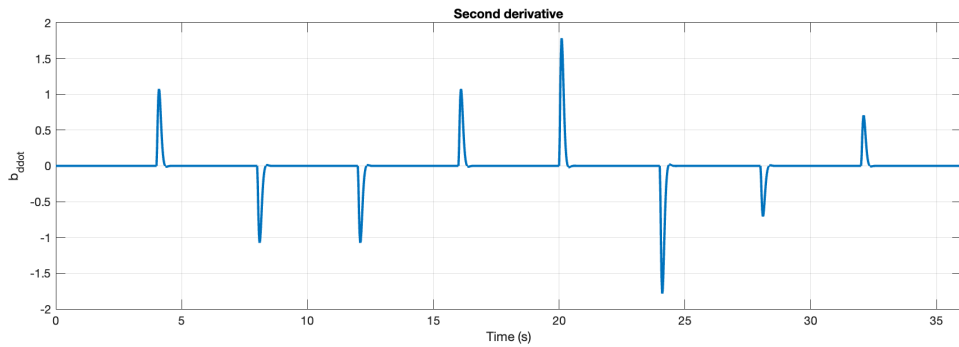


Figure 2.11: Second derivative of the reference signal

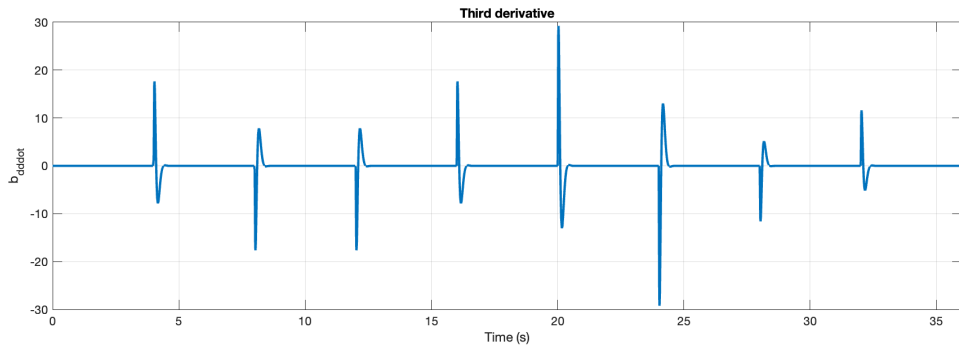


Figure 2.12: Third derivative of the reference signal

The control system development will be presented based on this specific reference until its completion. Subsequently, other signals will be introduced and utilized as references.

Chapter 3

Proposed solutions

3.1 Control Architecture

The system controlling the electric circuit and throttle valve can be represented as a system with inputs, consisting of the control action (such as the voltage applied to the motor) and exogenous elements (including references, sensor noises, and external disturbances)

The outputs are derived from the measurements collected by the sensors and the corresponding error values.

The control architecture for this system is divided into three main components:

- **Observer** processes the sensor measurements \mathbf{y} to provide an estimate of the state \mathbf{y}_o . This estimation is essential, as it supplies the necessary state information for the feedback control action;
- **Feedback Path** generates a control signal \mathbf{u}_{FB} that is proportional to both the state estimate and the integral of the error, utilizing the matrices \mathbf{K}_S and \mathbf{K}_I . This path ensures the system can correct deviations from desired values;
- **Feed-Forward Path** produces a control signal \mathbf{u}_{FF} , which is applied when the reference input or its time derivatives are known and vary over time. The feed-forward path is crucial for improving system response to dynamic reference changes.

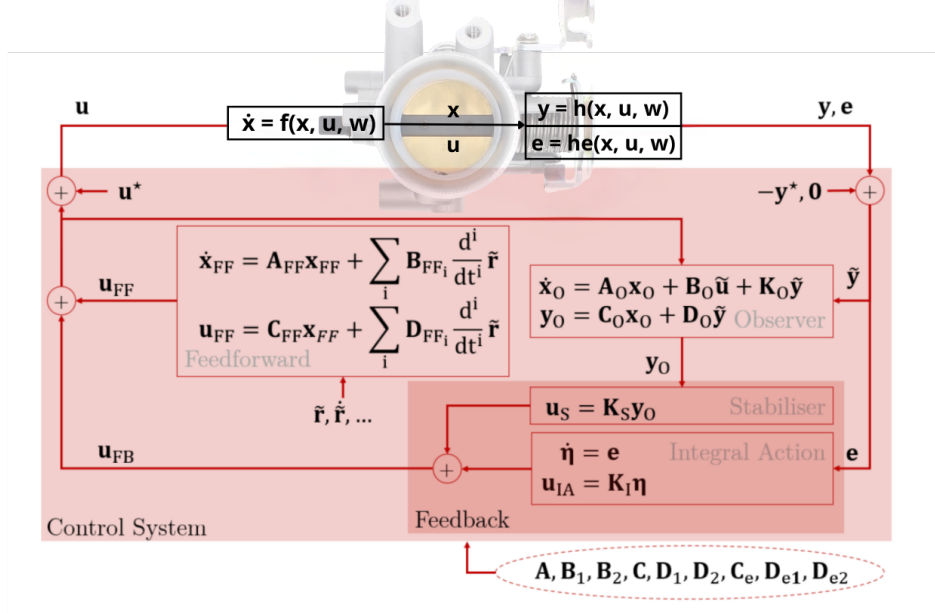


Figure 3.1: Control architecture

3.2 Optimal Control for the Feedback

The matrices \mathbf{K}_S and \mathbf{K}_I are determined by solving an optimal control problem aimed at balancing the minimization of error with the control cost. This approach may allow for a small error to prevent excessive control effort.

We start with the system:

$$\dot{\tilde{x}} = \mathbf{A}\tilde{x} + \mathbf{B}_1\tilde{u}$$

$$\mathbf{e} = \mathbf{C}_e\tilde{x} + \mathbf{D}_{1e}\tilde{u}$$

where the exogenous input \tilde{w} is omitted to simplify the design of a control law.

The dynamics of the extended state \tilde{x}_e are described as:

$$\dot{\tilde{x}}_e = \mathbf{A}_e\tilde{x}_e + \mathbf{B}_{1e}\tilde{u}$$

To identify suitable matrices, we modify the dynamics by introducing a parameter $\alpha \geq 0$, which reduces stability by shifting the eigenvalues of matrix \mathbf{A} , making them less negative. This modification ensures that if the

control law can handle a less stable system, it will be capable of controlling the actual system.

The modified equation is:

$$\dot{\tilde{\mathbf{x}}}_e = \mathbf{A}_e \tilde{\mathbf{x}}_e + \alpha \mathbf{I} \tilde{\mathbf{x}}_e + \mathbf{B}_{1e} \tilde{\mathbf{u}} \quad (3.1)$$

Here, the parameter α moves the eigenvalues closer to the imaginary axis, reducing stability and increasing robustness to uncertainties in the model.

Additionally, a virtual output ε is defined as a linear combination of the extended state \mathbf{x}_e and the control input $\tilde{\mathbf{u}}$.

$$\varepsilon = \mathbf{C}_\varepsilon \tilde{\mathbf{x}}_e + \mathbf{D}_\varepsilon \tilde{\mathbf{u}} \quad (3.2)$$

It is possible to define the matrices \mathbf{C}_ε and \mathbf{D}_ε as an identity matrix and a null one respectively. The reasons behind these choices will be explained further for the sake of clarity.

$$\mathbf{D}_\varepsilon = [0]$$

$$\mathbf{C}_\varepsilon = \begin{bmatrix} 1 & 0 & 0 & 0 \\ 0 & 1 & 0 & 0 \\ 0 & 0 & 1 & 0 \\ 0 & 0 & 0 & 1 \end{bmatrix}$$

3.2.1 Cost Function

The cost function J is defined as:

$$J = \int_0^{+\infty} (\varepsilon^\top \mathbf{Q} \varepsilon + \tilde{\mathbf{u}}^\top \mathbf{R} \tilde{\mathbf{u}}) dt \quad (3.3)$$

where $J > 0$ must be minimized through an optimal control input $\tilde{\mathbf{u}}$ that addresses the control objective.

The matrices \mathbf{Q} is required to be semi-positive definite. Another essential requirement is that the matrix $\bar{\mathbf{R}} = \mathbf{D}_\varepsilon^\top \mathbf{Q} \mathbf{D}_\varepsilon + \mathbf{R}$, which will be utilized later, must be positive definite. Setting $\mathbf{Q} = 0$ implies that the error is not prioritized, while \mathbf{R} represents the penalty on control effort.

To ensure $J > 0$, we select:

$$\mathbf{Q} \in \mathbb{R}^{n_e \times n_e}, \quad \mathbf{R} \in \mathbb{R}^{p \times p}$$

In this case, the matrices are defined as follows:

$$\mathbf{Q} = \frac{1}{n_e} \begin{bmatrix} \frac{1}{(\varepsilon_{1,\max})^2} & 0 & 0 & 0 \\ 0 & \frac{1}{(\varepsilon_{2,\max})^2} & 0 & 0 \\ 0 & 0 & \frac{1}{(\varepsilon_{3,\max})^2} & 0 \\ 0 & 0 & 0 & \frac{1}{(\varepsilon_{4,\max})^2} \end{bmatrix}$$

$$\mathbf{R} = \frac{1}{p} \begin{bmatrix} \frac{1}{(u_{\max})^2} \end{bmatrix}$$

where $\varepsilon_{i,\max}$ represents the maximum permissible error for each state variable \mathbf{x}_i , and the elements of \mathbf{R} regulate the use of control inputs.

The extended state \mathbf{x}_e is represented as:

$$\mathbf{x}_e = \begin{bmatrix} I_a \\ \theta \\ \dot{\theta} \\ \eta \end{bmatrix},$$

with:

- $\varepsilon_{1,\max}$: maximum allowable error in the current passing through the electric circuit I_a [A].
- $\varepsilon_{2,\max}$: maximum allowable error in the valve's angular position θ [rad].
- $\varepsilon_{3,\max}$: maximum allowable error in the valve's angular velocity $\dot{\theta}$ [$\frac{\text{rad}}{\text{s}}$].
- $\varepsilon_{4,\max}$: component related to the integral action [rad].
- u_{\max} : maximum allowable value for the control voltage input u [V].

3.2.2 Solution of the Optimal Control Problem

After analyzing the structure and meaning of the matrices, the optimal control problem must be solved. The previous analysis focuses on minimizing cost, so to ensure system stability and determine the most appropriate control $\tilde{\mathbf{u}}$, the following assumptions are verified:

- $(\mathbf{A}_e, \mathbf{C}_\varepsilon)$ is detectable;
- $(\mathbf{A}_e, \mathbf{B}_{1e})$ is stabilisable;
- $\tilde{\mathbf{u}}^\top \mathbf{R} \tilde{\mathbf{u}} > 0$;

- $\boldsymbol{\varepsilon}^\top \mathbf{Q} \boldsymbol{\varepsilon} \geq 0$ (with \mathbf{Q} semi-positive definite).

Recalling previous equations, the system is:

$$\begin{cases} \dot{\tilde{\mathbf{x}}}_e = \mathbf{A}_e \tilde{\mathbf{x}}_e + \alpha \mathbf{I} \tilde{\mathbf{x}}_e + \mathbf{B}_{1e} \tilde{\mathbf{u}} \\ \boldsymbol{\varepsilon} = \mathbf{C}_\varepsilon \tilde{\mathbf{x}}_e + \mathbf{D}_\varepsilon \tilde{\mathbf{u}} \\ J = \int_0^{+\infty} (\boldsymbol{\varepsilon}^\top \mathbf{Q} \boldsymbol{\varepsilon} + \tilde{\mathbf{u}}^\top \mathbf{R} \tilde{\mathbf{u}}) dt \end{cases}$$

The objective is to find \mathbf{u} that minimizes J and ensures closed-loop stability.

To proceed, we introduce the Hamiltonian function:

$$H(\tilde{\mathbf{x}}_e, \tilde{\mathbf{u}}, \boldsymbol{\lambda}) = \boldsymbol{\varepsilon}^\top \mathbf{Q} \boldsymbol{\varepsilon} + \tilde{\mathbf{u}}^\top \mathbf{R} \tilde{\mathbf{u}} + \boldsymbol{\lambda}^\top ((\mathbf{A}_e + \alpha \mathbf{I}) \tilde{\mathbf{x}}_e + \alpha \mathbf{B}_{1e} \tilde{\mathbf{u}}) \quad (3.4)$$

where $\boldsymbol{\lambda} \in \mathbb{R}^n$ is the co-state vector. For an optimal solution \mathbf{u}^* , the following necessary (but not sufficient) conditions must be met:

1.

$$\frac{d\boldsymbol{\lambda}}{dt} = - \left[\frac{\partial H}{\partial \mathbf{x}} \right]^\top$$

2.

$$\frac{\partial H}{\partial \tilde{\mathbf{u}}} \Big|_{\mathbf{u}=\mathbf{u}^*} = 0$$

From this second condition and using equation 3.2, it is possible to derive:

$$\mathbf{u}^* = -\frac{1}{2} \bar{\mathbf{R}}^{-1} (\mathbf{B}_{1e}^\top \boldsymbol{\lambda} + 2 \mathbf{D}_\varepsilon^\top \mathbf{Q} \mathbf{C}_\varepsilon) \tilde{\mathbf{x}}_e \quad (3.5)$$

where:

$$\bar{\mathbf{R}} = \mathbf{D}_\varepsilon^\top \mathbf{Q} \mathbf{D}_\varepsilon + \mathbf{R} \quad (3.6)$$

Defining $\boldsymbol{\lambda} = 2\mathbf{S}\tilde{\mathbf{x}}_e$, where \mathbf{S} is the stabilizing solution, one obtains:

$$\tilde{\mathbf{u}} = -\bar{\mathbf{R}}^{-1} (\mathbf{B}_{1e}^\top \mathbf{S} + \mathbf{D}_\varepsilon^\top \mathbf{Q} \mathbf{C}_\varepsilon) \tilde{\mathbf{x}}_e = \mathbf{K} \tilde{\mathbf{x}}_e = [\mathbf{K}_S \quad \mathbf{K}_I] \tilde{\mathbf{x}}_e$$

Through this procedure the structure of the matrix \mathbf{K} is shaped.

Setting $\dot{\mathbf{S}} = 0$ and using the first necessary condition, the algebraic Riccati equation (ARE) can be written:

$$\begin{aligned} \mathbf{S} \mathbf{B}_{1e} \bar{\mathbf{R}}^{-1} \mathbf{B}_{1e}^\top \mathbf{S} - \mathbf{S} (\mathbf{A}_e + \alpha \mathbf{I} - \mathbf{B}_{1e} \bar{\mathbf{R}}^{-1} \mathbf{D}_\varepsilon^\top \mathbf{Q} \mathbf{C}_\varepsilon) - (\mathbf{A}_e + \alpha \mathbf{I} + \\ - \mathbf{B}_{1e} \bar{\mathbf{R}}^{-1} \mathbf{D}_\varepsilon^\top \mathbf{Q} \mathbf{C}_\varepsilon)^\top \mathbf{S} - \mathbf{C}_\varepsilon^\top \mathbf{Q} (\mathbf{I} - \mathbf{D}_\varepsilon \bar{\mathbf{R}}^{-1} \mathbf{D}_\varepsilon^\top \mathbf{Q}) \mathbf{C}_\varepsilon = 0 \end{aligned} \quad (3.7)$$

The algebraic Riccati equation can be solved using the ‘icare’ function in Matlab, which outputs:

$$(\mathbf{X}_m, \mathbf{K}_m, \mathbf{L}_m) = \text{icare}(\mathbf{A}_m, \mathbf{B}_m, \mathbf{Q}_m, \mathbf{R}_m, \mathbf{S}_m, \mathbf{E}_m, \mathbf{G}_m) \quad (3.8)$$

where:

- $\mathbf{X}_m = \mathbf{S}$;
- $\mathbf{K}_m = -\mathbf{K} = -[\mathbf{K}_S \quad \mathbf{K}_I]$;
- \mathbf{L}_m ;
- $\mathbf{A}_m = \mathbf{A}_e + \alpha \mathbf{I}$;
- $\mathbf{B}_m = \mathbf{B}_{1e}$;
- $\mathbf{Q}_m = \mathbf{C}_\varepsilon^T \mathbf{Q} \mathbf{C}_\varepsilon$;
- $\mathbf{R}_m = \bar{\mathbf{R}}$;
- $\mathbf{S}_m = -\mathbf{C}_\varepsilon^T \mathbf{Q} \mathbf{D}_\varepsilon$;
- $\mathbf{E}_m = \mathbf{I}$;
- $\mathbf{G}_m = 0$

where the eigenvalues of the closed-loop system are listed in \mathbf{L}_m .

The subscript “m” refers to matrices used in Matlab.

```
>> RankStab=rank(ctrb(Ae,B1e));
if RankStab == length(Ae)
    disp('Stabilisability of (Ae,B1e) is verified')
else
    disp('Stabilisability of (Ae,B1e) is not verified')
end
Stabilisability of (Ae,B1e) is verified
>> RankStab=rank(obsv(Ae,Ceps));
if RankStab == length(Ae)
    disp('Detectability of (Ae,Ceps) is verified')
else
    disp('Detectability of (Ae,Ceps) is not verified')
end
Detectability of (Ae,Ceps) is verified
```

Since these two conditions are satisfied, the ‘icare’ function in Matlab will provide a valid solution, defining the stabilizing feedback gain matrix

required for optimal control. The ‘icare’ function will not provide a solution if the two necessary hypotheses are not satisfied. Specifically, the selected dimension of ϵ must ensure the detectability of $(\mathbf{A}_e, \mathbf{C}_\epsilon)$ and the stabilizability of $(\mathbf{A}_e, \mathbf{B}_{1e})$. In our case, both conditions have been thoroughly verified. The system design ensures that $(\mathbf{A}_e, \mathbf{C}_\epsilon)$ is detectable, meaning that all unstable modes of the system are observable through the output. Additionally, $(\mathbf{A}_e, \mathbf{B}_{1e})$ is stabilizable, guaranteeing that all unstable modes of the system can be controlled through the input.

```

alpha = 5;

Ceps = eye(4);
Deps = zeros(length(Ae),1);

n_e=length(Ae);
Q = (1/n_e)*diag([eps1max^(-2),eps2max^(-2),eps3max^(-2),eps4max^(-2)]);

p=1;
Rs = (1/p)*mu_max^-2;

Am = Ae+alpha*eye(length(Ae));
Bm = B1e;
Qm = (Ceps')*Q*Ceps;
barR = Rs + (Deps')*Q*Deps;
Rm = barR;
Em = eye(length(Ae));
Gm = 0;
Sm = (Deps'*Q*Ceps)';
[S,Km,L] = icare(Am,Bm,Qm,Rm,Sm,Em,Gm);

```

Here, \mathbf{C}_ϵ is set to the identity matrix, while \mathbf{D}_ϵ is zero, ensuring observability of $(\mathbf{A}_e, \mathbf{C}_\epsilon)$ and simplifying the tuning of the matrices \mathbf{Q} and \mathbf{R} .

By setting $\mathbf{D}_\epsilon = 0$, the virtual output ϵ becomes independent of $\tilde{\mathbf{u}}$, thereby minimizing the control’s influence on the virtual output.

The matrix $\bar{\mathbf{R}} = \mathbf{D}_\epsilon^\top \mathbf{Q} \mathbf{D}_\epsilon + \mathbf{R}$ reflects control costs. With $\mathbf{D}_\epsilon = 0$, the contribution of \mathbf{Q} to $\bar{\mathbf{R}}$ is eliminated, effectively reducing the associated costs. Conversely, if $\mathbf{D}_\epsilon \neq 0$, \mathbf{Q} would increase $\bar{\mathbf{R}}$, resulting in higher control costs. Thus, $\mathbf{D}_\epsilon = 0$ is chosen to maintain efficiency and simplicity.

3.2.3 Tuning of \mathbf{K}_S and \mathbf{K}_I

The design of matrices \mathbf{K}_S and \mathbf{K}_I requires a proper tuning of the matrices \mathbf{Q} and \mathbf{R} , so the right values must be assigned to $\epsilon_{i,\max}$ and u_{\max} . The balance between these parameters is crucial, as the ratio between \mathbf{Q} and \mathbf{R}

directly affects system performance.

3.2.4 Selection of Q and R

The values of $\varepsilon_{i,\max}$ are defined to account for different aspects of the vehicle's dynamics:

- $\varepsilon_{1,\max}$ represents the maximum allowable error in the current passing through the electric circuit I_a . For this system, an acceptable error is calculated as 5% of the nominal current. This level is generally precise enough to keep the valve close to the target position, ensuring proper regulation of airflow.

$$\begin{aligned} V_{DC} &= 12 \text{ V} \\ I_{\text{nom}} &= \frac{V_{DC} K_d}{R_a} = 18 \text{ A} \\ \varepsilon_{1,\max} &= 0.05 \cdot I_{\text{nom}} = 0.9 \text{ A} \end{aligned} \quad (3.9)$$

- $\varepsilon_{2,\max}$ is the maximum allowable error in the valve's angular position θ . An angular error of approximately 0.05 radians can be considered acceptable for a throttle valve. This represents a deviation that is regarded as reasonably small and that does not significantly affect the quality of the air-fuel mixture.

$$\varepsilon_{2,\max} = 0.05 \text{ rad} \quad (3.10)$$

- $\varepsilon_{3,\max}$: maximum allowable error in the valve's angular velocity $\dot{\theta}$. A value of $0.1 \frac{\text{rad}}{\text{s}}$ is considered an ideal compromise for most automotive applications, ensuring good responsiveness and stability.

$$\varepsilon_{3,\max} = 0.1 \frac{\text{rad}}{\text{s}} \quad (3.11)$$

- $\varepsilon_{4,\max}$: component related to the integral action. An acceptable value could be 0.02 radians, allowing the error to be reduced with precision.

$$\varepsilon_{4,\max} = 0.02 \text{ rad} \quad (3.12)$$

The choice of **R** depends on the desired configuration.

For this specific application the choice of the u_{\max} , the maximum allowable value for the control voltage input, fell on $u_{\max} = 12 \text{ V}$.

$$\mathbf{Q} = \begin{bmatrix} 0.3086 & 0 & 0 & 0 \\ 0 & 100 & 0 & 0 \\ 0 & 0 & 25 & 0 \\ 0 & 0 & 0 & 625 \end{bmatrix} \quad (3.13)$$

$$\mathbf{R} = [0.0069] \quad (3.14)$$

The overall tuning process of \mathbf{Q} and \mathbf{R} is designed to balance control accuracy and cost while maintaining robust performance in all vehicle configurations. This careful selection ensures accurate airflow regulation, minimizes angular position error and guarantees excellent responsiveness and stability.

Following the choice of this configuration, the matrices \mathbf{K}_S and \mathbf{K}_I are derived and reported below.

$$\mathbf{K}_S = [-6.0554 \quad -2.9124 \times 10^3 \quad -254.6160] \quad (3.15)$$

$$\mathbf{K}_I = [-1.1015 \times 10^4] \quad (3.16)$$

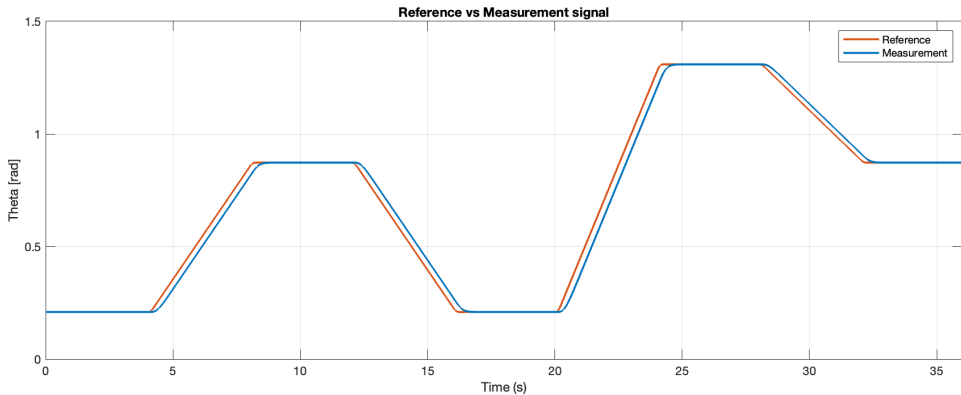


Figure 3.2: Reference vs Measurement signal with feedback

The contribution provided by \mathbf{K}_S and \mathbf{K}_I alone is not enough to accurately follow the reference signal, especially when rapid changes occur. This behavior is highlighted in figure 3.2, where the actual throttle angular position has some delay with respect to the desired one.

For completeness, also the other plant quantities are represented in order to provide a clear initial understanding of how these are correlated among them.

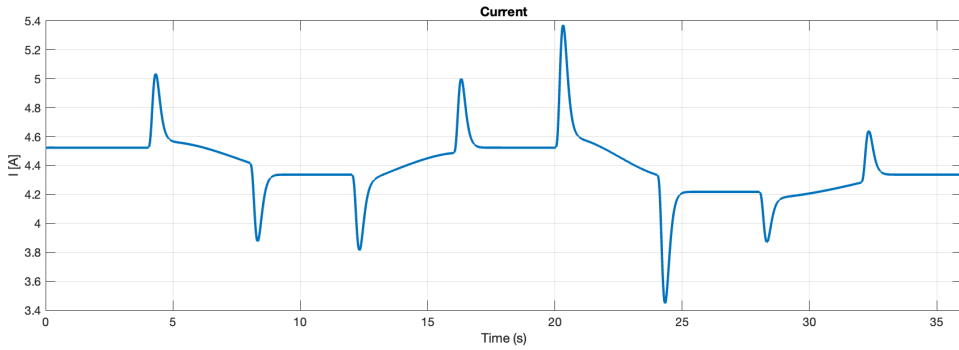


Figure 3.3: Current signal with feedback

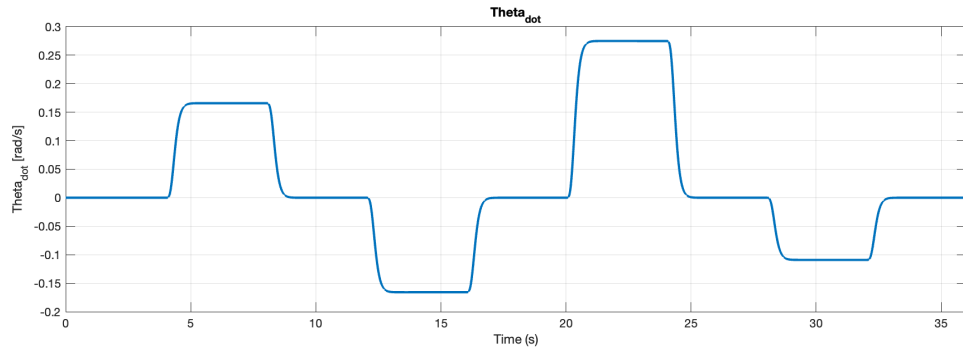


Figure 3.4: $\dot{\theta}$ signal with feedback

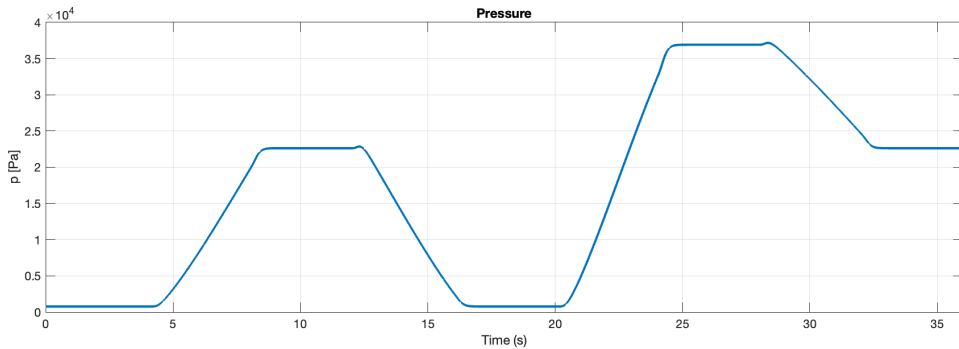


Figure 3.5: Pressure signals with feedback

In addition to what has been shown so far, the input voltage signal used as control, along with the corresponding error between the measurement and

the reference, is also provided. By doing this, a more complete overview can be obtained.

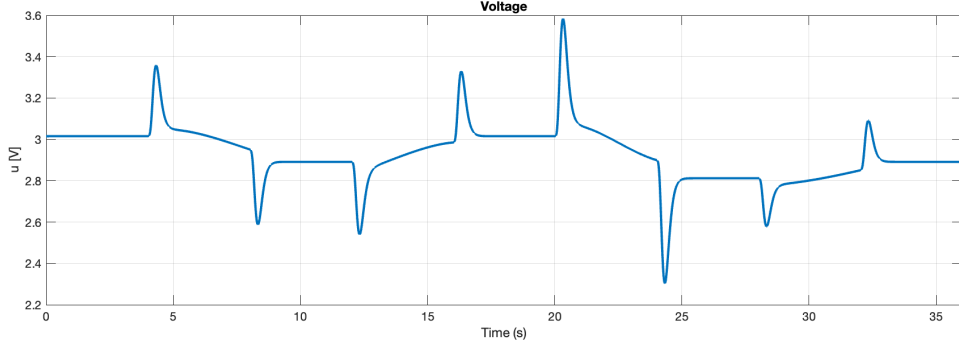


Figure 3.6: Control signal with feedback

This allows the close correlation between voltage and current to be clearly observed at the graphical level.

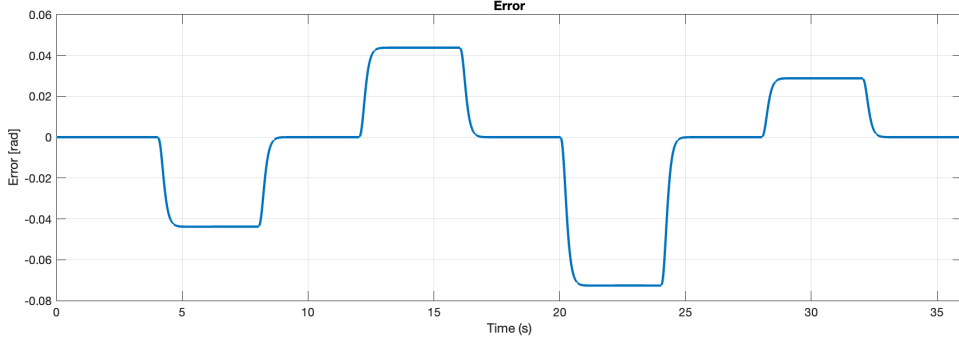


Figure 3.7: Error signal with feedback

Furthermore, it is shown that the maximum error peak corresponds to just under -0.08 rad , which is approximately -4.58° , and that, in general, the error is nonzero during transients following changes in the reference slope. This further supports the implementation of a feed-forward control strategy, as it highlights the need for the control system to provide a greater impulse to better track variations in the desired signal.

3.3 Observer

To implement the control law $\tilde{\mathbf{u}} = \mathbf{K}_S \tilde{\mathbf{x}}$, the state $\tilde{\mathbf{x}}$ must be estimated since it is not directly measurable. Therefore, an observer system capable of estimating the state using sensor measurements is required.

The plant is equipped with one sensor, the MA600, a magnetic rotary position sensor with a high-resolution encoder used to measure the angular position θ .

Given that the pair (\mathbf{A}, \mathbf{C}) is fully observable, it is possible to define an observer gain matrix \mathbf{K}_O such that $\mathbf{A} - \mathbf{K}_O \mathbf{C}$ is Hurwitz, ensuring stability of the observer.

3.3.1 Observer Dynamics

The computed observer gain \mathbf{K}_O is implemented in the observer system as and its dynamics are then described as:

$$\dot{\hat{\mathbf{x}}} = \mathbf{A}\hat{\mathbf{x}} + \mathbf{B}_1\mathbf{u} + \mathbf{B}_2\hat{\mathbf{w}} - \mathbf{K}_o\mathbf{e}_y; \quad (3.17)$$

The estimated output and the estimation error can instead be computed in the following way:

$$\hat{\mathbf{y}} = \mathbf{C}\hat{\mathbf{x}} + \mathbf{D}_1\mathbf{u} + \mathbf{D}_2\hat{\mathbf{w}}; \quad (3.18)$$

$$\mathbf{e}_y = \hat{\mathbf{y}} - \mathbf{y}; \quad (3.19)$$

This ensures that the state $\tilde{\mathbf{x}}$ is accurately estimated and provided to the control system. This statement will be visually validated in the following sections, by plotting the difference between the evolutions of each state obtained with and without the observer.

3.3.2 Dual System

To compute the observer gain \mathbf{K}_O , a dual system is introduced:

$$\begin{aligned} \dot{\chi} &= \mathbf{A}^\top \chi + \mathbf{C}^\top \nu \\ \mu &= \mathbf{B}_2^\top \chi + \mathbf{D}_2^\top \nu \end{aligned}$$

where the dual variables belong to the same spaces as the original system but are not directly related.

$$\begin{aligned}\boldsymbol{\chi} &\in \mathbb{R}^n \\ \boldsymbol{\nu} &\in \mathbb{R}^q \\ \boldsymbol{\mu} &\in \mathbb{R}^r\end{aligned}$$

The system represents the dual system associated with the primary one. The primary and dual systems are two equivalent representations of the same mathematical model, and, therefore, any property possessed by the primary system can be translated into an equivalent property of its dual.

The Optimal Control approach applied to the primary system to obtain the matrices \mathbf{K}_S and \mathbf{K}_I can also be applied to the dual system to derive the matrix \mathbf{K}_{sd} , such that $(\mathbf{A}^\top + \mathbf{C}^\top \mathbf{K}_{sd})$ is Hurwitz.

Three important properties relate the primary system and its dual:

- if the primary system is fully reachable, then the dual system is fully observable, and vice versa;
- if the primary system is fully observable, then the dual system is fully reachable, and vice versa;
- if the primary system is BIBO stable, then the dual system is also BIBO stable, and vice versa.

Since the primary system is fully observable, there exists \mathbf{K}_O such that the state estimator error:

$$\hat{\mathbf{e}}_x = \hat{\mathbf{x}} - \mathbf{x}$$

This estimation error is governed by the dynamics:

$$\dot{\hat{\mathbf{e}}}_x = (\mathbf{A} - \mathbf{K}_O \mathbf{C}) \hat{\mathbf{e}}_x$$

whose dual system is:

$$\dot{\epsilon} = (\mathbf{A}^\top - \mathbf{C}^\top \mathbf{K}_O^\top) \epsilon$$

Now, since the dual system is fully reachable, there exists a matrix \mathbf{K}_{sd} such that:

$$\boldsymbol{\nu} = \mathbf{K}_{sd} \boldsymbol{\chi}$$

leading to:

$$\dot{\boldsymbol{\chi}} = (\mathbf{A}^\top + \mathbf{C}^\top \mathbf{K}_{sd}) \boldsymbol{\chi}$$

The matrices $(\mathbf{A}^\top - \mathbf{C}^\top \mathbf{K}_O^\top)$ and $(\mathbf{A}^\top + \mathbf{C}^\top \mathbf{K}_{sd})$ are equal if:

$$\mathbf{K}_O = -\mathbf{K}_{sd}^\top. \quad (3.20)$$

Consequently, the solution \mathbf{K}_O of the observability problem for the primary system will be the solution of the Optimal Control problem for the dual system, and is given by equation (3.20), shown right before.

3.3.3 Optimal Control for the Observer

As previously mentioned, the observability problem for the primary system can be solved using the optimal control approach applied to the dual system. This results in the observer gain matrix \mathbf{K}_O , computed as:

$$\mathbf{K}_O = -\mathbf{K}_{sd}^\top$$

where \mathbf{K}_{sd} is derived through the ARE applied to the dual system:

$$\begin{cases} \dot{\chi} = (\mathbf{A}^\top + \alpha_d \mathbf{I})\chi + \mathbf{C}^\top \boldsymbol{\nu} \\ \boldsymbol{\mu} = \mathbf{B}_2^\top \chi + \mathbf{D}_2^\top \boldsymbol{\nu} \\ J = \int_0^\infty (\boldsymbol{\mu}^\top \mathbf{Q}_d \boldsymbol{\mu} + \boldsymbol{\nu}^\top \mathbf{R}_d \boldsymbol{\nu}) dt \end{cases}$$

The matrices that enter the ARE are written as:

$$\mathbf{A}_d = \mathbf{A}^\top, \quad \mathbf{B}_d = \mathbf{C}^\top, \quad \mathbf{C}_d = \mathbf{B}_2^\top, \quad \mathbf{D}_d = \mathbf{D}_2^\top$$

The ARE is solved using the ‘icare’ function in Matlab, which minimizes the cost function J .

$$(\mathbf{X}_{md}, \mathbf{K}_{md}, \mathbf{L}_{md}) = \text{icare}(\mathbf{A}_{md}, \mathbf{B}_{md}, \mathbf{Q}_{md}, \mathbf{R}_{md}, \mathbf{S}_{md}, \mathbf{E}_{md}, \mathbf{G}_{md})$$

where:

- $\mathbf{A}_{md} = \mathbf{A}^\top + \alpha_d \mathbf{I}$
- $\mathbf{B}_{md} = \mathbf{C}^\top$
- $\mathbf{Q}_{md} = \mathbf{C}_d^\top \mathbf{Q}_d \mathbf{C}_d$
- $\mathbf{R}_{md} = \bar{\mathbf{R}}_d = \mathbf{R}_d + \mathbf{D}_d^\top \mathbf{Q}_d \mathbf{D}_d$
- $\mathbf{S}_{md} = \mathbf{S} = \mathbf{C}_d^\top \mathbf{Q}_d \mathbf{D}_d$
- $\mathbf{E}_{md} = \mathbf{I}$

- $\mathbf{G}_{md} = 0$
- $\mathbf{K}_{md} = -\mathbf{K}_{sd}$

Following these steps, the solution of the optimization problem gives:

$$\mathbf{K}_{sd} = -\bar{\mathbf{R}}_d^{-1}(\mathbf{C}_d^\top \mathbf{Q}_d \mathbf{D}_d + \mathbf{B}_d^\top \mathbf{S}).$$

Generally, matrices \mathbf{Q}_d and \mathbf{R}_d are defined as follows:

$$\mathbf{Q}_d = \begin{bmatrix} Q_{d11} & Q_{d12} & Q_{d13} \\ Q_{d12}^\top & Q_{d22} & Q_{d23} \\ Q_{d13}^\top & Q_{d23}^\top & Q_{d33} \end{bmatrix}$$

then we have:

$$\begin{aligned} \bar{\mathbf{R}}_d &= Q_{d22} + \mathbf{R}_d, \\ \mathbf{D}_2 \mathbf{Q}_d \mathbf{B}_2^\top &= Q_{d12}^\top \mathbf{B}_{21}^\top, \\ \mathbf{B}_2 \mathbf{Q}_d \mathbf{B}_2^\top &= \mathbf{B}_{21} Q_{d11} \mathbf{B}_{21}^\top. \end{aligned}$$

The gain \mathbf{K}_{sd} represents a balance between the reliability of the model and the reliability of the measurements. \mathbf{K}_{sd} is directly proportional to \mathbf{S} , which in turn depends on Q_{d11} , a term representing the uncertainties associated to the equations, and to $(Q_{d22} + \mathbf{R}_d)^{-1}$, which instead is related to the covariance of noise.

Larger values of Q_{d11} or smaller values of $(Q_{d22} + \mathbf{R}_d)^{-1}$ indicate that the model is less reliable compared to the measurements, and vice versa. The designer can adjust the magnitudes of Q_{d11} and $Q_{d22} + \mathbf{R}_d$ to achieve the desired balance between utilizing the model and relying on the measurements.

In this system, matrices \mathbf{Q}_d and \mathbf{R}_d are the following:

$$\begin{aligned} \mathbf{Q}_d &= \begin{bmatrix} 0 & 0 & 0 \\ 0 & q_{22}^2 & 0 \\ 0 & 0 & 0 \end{bmatrix} \\ \mathbf{R}_d &= [\text{std}_{\text{sensor}}^2] \end{aligned}$$

The matrix \mathbf{R}_d is fixed once the most suitable sensor for the plant is selected, as it contains the standard deviation of the sensor's measurement error. In contrast, the values of \mathbf{Q}_d and the parameter α_d can be adjusted to optimize the observer \mathbf{K}_O . Due to the fact that \mathbf{B}_2 is null, according to the terms involved in the Riccati equation, the only relevant element is q_{22} , the noise covariance, set to 1 in this specific case considering the reliability of our sensor.

3.3.4 Tuning of \mathbf{Q}_d and \mathbf{R}_d

Based on the previous discussion, the design of \mathbf{K}_O can only be adjusted through two tuning parameters: α_d and \mathbf{Q}_d , as \mathbf{R}_d is fixed. In our system, since the matrix \mathbf{B}_2 is null due to the fact that our disturbances are embedded in the state, we are not able to define, through the matrix \mathbf{Q}_d , a level of uncertainty of the equations. This means that the output of the optimal control problem results in null \mathbf{K}_O . Through this process, we are assessing that our model is perfectly reliable, and an identity observer is sufficient for the estimation of the state. Clearly, due to the mathematical constraints of the approach, we are ignoring the approximation introduced by linearisation and the effect of disturbances on the system.

In order to solve the problem, two possible approaches could be exploited:

- Introduction of a dummy matrix $\bar{\mathbf{Q}}$ in \mathbf{Q}_{md} , which takes into account the missing knowledge related to the model.
- Modification of the dynamics in the Jordan form of the system by using different parameters α_d for each eigenvalue, being able to act precisely on the less stable portion of the system.

The first tuning is performed ignoring the presence of noise and focusing only on minimizing the estimation error, in order to be afraid about the effect on \mathbf{K}_O by the different design parameters.

Without any additional parameter and with $\alpha_d = 0$, the \mathbf{K}_O values are zero. This approach essentially assumes that there are no corrections made to the model state estimation.

In the following case, α_d is set to an integer number, specifically it is set to 5. This is the most basic form of tuning and leads to the following \mathbf{K}_O values:

$$\mathbf{K}_O = \begin{bmatrix} -4.7100 \\ 19.6060 \\ 94.1683 \end{bmatrix}$$

The corresponding estimation error is shown in figure 3.8.

At this point, a more accurate tuning is done by directly working with the canonical form of the system using different parameters for each eigenvalue. Particularly, the values of α_d are set in order to move the eigenvalues associated with the angular position and the angular velocity, which are less stable than the one associated to the current.

$$\boldsymbol{\alpha}_d = \begin{bmatrix} 0 & 0 & 0 \\ 0 & 30 & 0 \\ 0 & 0 & 30 \end{bmatrix}$$

$$\mathbf{A}_{mo} = \mathbf{A}_d + \mathbf{V}\boldsymbol{\alpha}_d\mathbf{V}^{-1}$$

These operations led to the following \mathbf{K}_O values:

$$\mathbf{K}_O = \begin{bmatrix} -0.1783 \times 10^3 \\ 0.1196 \times 10^3 \\ 3.5646 \times 10^3 \end{bmatrix}$$

The corresponding estimation error is shown in figure 3.9.

Alongside $\boldsymbol{\alpha}_d$, with the introduction of the dummy matrix $\bar{\mathbf{Q}}$, the system is further tuned by defining this extra matrix and by including it in the tuning process.

$$\bar{\mathbf{Q}} = \begin{bmatrix} 0 & 0 & 0 \\ 0 & 2000 & 0 \\ 0 & 0 & 2000 \end{bmatrix}$$

$$\mathbf{Q}_{mo} = \mathbf{C}_d^\top \mathbf{Q}_d \mathbf{C}_d + \bar{\mathbf{Q}}$$

The results are in the following \mathbf{K}_O values:

$$\mathbf{K}_O = \begin{bmatrix} -0.2494 \times 10^3 \\ 0.1435 \times 10^3 \\ 4.9866 \times 10^3 \end{bmatrix}$$

The corresponding estimation error is shown in figure 3.10.

It is important to visualize that, the introduction of $\bar{\mathbf{Q}}$ enables finer adjustments to the coefficient \mathbf{K}_O , being able to have high accuracy in parameters selection. Conversely, by changing the dynamics of the system through $\boldsymbol{\alpha}_d$, even a small perturbation of the eigenvalues position generates a significant effect on the values of \mathbf{K}_O .

Clearly, what has been seen up to now is valid under the condition of zero noise. This assumption allows us to focus solely on minimizing the estimation error, which leads to the selection of high \mathbf{K}_O values without considering the potential impact of noise. However, extremely high values of \mathbf{K}_O could result in the propagation of errors during the estimation process. Therefore, as the control system development progresses and noise is introduced, a new tuning process will be carried out, and updated \mathbf{K}_O values will be determined taking also the noise effects into account.

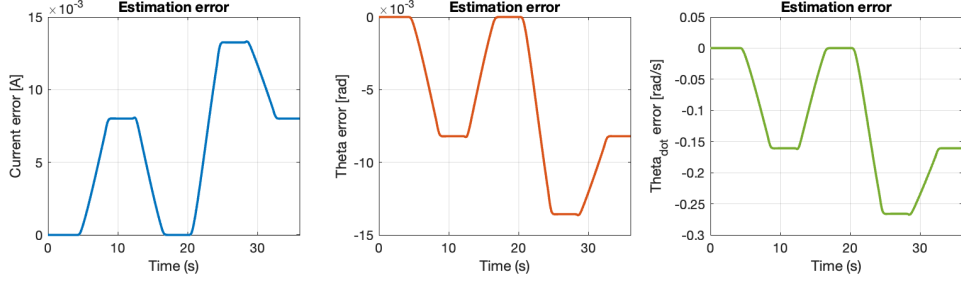


Figure 3.8: Estimation error with $\alpha_d = 5$

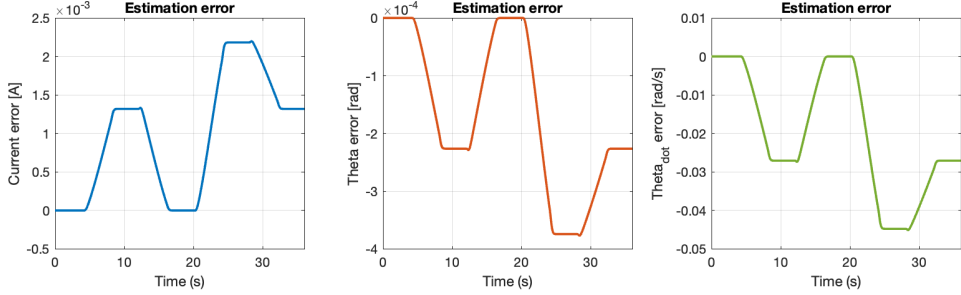


Figure 3.9: Estimation error with α_d

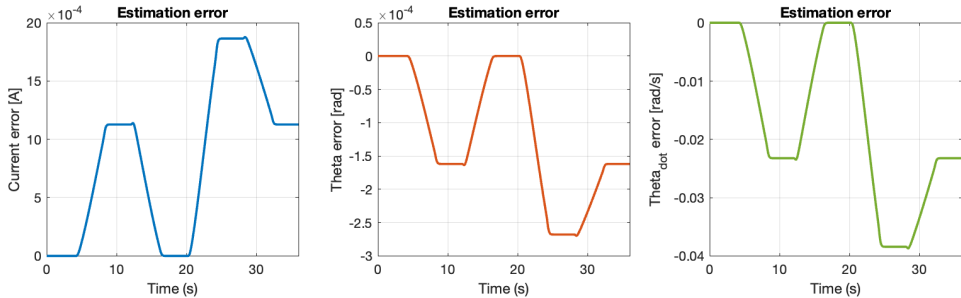


Figure 3.10: Estimation error with α_d and \bar{Q}

As stated, the observer accurately estimates \tilde{x} . Indeed, from the plots included in figure 3.10, it can be observed that the order of magnitude of the estimation error ranges from $10^{-2} \frac{\text{rad}}{\text{s}}$ for angular velocity to 10^{-4} rad for angular position. The estimation error for the current is of the order of 10^{-3} A .

As can be seen, the model is not capable of estimating \tilde{x} such that the estimation error reaches zero after convergence. However, since the observer

implementation does not account for exogenous, a constant estimation bias is expected when $\tilde{w} \neq 0$. Furthermore, in the non-linear plant, this bias can also arise due to the non-linearities and the model mismatch between the linear and non-linear cases.

3.4 Noise

During the measurements, the noise ν has a significant impact that cannot be neglected. The output given by the sensor is $y = \theta + \nu$, where ν represents the noise. From the sensor datasheet, the value of ν was retrieved. In Simulink, this was implemented using a zero-mean block that generates a value within the range $[-\nu, \nu]$ at each time step.

The presence of the noise has some implications on the tuning of the K_O values. Alongside the objective of minimising the estimation error, now it is important to consider also the possible noise propagation due to improperly high coefficients. Furthermore, an additional tuning must be performed in order to get K_O values that allow for a trade-off between the reliability of the linearized model and the reliability of sensor measurements, which inherently include some level of noise. This approach, however, comes at the cost of slightly reduced accuracy and slower convergence toward the desired goals.

From the sensor datasheet it is possible to derive the measurement noise. It is implemented in simulink through a band-limited white noise.

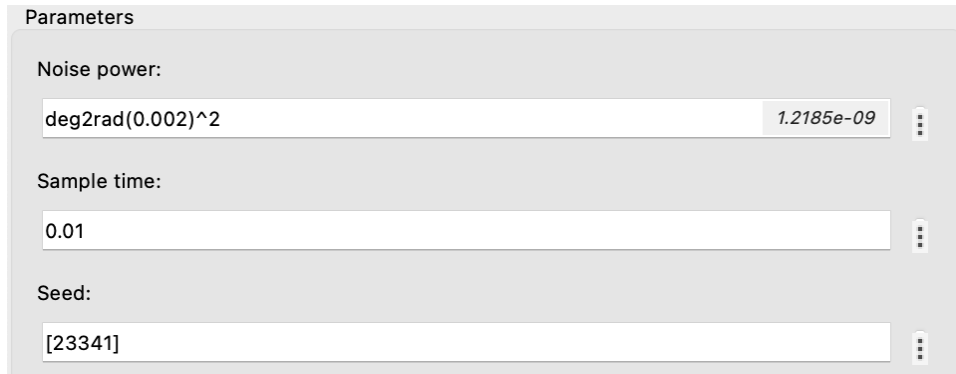


Figure 3.11: Tuning window of the band-limited white noise block

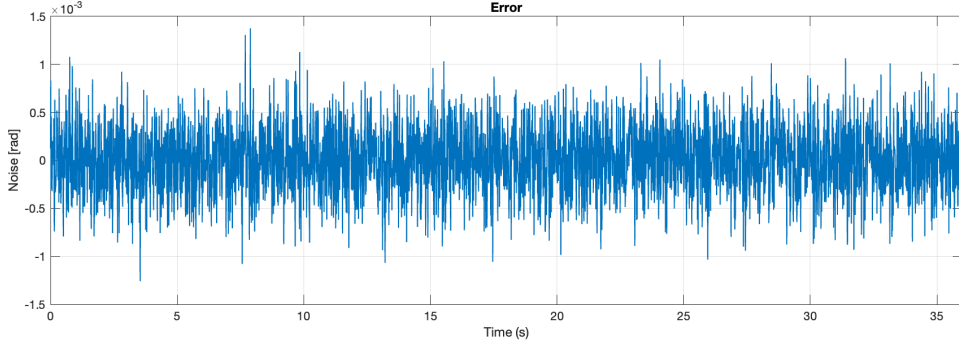


Figure 3.12: Noise signal

The output of the new tuning process is:

$$\mathbf{K}_O = \begin{bmatrix} -33.7193 \\ 52.1339 \\ 674.2308 \end{bmatrix}$$

This result is obtained combining both the previously mentioned methods: a dummy matrix is introduced and the dynamics in the Jordan form are changed using different coefficients for the eigenvalues.

$$\bar{\mathbf{Q}} = \begin{bmatrix} 0 & 0 & 0 \\ 0 & 14 & 0 \\ 0 & 0 & 14 \end{bmatrix}$$

$$\boldsymbol{\alpha}_d = \begin{bmatrix} 0 & 0 & 0 \\ 0 & 13 & 0 \\ 0 & 0 & 13 \end{bmatrix}$$

The need of limiting the error propagation led to significantly lower values than before at the cost of increasing a bit the estimation error. Furthermore, in order to avoid too high back propagation of noise through the feedback path, an additional tuning of the parameters \mathbf{K}_S and \mathbf{K}_I is required.

In particular, these values are significantly reduced with respect to the previous tuning by setting the parameter $\alpha = 0.1$.

Moreover, in order to steer the error to zero also the maximum allowable error associated to the integral action is reduced, imposing a value of $\varepsilon_{4,\max}$ equal to 0.007 rad .

The updated matrix \mathbf{Q} becomes:

$$\mathbf{Q} = \begin{bmatrix} 0.3086 & 0 & 0 & 0 \\ 0 & 100 & 0 & 0 \\ 0 & 0 & 25 & 0 \\ 0 & 0 & 0 & 5120 \end{bmatrix} \quad (3.21)$$

and the updated \mathbf{K}_S and \mathbf{K}_I :

$$\mathbf{K}_S = [-6.0410 \quad -4.4247 \times 10^2 \quad -1.0022 \times 10^2]$$

$$\mathbf{K}_I = [-9.0118 \times 10^2]$$

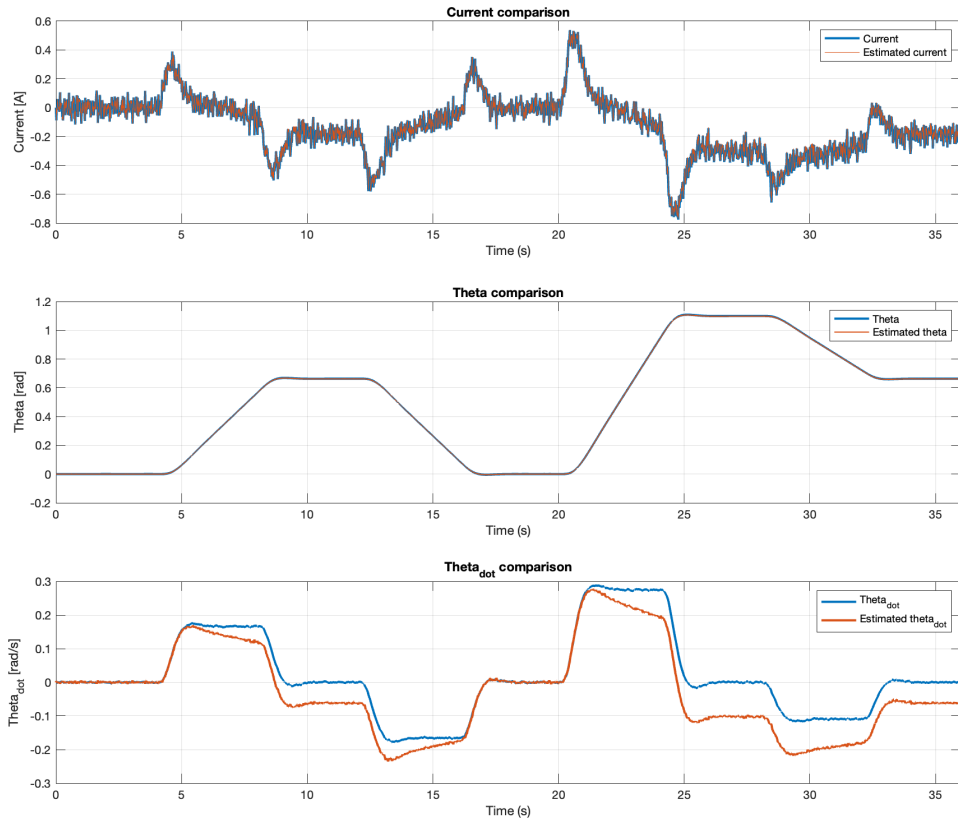


Figure 3.13: States vs Estimated states comparison

Figure 3.13 illustrates that, although the estimation error values are noticeably larger than before, they remain within an acceptable range.

For completeness all the other quantities are reported below.

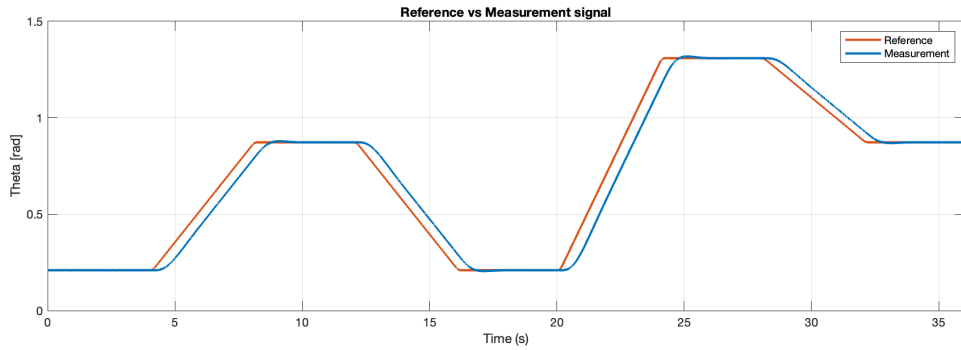


Figure 3.14: Reference vs Measurement with noise

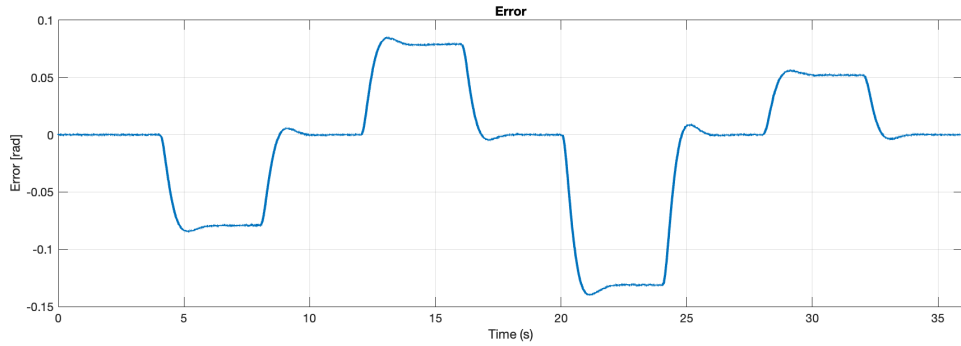


Figure 3.15: Error signal with noise

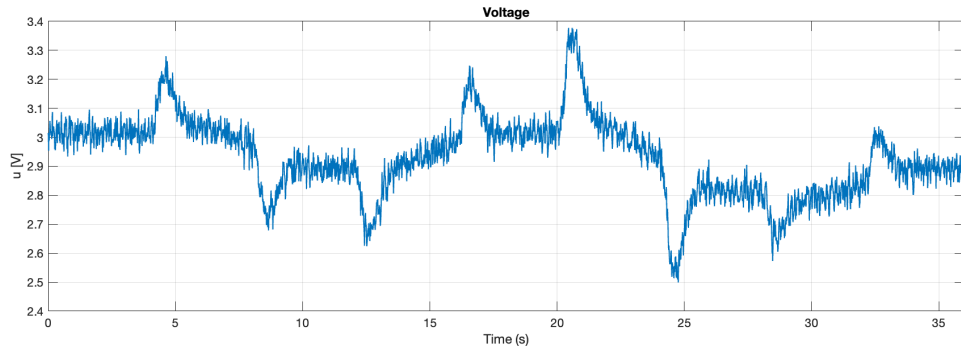


Figure 3.16: Control signal with noise

Specifically from the error in figure 3.15, the voltage in figure 3.16 and the current in figure 3.17, one can get a first idea of how the noise introduced

from the sensor propagates and affects other variables.

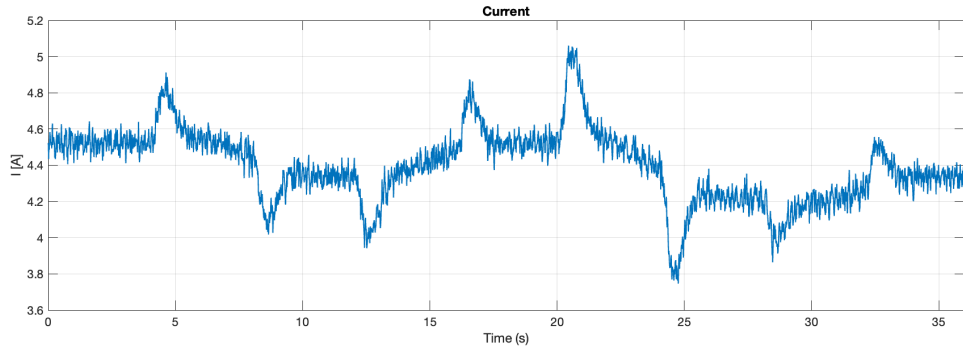


Figure 3.17: Current signal with noise

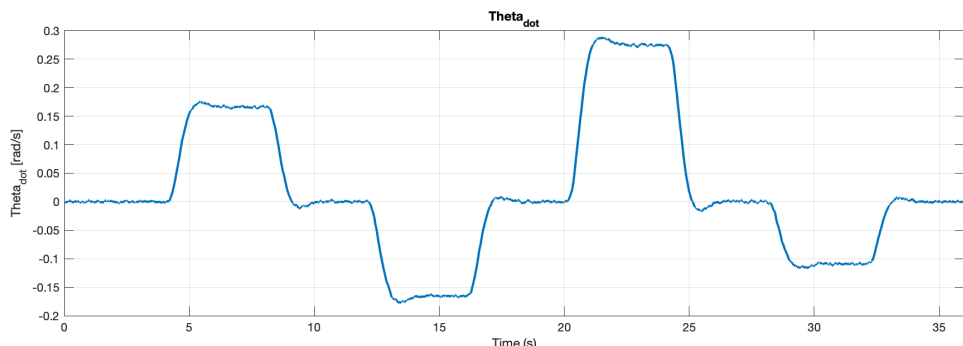


Figure 3.18: $\dot{\theta}$ signal with noise

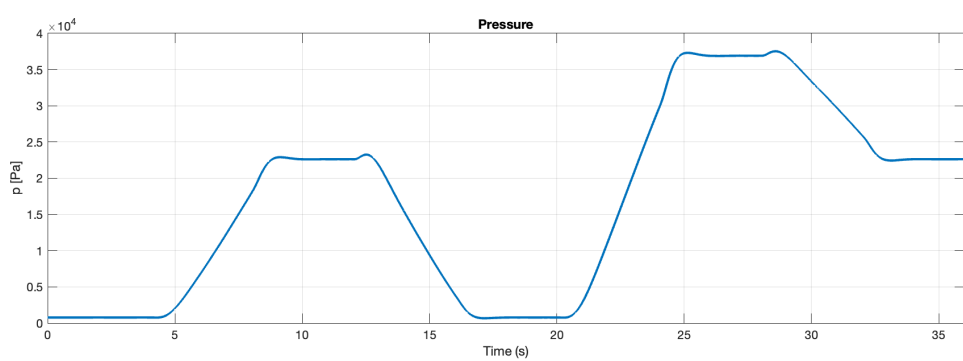


Figure 3.19: Pressure signal with noise

3.5 Linear Feed-Forward Control

The stabilizer and integral action have been introduced to provide stability, robustness, and ensure the system is BIBS stable. Additionally, the observer has been implemented to provide state knowledge of the system. However, in order to enhance performance, a feed-forward action is required.

This is a crucial tool in automatic control systems when managing tracking references that change over time.

The goal of feed-forward is to design a control law that ensures the error tends to zero asymptotically:

$$\lim_{t \rightarrow \infty} \mathbf{e}(t) = 0.$$

A critical feature is its reliance on references rather than real-time measurements from sensors. This approach allows the system to anticipate variations in the reference, independent of the current state. As a result, feed-forward can reduce the gains of the \mathbf{K} matrices of the feedback control system. In an ideal scenario, feedback would not be required if feed-forward control worked perfectly. However, in real-world applications, feedback is still necessary to compensate for modeling errors or unexpected disturbances.

The inclusion of this control part places the system in a more "favorable" condition, enabling precise reference tracking and requiring only minor adjustments from the stabilizer to handle residual errors.

3.5.1 System Dynamics

The original system equations for state dynamics and error are defined as:

$$\begin{aligned}\dot{\tilde{\mathbf{x}}} &= \mathbf{A}\tilde{\mathbf{x}} + \mathbf{B}_1\tilde{\mathbf{u}} + \mathbf{B}_2\tilde{\mathbf{w}}, \\ \tilde{\mathbf{e}} &= \mathbf{C}_e\tilde{\mathbf{x}} + \mathbf{D}_{1e}\tilde{\mathbf{u}} + \mathbf{D}_{2e}\tilde{\mathbf{w}}.\end{aligned}$$

Recalling that both \mathbf{D}_{1e} and \mathbf{B}_2 are null matrices and defining the new matrix $\mathbf{D}'_{2e} = \mathbf{D}_{2e}(3) = [-1]$, the system can be rewritten as:

$$\begin{aligned}\dot{\tilde{\mathbf{x}}} &= \mathbf{A}\tilde{\mathbf{x}} + \mathbf{B}_1\tilde{\mathbf{u}}, \\ \tilde{\mathbf{e}} &= \mathbf{C}_e\tilde{\mathbf{x}} + \mathbf{D}'_{2e}\tilde{\mathbf{w}} = \mathbf{C}_e\tilde{\mathbf{x}} - \tilde{\mathbf{r}}.\end{aligned}$$

Differentiating the error, the first derivative is:

$$\dot{\tilde{\mathbf{e}}} = \mathbf{C}_e\dot{\tilde{\mathbf{x}}} - \dot{\tilde{\mathbf{r}}}$$

Substituting $\dot{\tilde{\mathbf{x}}} = \mathbf{A}\tilde{\mathbf{x}} + \mathbf{B}_1\tilde{\mathbf{u}}$, the equation becomes:

$$\dot{\tilde{\mathbf{e}}} = \mathbf{C}_e \mathbf{A} \tilde{\mathbf{x}} + \mathbf{C}_e \mathbf{B}_1 \tilde{\mathbf{u}} - \dot{\tilde{\mathbf{r}}}$$

Higher-order derivatives of $\tilde{\mathbf{e}}$ are calculated to evaluate the relative degree of the system. The k -th derivative is expressed as:

$$\frac{d^k \tilde{\mathbf{e}}}{dt^k} = \mathbf{C}_e \mathbf{A}^{k-1} \mathbf{B}_1$$

Moreover r_{\max} is defined as:

$$r_{\max} \in \mathbb{N} \mid \mathbf{C}_e \mathbf{A}^{r_{\max}-1} \mathbf{B}_1 \neq 0$$

To determine the relative degree, successive powers of \mathbf{A} must be computed and the terms $\mathbf{C}_e \mathbf{A}^{k-1} \mathbf{B}_1$ must be evaluated.

The process continues until $\mathbf{C}_e \mathbf{A}^{k-1} \mathbf{B}_1 \neq 0$. The value of r_{\max} corresponds to the smallest k satisfying this condition.

If $r_{\max} = n$, where n is the dimension of the state $\tilde{\mathbf{x}}$, the system has a vector relative degree. This ensures that the system dynamics can be effectively controlled using feed-forward control, leveraging the properties of the transformed coordinates.

$$\mathbf{C}_e \mathbf{A}^0 \mathbf{B}_1 = \mathbf{C}_e \mathbf{B}_1 = [0 \ 1 \ 0] \begin{bmatrix} 1764.7 \\ 0 \\ 0 \end{bmatrix} = 0$$

$$\mathbf{C}_e \mathbf{A} \mathbf{B}_1 = [0 \ 1 \ 0] \begin{bmatrix} -1176.5 & 0 & -58.8235 \\ 0 & 0 & 1 \\ 0.9091 & -0.9697 & -0.1515 \end{bmatrix} \begin{bmatrix} 1764.7 \\ 0 \\ 0 \end{bmatrix} = 0$$

$$\mathbf{C}_e \mathbf{A}^2 \mathbf{B}_1 = [0 \ 1 \ 0] \begin{bmatrix} -1176.5 & 0 & -58.8235 \\ 0 & 0 & 1 \\ 0.9091 & -0.9697 & -0.1515 \end{bmatrix}^2 \begin{bmatrix} 1764.7 \\ 0 \\ 0 \end{bmatrix} = 1604.3$$

3.5.2 Change of Coordinates

Given that $r_{\max} = n$, the condition holds, so the transformation matrix \mathbf{T} is defined as:

$$\mathbf{T} = \begin{bmatrix} \mathbf{C}_e \\ \mathbf{C}_e \mathbf{A} \\ \mathbf{C}_e \mathbf{A}^2 \end{bmatrix}$$

$$\mathbf{T} = \begin{bmatrix} 0 & 1 & 0 \\ 0 & 0 & 1 \\ 0.9091 & -0.9697 & -0.1515 \end{bmatrix}$$

By defining a new state ζ such that $\zeta = \mathbf{T}\tilde{\mathbf{x}}$ and $\tilde{\mathbf{x}} = \mathbf{T}^{-1}\zeta$, the system can be expressed as:

$$\begin{cases} \dot{\zeta} = \mathbf{A}_\zeta \zeta + \mathbf{B}_{1\zeta} \tilde{\mathbf{u}} \\ \tilde{\mathbf{e}} = \mathbf{C}_{e\zeta} \zeta + \mathbf{D}_{2e} \tilde{\mathbf{w}} \end{cases}$$

where $\mathbf{A}_\zeta = \mathbf{T}\mathbf{A}\mathbf{T}^{-1}$, $\mathbf{B}_{1\zeta} = \mathbf{T}\mathbf{B}_1$ and $\mathbf{C}_{e\zeta} = \mathbf{C}_e\mathbf{T}^{-1}$ are the transformed system matrices and depend on the chosen coordinates.

$$\begin{aligned} \mathbf{A}_\zeta &= \begin{bmatrix} 0 & 1 & 0 \\ 0 & 0 & 1 \\ -1.1408 \times 10^3 & -232.6988 & -1.1766 \times 10^3 \end{bmatrix} \\ \mathbf{B}_\zeta &= \begin{bmatrix} 0 \\ 0 \\ 1604.3 \end{bmatrix} \\ \mathbf{C}_{e\zeta} &= [1 \ 0 \ 0] \end{aligned}$$

At this point, assuming $\mathbf{e}(0) = 0$, it is possible to design a control action that keeps the error equal to zero forever. To find that control law named \mathbf{u}_{FF1} , the procedure is the following:

$$\tilde{\mathbf{e}} = \mathbf{C}_{e\zeta} \zeta - \tilde{\mathbf{r}} = \zeta(1) - \tilde{\mathbf{r}} = 0$$

$$\zeta_{1r} = \tilde{\mathbf{r}}$$

The symbol ζ_{1r} denotes the first component of the reference state in the new coordinates. The first derivative of the error is equal to:

$$\begin{aligned} \dot{\tilde{\mathbf{e}}} &= \mathbf{C}_{e\zeta} \dot{\zeta} - \dot{\tilde{\mathbf{r}}} = \mathbf{C}_{e\zeta} (\mathbf{A}_\zeta \zeta + \mathbf{B}_{1\zeta} \tilde{\mathbf{u}}) - \dot{\tilde{\mathbf{r}}} = \zeta(2) - \dot{\tilde{\mathbf{r}}} = 0 \\ \zeta_{2r} &= \dot{\tilde{\mathbf{r}}} \end{aligned}$$

where ζ_{2r} denotes the second component of the reference state in the new coordinates.

The second derivative of the error is equal to:

$$\begin{aligned} \ddot{\tilde{\mathbf{e}}} &= \mathbf{C}_{e\zeta} \ddot{\zeta} - \ddot{\tilde{\mathbf{r}}} = \mathbf{C}_{e\zeta} (\mathbf{A}_\zeta^2 \zeta + \mathbf{A}_\zeta \mathbf{B}_{1\zeta} \tilde{\mathbf{u}}) - \ddot{\tilde{\mathbf{r}}} = \zeta(3) - \ddot{\tilde{\mathbf{r}}} = 0 \\ \zeta_{3r} &= \ddot{\tilde{\mathbf{r}}} \end{aligned}$$

where ζ_{3r} denotes the third component of the reference state in the new coordinates.

After this computation, the reference state ζ_r in the new coordinates is retrieved. Specifically, that vector contains the reference $\tilde{\mathbf{r}}$ and its derivatives up to the $(n - 1)$ -th order.

$$\zeta_r = \begin{bmatrix} \zeta_{1r} \\ \zeta_{2r} \\ \zeta_{3r} \end{bmatrix} = \begin{bmatrix} \tilde{\mathbf{r}} \\ \dot{\tilde{\mathbf{r}}} \\ \ddot{\tilde{\mathbf{r}}} \end{bmatrix}$$

It is clear that, to ensure the control system effectively tracks the desired reference, it is necessary to define a reference signal $\tilde{\mathbf{r}}$ that is sufficiently continuous, allowing it to be differentiated three times. This continuity guarantees that the control input $\tilde{\mathbf{u}}$, derived from $\tilde{\mathbf{r}}$, will also be continuous, without discontinuities, which would not be implementable in a real application.

By this point, the first component of the feed-forward action can be written as:

$$\tilde{\mathbf{u}}_{FF1} = \mathbf{b}_3^{-1} \left[\frac{d^3 \tilde{\mathbf{r}}}{dt^3} - [a_{31} \ a_{32} \ a_{33}] \zeta_r \right]$$

where a_{31} , a_{32} and a_{33} are the three elements of the last row of the matrix \mathbf{A}_ζ , and b_3 is the last element of the vector $\mathbf{B}_{1\zeta}$.

The feed-forward control is not complete as it stands, because a second part must be added to cope with situations in which the initial state does not correspond to reference conditions.

This part, named $\tilde{\mathbf{u}}_{FF2}$, is equal to:

$$\tilde{\mathbf{u}}_{FF2} = -\mathbf{K}_S \tilde{\mathbf{x}}_r = -\mathbf{K}_S \mathbf{T}^{-1} \zeta_r$$

The overall feed-forward control action results in:

$$\tilde{\mathbf{u}}_{FF} = \tilde{\mathbf{u}}_{FF1} + \tilde{\mathbf{u}}_{FF2} = \mathbf{b}_3^{-1} \left[\frac{d^3 \tilde{\mathbf{r}}}{dt^3} - [a_{31} \ a_{32} \ a_{33}] \zeta_r \right] - \mathbf{K}_S \mathbf{T}^{-1} \zeta_r$$

The overall control action, including the feedback and feed-forward parts, is equal to:

$$\tilde{\mathbf{u}} = \tilde{\mathbf{u}}_{FF} + \tilde{\mathbf{u}}_{FB} = \mathbf{b}_3^{-1} \left[\frac{d^3 \tilde{\mathbf{r}}}{dt^3} - [a_{31} \ a_{32} \ a_{33}] \tilde{\zeta}_r \right] + \mathbf{K}_S (\tilde{\mathbf{x}} - \tilde{\mathbf{x}}_r) + \mathbf{K}_I \boldsymbol{\eta}$$

where the feedback control is composed of the stabilizer action $\mathbf{K}_S \tilde{\mathbf{x}}$ and the integral action $\mathbf{K}_I \boldsymbol{\eta}$.

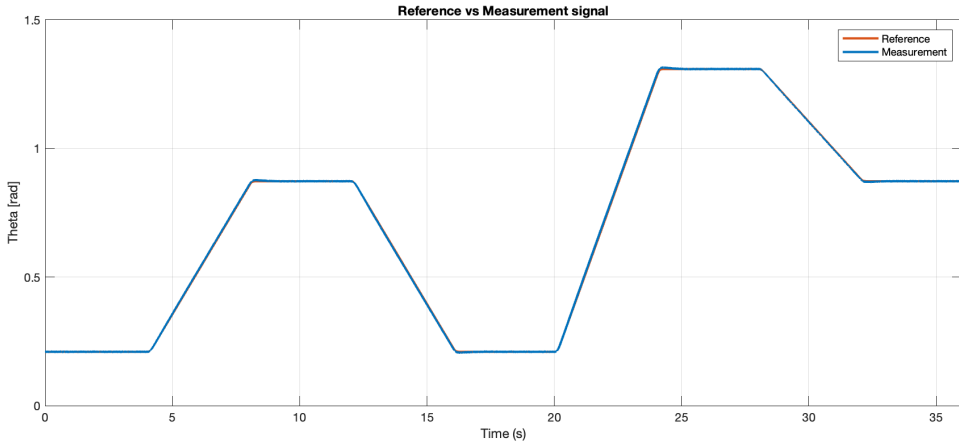


Figure 3.20: Reference vs Measurement signal with feed-forward

To better illustrate that the noise is considered in this simulation, the segment of the plot between 24 and 28 seconds is magnified.

The irregular trace of the blue signal in figure 3.21 clearly highlights this phenomenon.

Obviously, this specific segment was chosen as an example; however, the noisy behavior is characteristic of the entire signal.

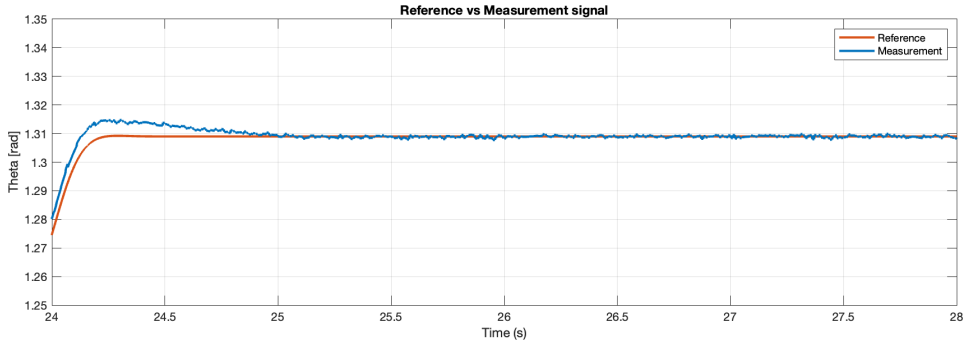


Figure 3.21: Zoom-in

With the implementation of the feed-forward, the throttle valve control achieves greater responsiveness, which is evident both now with the actual reference and later with the introduction of more complex signals to follow.

As before, all relevant plots of noteworthy signals are presented below, one by one.

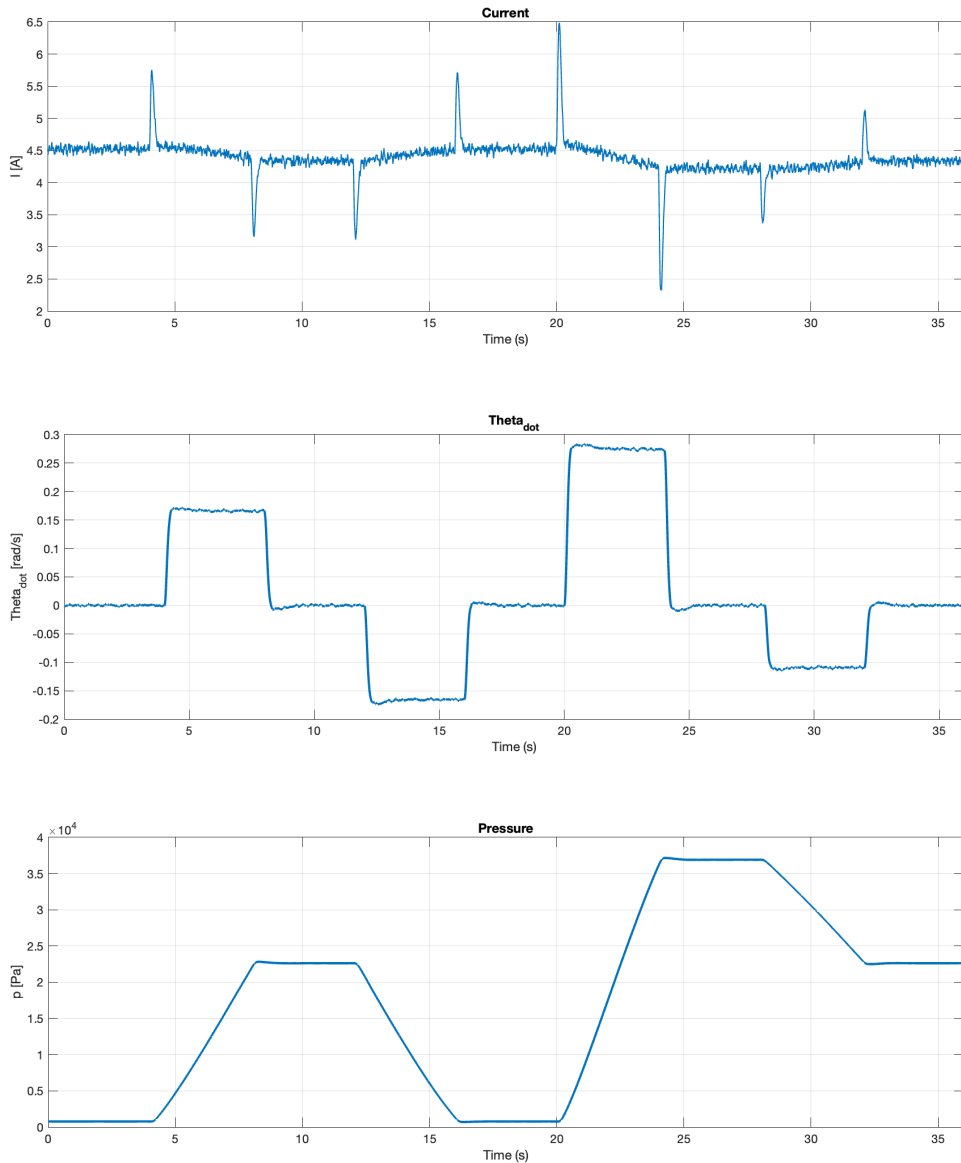


Figure 3.22: Current, $\dot{\theta}$ and pressure signals with feed-forward

It is important to comment on the control action, which now provides greater contribution peaks than before, ensuring that the throttle angle tracks the desired reference with such accuracy that the two signals in figure 3.20 appear almost perfectly overlapped.

This is particularly evident in the higher voltage peaks, which result in a current sufficient to generate the torque required to closely follow the reference during transitions and variations. These peaks occur at critical moments where the reference slope changes, ensuring the system maintains its accuracy and responsiveness.

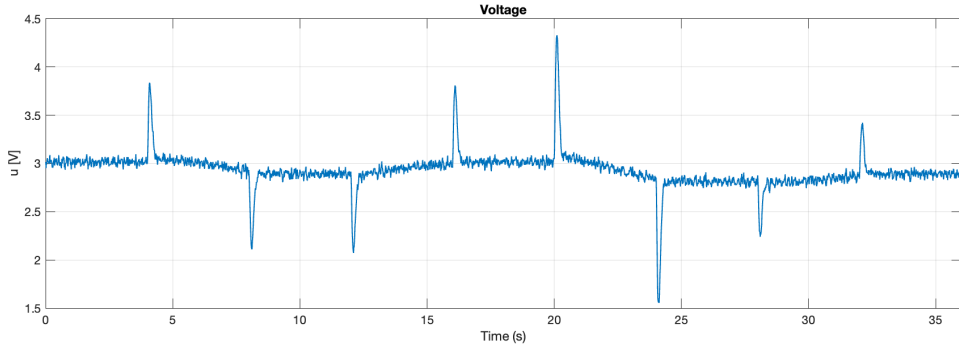


Figure 3.23: Control signal with feed-forward

Consequently, the error remains close to zero across almost the entire operating range, with an order of magnitude of 10^{-2} rad, significantly improving the performance achievable solely with feedback control.

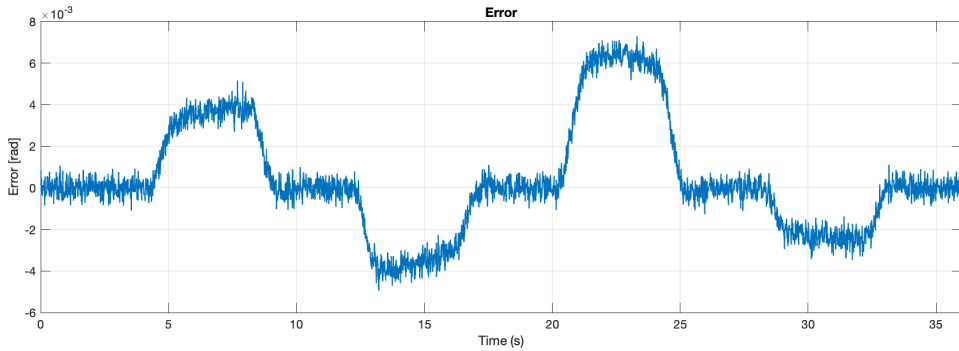


Figure 3.24: Error signal with feed-forward

This highlights the essential role of feed-forward in addressing the limitations of feedback alone, particularly during dynamic phases where higher precision and faster response are required.

These results have been achieved using the state estimated by the observer. In this context, it is also essential to present the estimation error to further validate the conclusions drawn so far regarding the feed-forward.

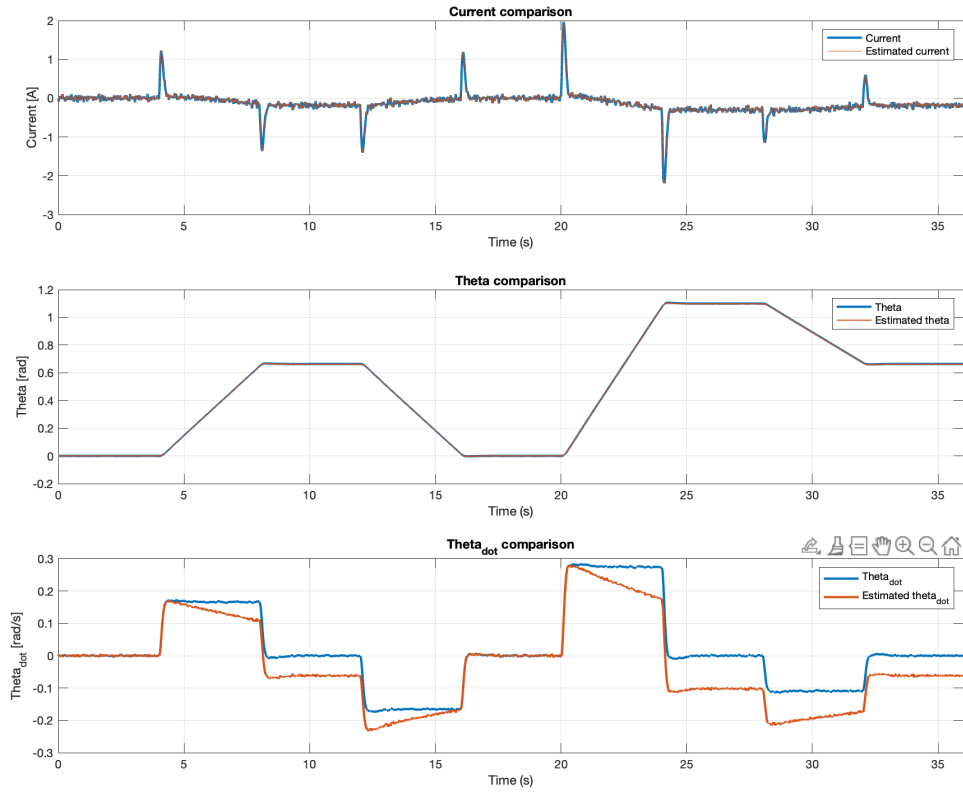


Figure 3.25: States vs Estimated states with feed-forward

It is worth noting that in figure 3.25, for each state, the 2 signals used for the comparison are almost completely overlapped, implying that the error values are small, confirming the effectiveness of the observer in accurately estimating the state.

Chapter 4

Case studies

4.1 References

As discussed in one of the previous sections, various reference signals are required to evaluate whether the control system functions effectively.

While the signal used so far exhibited relatively simple characteristics and dynamics that were easy to track, the system will now be subjected to more challenging signals that increasingly reflect the potential operating conditions of a vehicle on the road in real-world scenarios.

The signals used so far have been relatively simple, with straightforward dynamics that allowed the valve to operate under manageable conditions. However, the system will now be exposed to more challenging signals. For example, the duration of each segment in the piecewise functions will be reduced, requiring the valve to reach specific openings in a shorter time frame. Additionally, during constant segments, the valve will have less time to stabilize following potential overshoots caused by the sharp dynamics of transients.

A subsequent level of difficulty can involve increasing the differences between the initial and final angles of each segment, resulting in steeper and more demanding transients, while simultaneously further reducing the duration of each step. This would better simulate the instantaneous and "demanding" variations typically required by a driver in real-world conditions.

As another potential complication, the nature of the ascending and descending segments could be altered. Instead of linear transitions, non-linear profiles, such as exponential curves, could be introduced. This approach would more closely resemble the signal generated by the accelerator pedal

pressed by a driver, adding a layer of realism and complexity to the system's operation.

Another step can be taken by introducing multiple transients consecutively, effectively eliminating any potential constant segments that serve to stabilize the system.

Additionally, a signal can be analyzed that aims to cover the widest possible range of angles, allowing the control system's stability to be evaluated across the full operational range of the valve. This approach ensures that the system is tested under diverse conditions, verifying its ability to maintain stability and performance throughout its entire range of action.

In the end, after addressing each step individually, all these dynamics and characteristics that progressively complicate the signal will be combined into a single reference. This unified reference will fully simulate the potential evolution of the throttle valve opening in a realistic urban driving scenario.

Moreover, other cases, less complex but equally representative of common real-world situations, will also be developed and analyzed.

4.2 Fast Transitions

Compared to the initial reference, the time intervals have been reduced from 4 seconds to 2 seconds, increasing the system's response demands.

$$r(t) = \begin{cases} 0.2094 & t < 4\text{ s} \\ 0.2094 + \frac{0.8727 - 0.2094}{2}(t - 4) & 4\text{ s} \leq t < 6\text{ s} \\ 0.8727 & 6\text{ s} \leq t < 8\text{ s} \\ 0.8727 - \frac{0.8727 - 0.2094}{2}(t - 8) & 8\text{ s} \leq t < 10\text{ s} \\ 0.2094 & 10\text{ s} \leq t < 12\text{ s} \\ 0.2094 + \frac{1.3089 - 0.2094}{2}(t - 12) & 12\text{ s} \leq t < 14\text{ s} \\ 1.3089 & 14\text{ s} \leq t < 16\text{ s} \\ 1.3089 - \frac{1.3089 - 0.8727}{2}(t - 16) & 16\text{ s} \leq t < 18\text{ s} \\ 0.8727 & t \geq 18\text{ s} \end{cases}$$

Each interval is described as follows:

- Interval $t < 4\text{ s}$: stabilization at 0.2094 rad .

During this time, the reference signal stays constant at $r(t) = 0.2094\text{ rad}$ (12°), representing a stabilization phase.

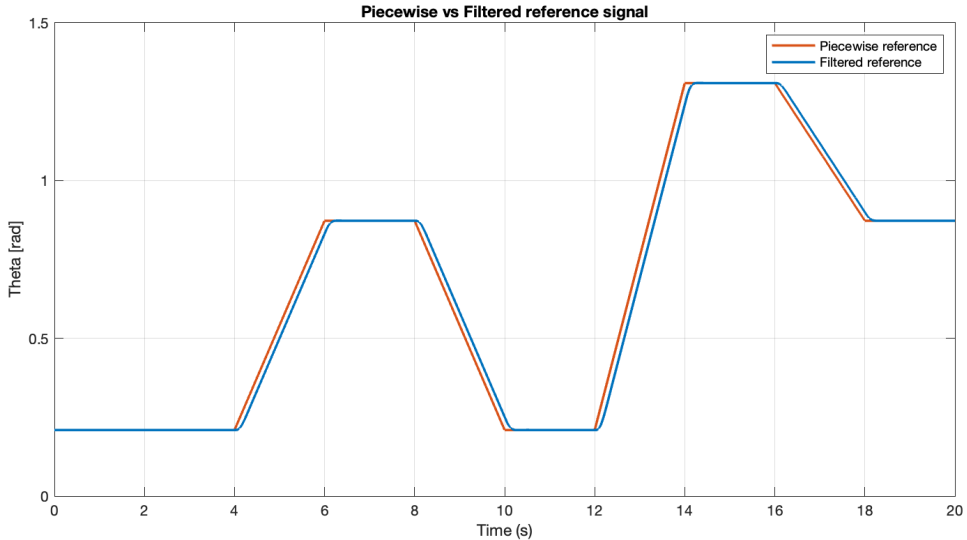


Figure 4.1: Pre and post-filtering reference signal

- Interval $4 \text{ s} \leq t < 6 \text{ s}$: linear transition from 0.2094 rad to 0.8727 rad . Over 2 seconds, the reference signal increases linearly from 0.2094 rad (12°) to 0.8727 rad (50°), representing a controlled opening of the throttle.
- Interval $6 \text{ s} \leq t < 8 \text{ s}$: stabilization at 0.8727 rad . The reference signal remains constant at $r(t) = 0.8727 \text{ rad}$ (50°) for 2 seconds, maintaining the throttle at the larger opening.
- Interval $8 \text{ s} \leq t < 10 \text{ s}$: linear transition from 0.8727 rad to 0.2094 rad . During the 2 seconds of this interval, the reference signal decreases linearly from 0.8727 rad (50°) to 0.2094 rad (12°), simulating a controlled closing of the throttle.
- Interval $10 \text{ s} \leq t < 12 \text{ s}$: stabilization at 0.2094 rad . The reference signal remains constant at $r(t) = 0.2094 \text{ rad}$ (12°), representing a new stabilization phase.
- Interval $12 \text{ s} \leq t < 14 \text{ s}$: linear transition from 0.2094 rad to 1.3089 rad . Over this interval, the reference increases linearly from 0.2094 rad (12°) to 1.3089 rad (75°), representing a wider throttle opening.
- Interval $14 \text{ s} \leq t < 16 \text{ s}$: stabilization at 1.3089 rad .

The reference signal is held constant at $r(t) = 1.3089 \text{ rad}$ (75°), maintaining the wide-open throttle.

- Interval $16 \text{ s} \leq t < 18 \text{ s}$: linear transition from 1.3089 rad to 0.8727 rad . During these other 2 seconds, the reference signal decreases linearly from 1.3089 rad (75°) to 0.8727 rad (50°), representing a partial throttle closing.
- Interval $t \geq 18 \text{ s}$: stabilization at 0.8727 rad . For $t \geq 18 \text{ s}$, the reference signal remains constant at $r(t) = 0.8727 \text{ rad}$ (50°), entering the final stabilization phase.

As in the previous chapters, all the relevant plots are reported below.

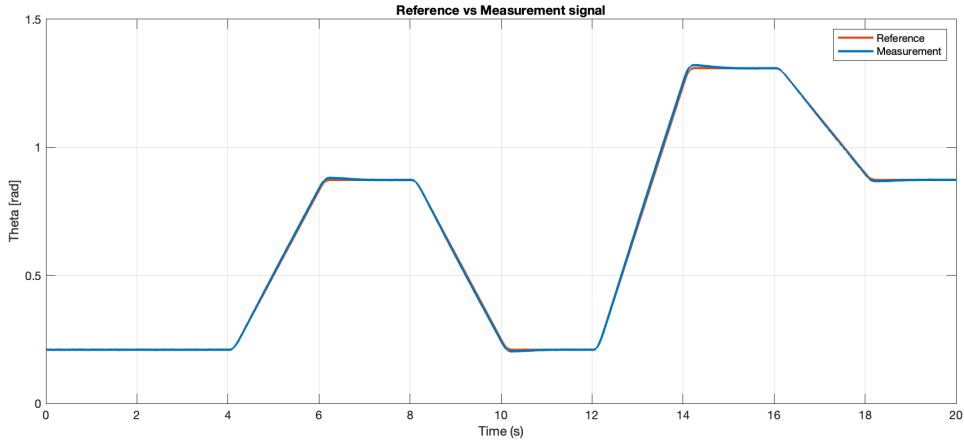


Figure 4.2: Reference vs Measurement

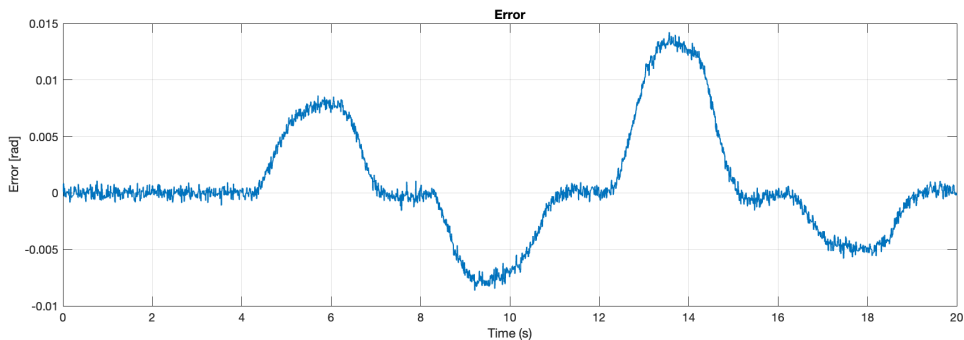


Figure 4.3: Error signal

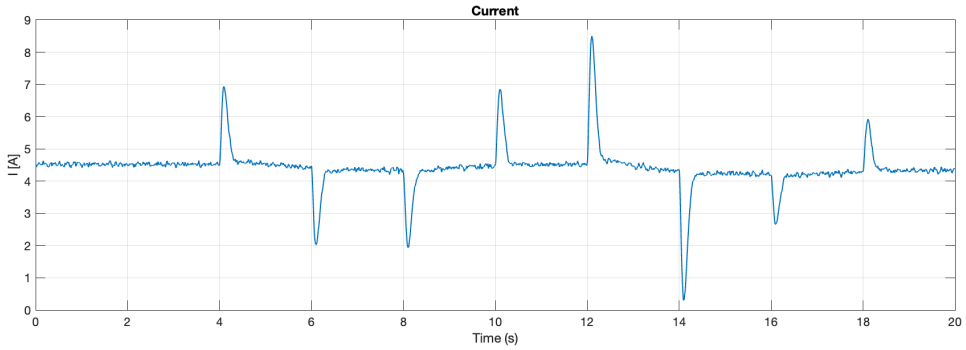


Figure 4.4: Current signal

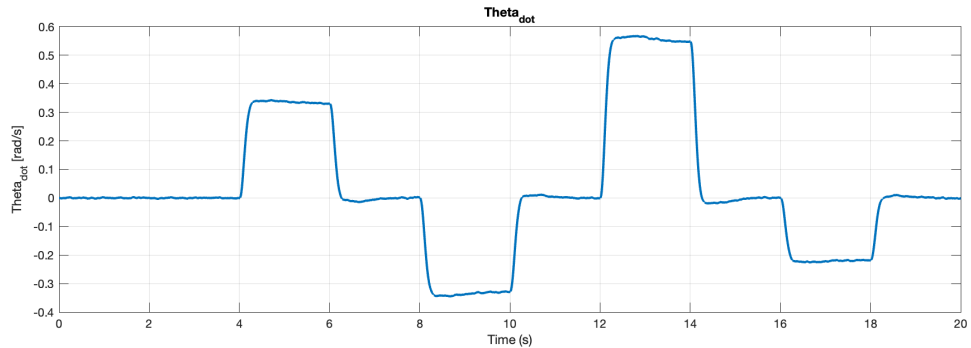


Figure 4.5: $\dot{\theta}$ signal

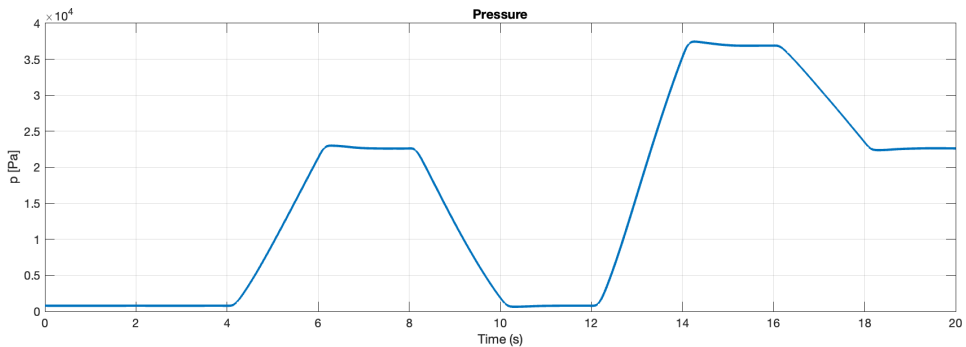


Figure 4.6: Pressure signal

The results carried out confirm that the developed control architecture allows to follow this reference signal in an accurate way.

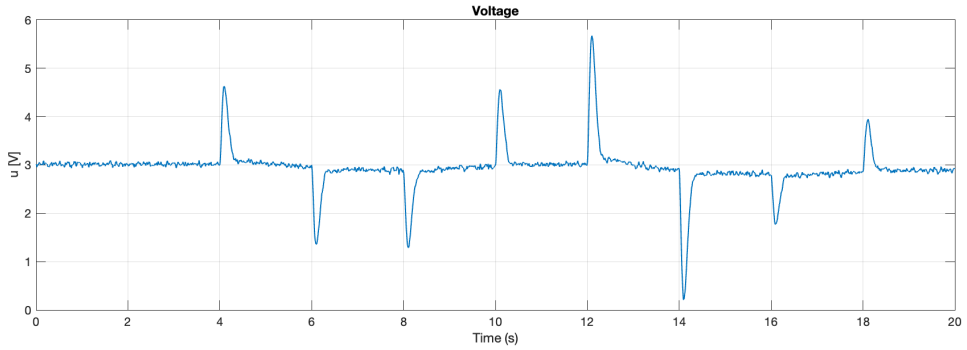


Figure 4.7: Control signal

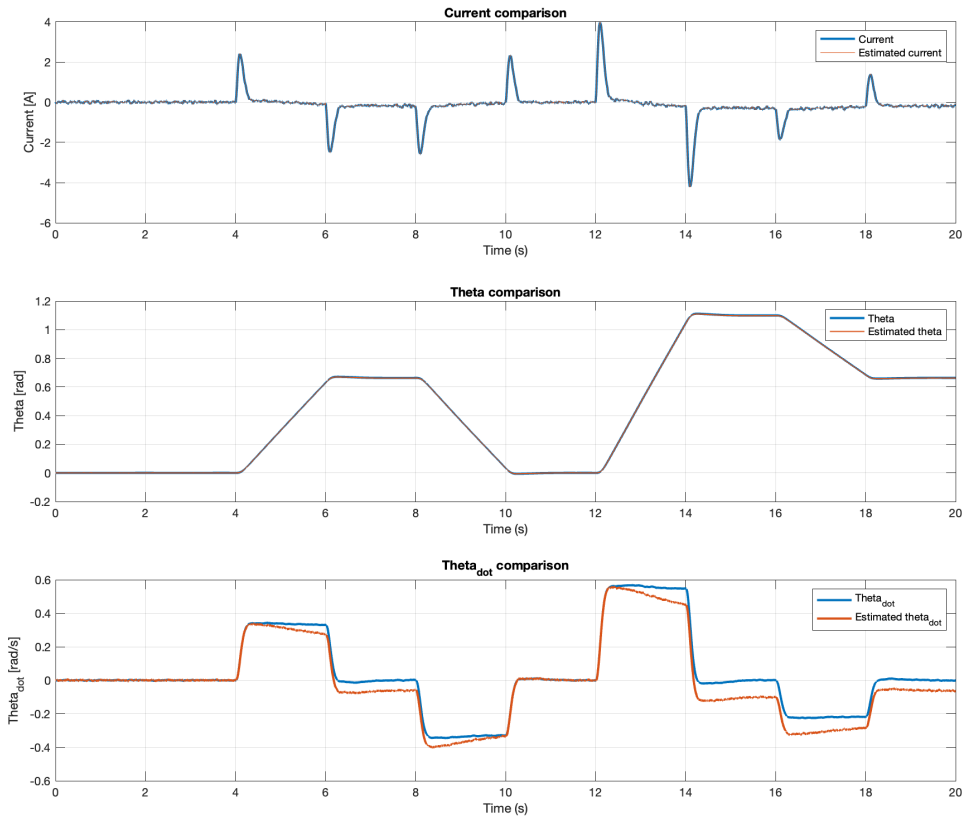


Figure 4.8: States vs Estimated states comparison

The next step is to track a shorter and steeper reference.

4.3 Faster Transitions

Compared to the previous reference, the time intervals have been further reduced to just 1 second, and the differences between the constant levels have been significantly increased.

These adjustments place greater demands on the system, requiring faster transitions and a more precise control response. The updated reference signal is described as follows:

$$\mathbf{r}(t) = \begin{cases} 0.2094 & t < 4\text{ s}, \\ 0.2094 + (1.3089 - 0.2094)(t - 4) & 4\text{ s} \leq t < 5\text{ s} \\ 1.3089 & 5\text{ s} \leq t < 6\text{ s} \\ 1.3089 - (1.3089 - 0.2094)(t - 6) & 6\text{ s} \leq t < 7\text{ s} \\ 0.2094 & 7\text{ s} \leq t < 8\text{ s} \\ 0.2094 + (0.8727 - 0.2094)(t - 8) & 8\text{ s} \leq t < 9\text{ s} \\ 0.8727 & 9\text{ s} \leq t < 10\text{ s} \\ 0.8727 - (0.8727 - 0.2094)(t - 10) & 10\text{ s} \leq t < 11\text{ s} \\ 0.2094 & t \geq 11\text{ s} \end{cases}$$

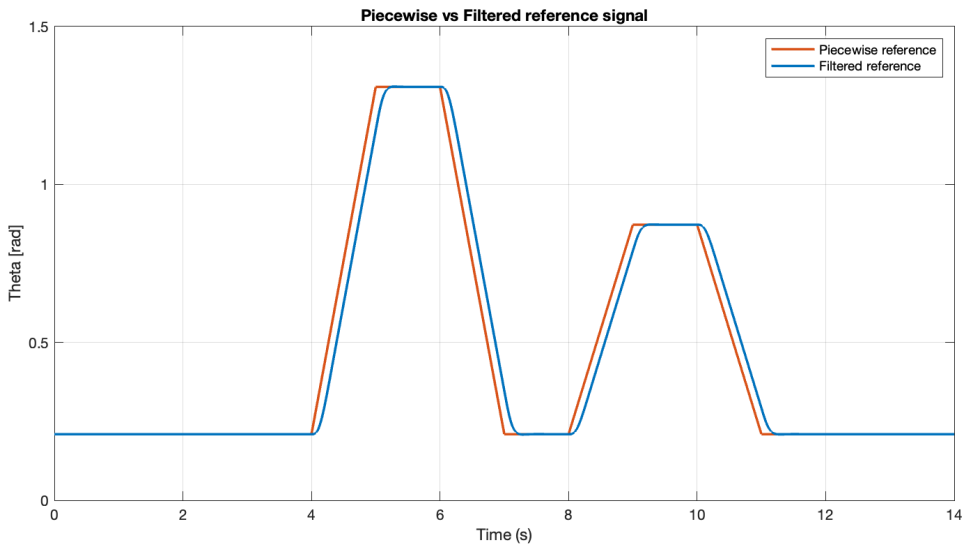


Figure 4.9: Pre and post-filtering reference signal

Each interval is described as follows:

- Interval $t < 4 \text{ s}$: stabilization at 0.2094 rad .
During this time, the reference signal stays constant at $r(t) = 0.2094 \text{ rad}$ (12°), representing an initial stabilization phase.
- Interval $4 \text{ s} \leq t < 5 \text{ s}$: linear transition from 0.2094 rad to 1.3089 rad .
Over just 1 second, the reference signal increases sharply from 0.2094 rad (12°) to 1.3089 rad (75°), simulating a rapid throttle opening.
- Interval $5 \text{ s} \leq t < 6 \text{ s}$: stabilization at 1.3089 rad .
The reference signal is held constant at $r(t) = 1.3089 \text{ rad}$ (75°), maintaining the throttle valve at its maximum opening.
- Interval $6 \text{ s} \leq t < 7 \text{ s}$: linear transition from 1.3089 rad to 0.2094 rad .
During this second, the reference decreases sharply from 1.3089 rad (75°) to 0.2094 rad (12°), simulating a rapid throttle closing.
- Interval $7 \text{ s} \leq t < 8 \text{ s}$: stabilization at 0.2094 rad .
The reference signal remains constant at $r(t) = 0.2094 \text{ rad}$ (12°), representing another stabilization phase.
- Interval $8 \text{ s} \leq t < 9 \text{ s}$: linear transition from 0.2094 rad to 0.8727 rad .
Over this interval, the reference signal increases from 0.2094 rad (12°) to 0.8727 rad (50°), simulating a moderate throttle opening.
- Interval $9 \text{ s} \leq t < 10 \text{ s}$: stabilization at 0.8727 rad .
The reference signal remains constant at $r(t) = 0.8727 \text{ rad}$ (50°), maintaining a partial throttle opening.
- Interval $10 \text{ s} \leq t < 11 \text{ s}$: linear transition from 0.8727 rad to 0.2094 rad .
During this second, the reference signal decreases from 0.8727 rad (50°) to 0.2094 rad (12°), simulating a gradual throttle closing.
- Interval $t \geq 11 \text{ s}$: stabilization at 0.2094 rad .
For $t \geq 11 \text{ s}$, the reference signal remains constant at $r(t) = 0.2094 \text{ rad}$ (12°), entering the final stabilization phase.

All the plots are presented in the same order as those used to illustrate the results of the simulation with the previous target.

This approach allows for a clear comparison of the differences between each case while highlighting the correlations among the reported quantities.

In this scenario as well, the control system demonstrates effective tracking, enabling nearly the entire throttle valve angular range to be spanned within 1 second.

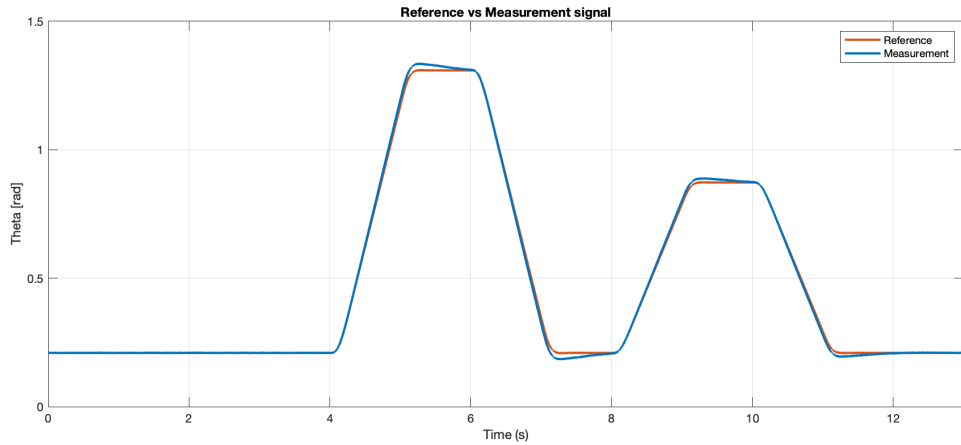


Figure 4.10: Reference vs Measurement

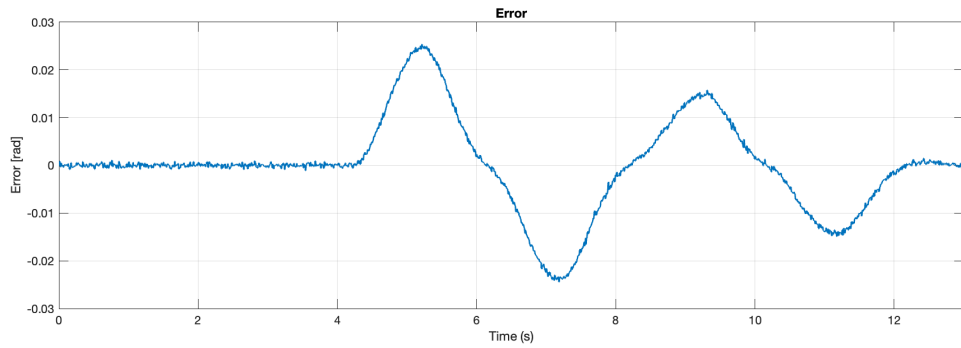


Figure 4.11: Error signal

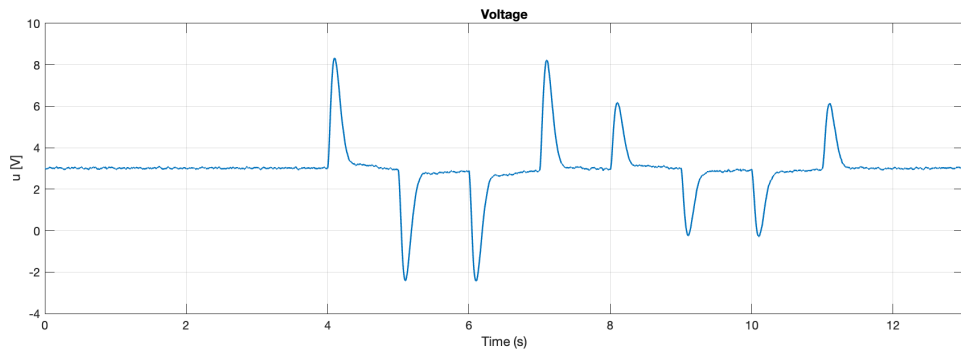


Figure 4.12: Control signal

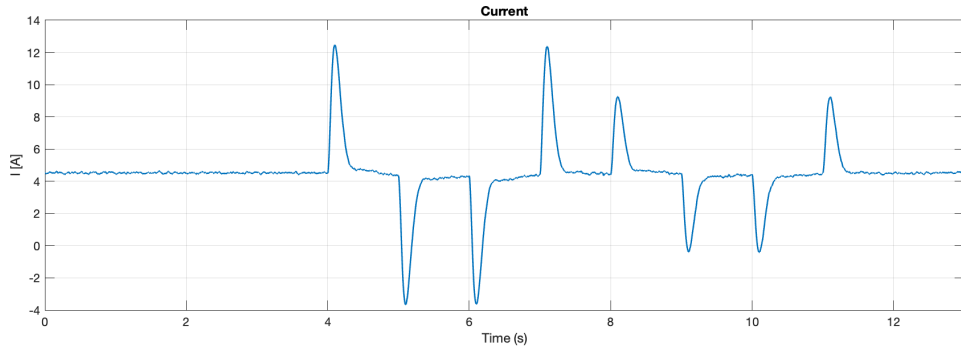


Figure 4.13: Current signal

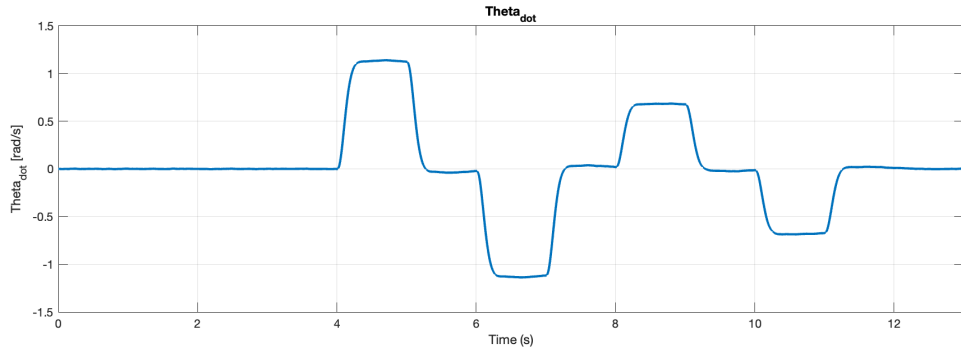


Figure 4.14: $\dot{\theta}$ signal

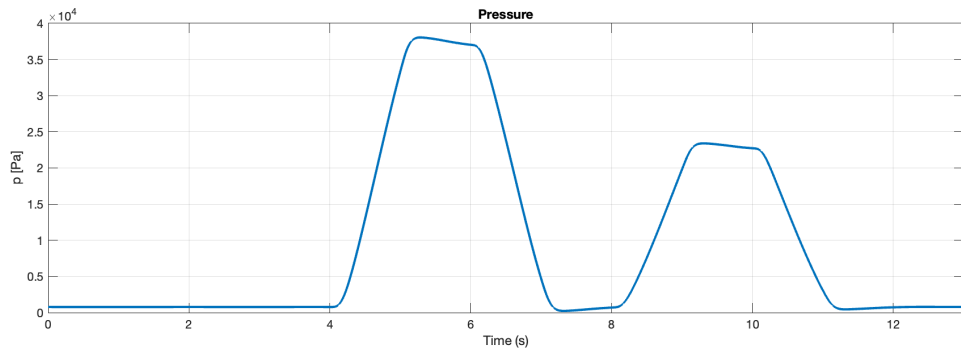


Figure 4.15: Pressure signal

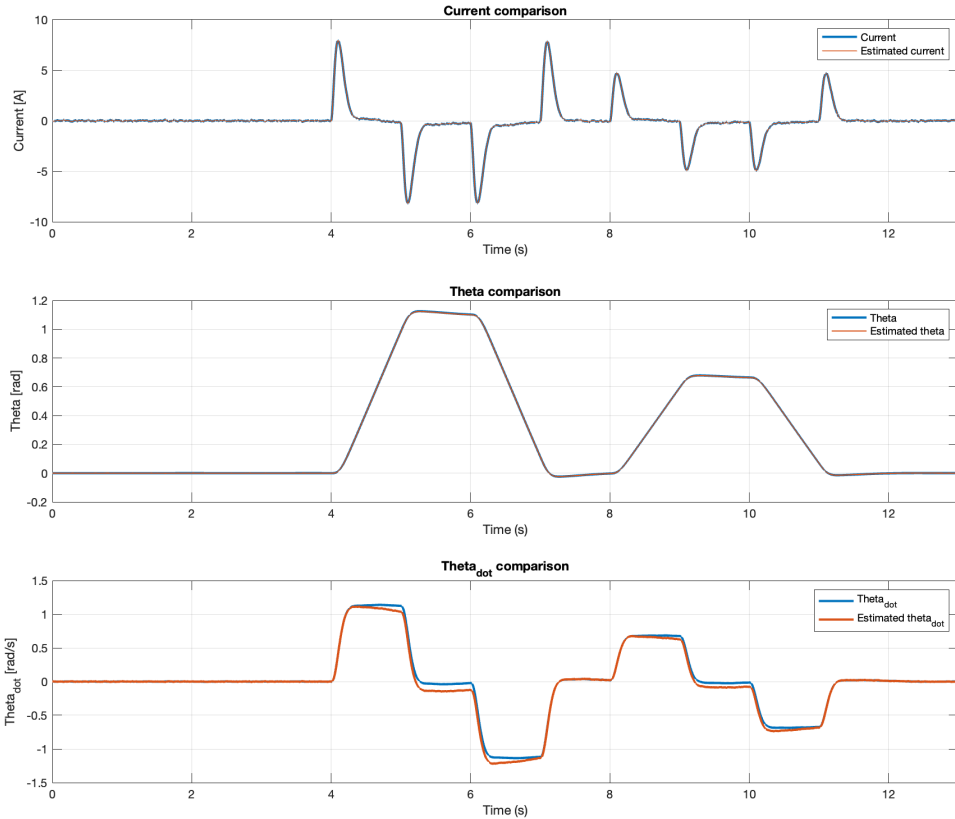


Figure 4.16: States vs Estimated states comparison

4.4 Sharp Peaks and Cusps Test

In this reference signal, sharp peaks and cusps have been introduced, and stabilization phases have been entirely removed. Previously, we primarily demanded higher speed from the control system by shortening the duration of the transitions, thus requiring faster dynamics. However, this approach mainly emphasized speed and responsiveness.

Now, the focus shifts to accuracy. While faster control dynamics are essential, they can lead to overshoots, particularly in systems with rapid transitions and no stabilization phases. In this context, overshoots become unacceptable, as there is no time for the system to stabilize. Therefore, this signal challenges the control system to maintain precise tracking of the reference without introducing oscillations or inaccuracies.

The signal is defined as follows:

$$r(t) = \begin{cases} 0.2094 & t < 4 \text{ s} \\ 0.2094 + (1.3089 - 0.2094)(t - 4) & 4 \text{ s} \leq t < 5 \text{ s} \\ 1.3089 - (1.3089 - 0.2094)(t - 5) & 5 \text{ s} \leq t < 6 \text{ s} \\ 0.2094 + (0.8727 - 0.2094)(t - 6) & 6 \text{ s} \leq t < 7 \text{ s} \\ 0.8727 - (0.8727 - 0.2094)(t - 7) & 7 \text{ s} \leq t < 8 \text{ s} \\ 0.2094 & t \geq 8 \text{ s} \end{cases}$$

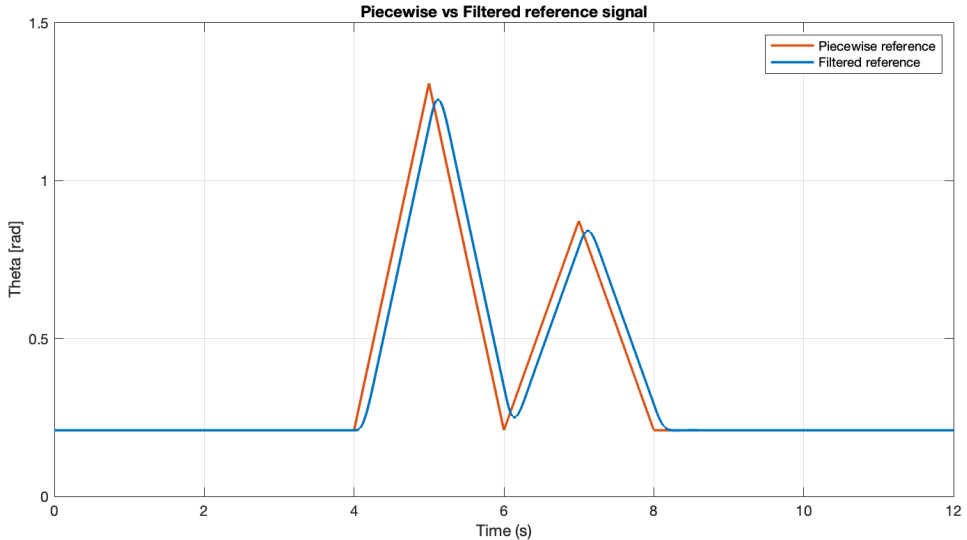


Figure 4.17: Pre and post-filtering reference signal

Each interval is described as follows:

- Interval $t < 4 \text{ s}$: stabilization at 0.2094 rad .
The throttle remains constant at 12° , representing an initial phase of constant demand.
- Interval $4 \text{ s} \leq t < 5 \text{ s}$: linear increase from 0.2094 rad to 1.3089 rad .
The throttle rapidly increases from 12° to 75° over 1 second, simulating a sharp acceleration demand.
- Interval $5 \text{ s} \leq t < 6 \text{ s}$: linear decrease from 1.3089 rad to 0.2094 rad .
The throttle quickly decreases from 75° to 12° within 1 second, reflecting a steep deceleration.

- Interval $6 \text{ s} \leq t < 7 \text{ s}$: linear increase from 0.2094 rad to 0.8727 rad .
The throttle rises again, this time reaching 50° over 1 second, simulating a moderate acceleration.
- Interval $7 \text{ s} \leq t < 8 \text{ s}$: linear decrease from 0.8727 rad to 0.2094 rad .
The throttle closes from 50° back to 12° over 1 second, reflecting a controlled deceleration.
- Interval $t \geq 8 \text{ s}$: stabilization at 0.2094 rad .
The throttle remains constant at 12° , representing a final phase of low demand.

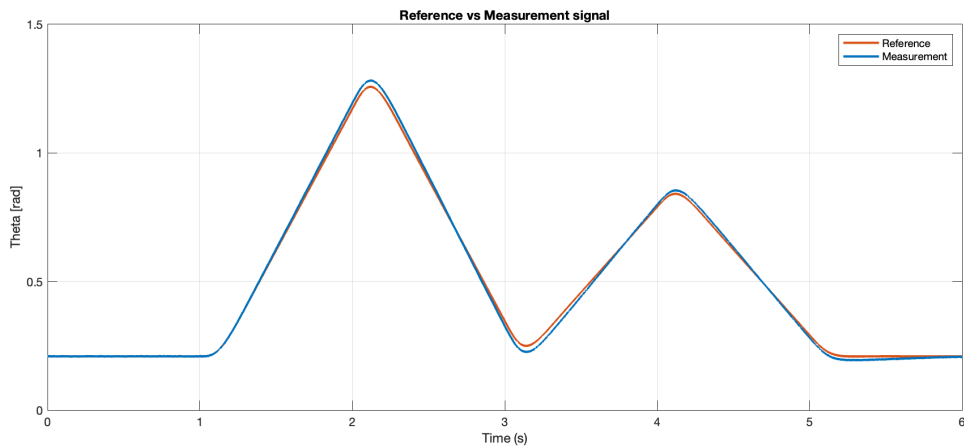


Figure 4.18: Reference vs Measurement

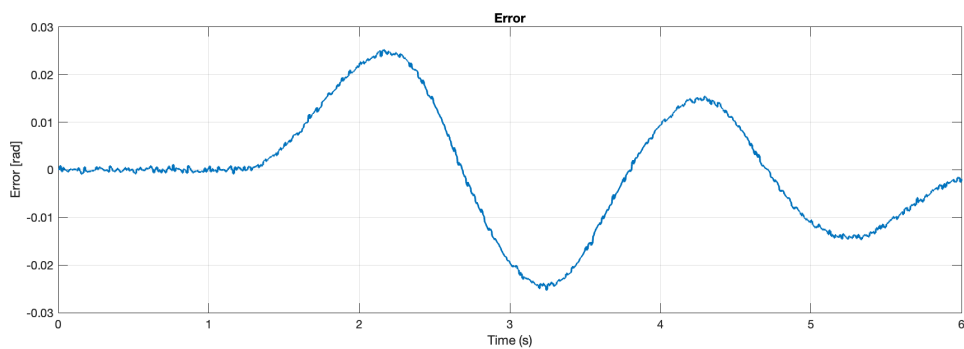


Figure 4.19: Error signal

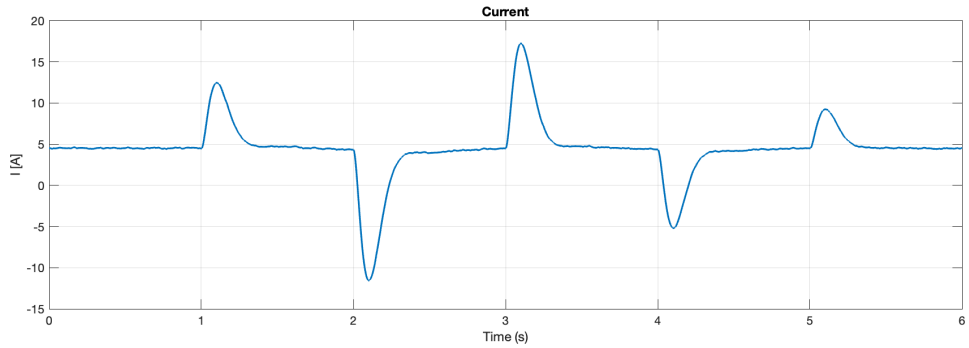


Figure 4.20: Current signal

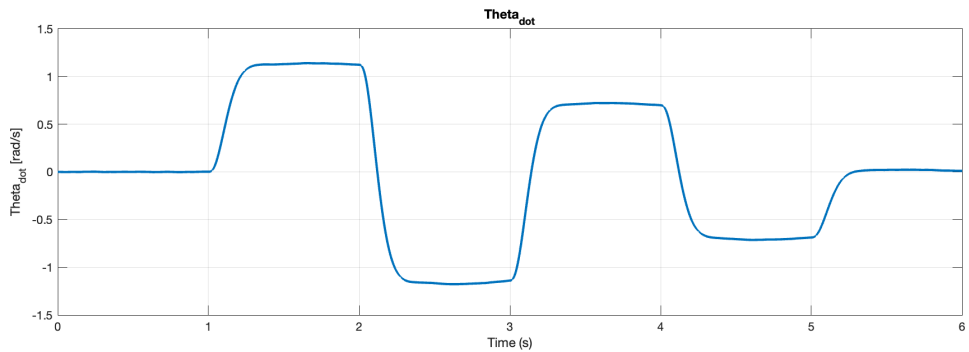


Figure 4.21: $\dot{\theta}$ signal

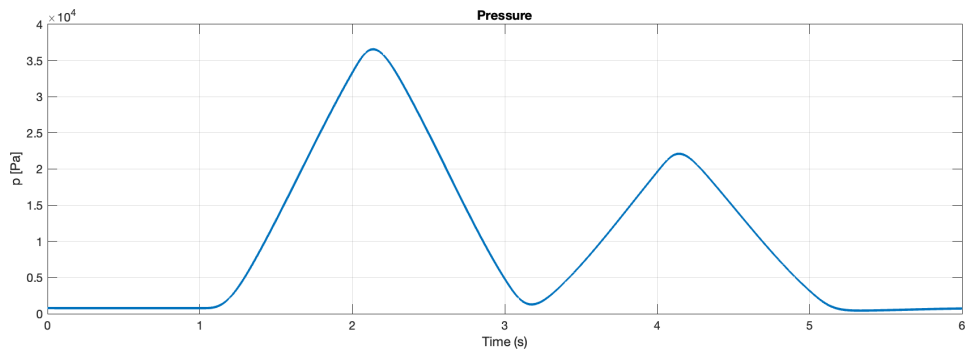


Figure 4.22: Pressure signal

All the behaviors depicted in the figures demonstrate the system's ability to effectively handle a highly demanding signal in terms of responsiveness.

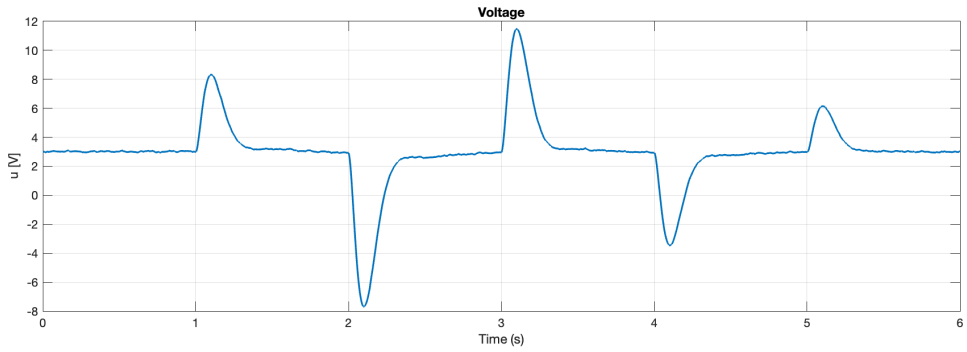


Figure 4.23: Control signal

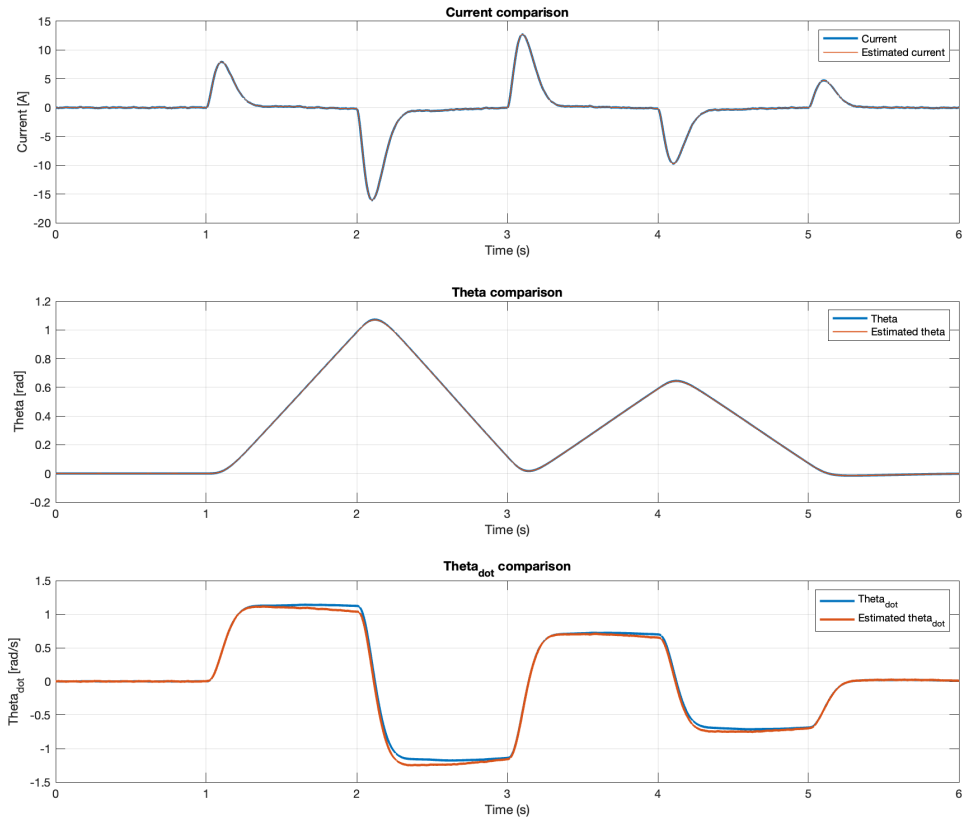


Figure 4.24: States vs Estimated states comparison

The absence of stationary parts among transients, and so the presence

of consecutive peaks and valleys, represents a challenging scenario that this control system is able to face.

After verifying this characteristic, it is time to subject the throttle valve to one of the most challenging tests it can undergo: a telemetry test. Naturally, this will not involve the highly variable telemetry typical of motorsport applications, as this is not the intended use case for a road car engine. However, the telemetry will be dynamic enough to demand a robust control architecture.

4.5 Complex Driving Cycle

The following reference signal $\mathbf{r}(t)$ combines all the complexities introduced in the previous references, simulating a realistic urban driving scenario where the driver's demands are highly variable and change rapidly. This signal includes stabilization phases, linear and exponential transitions, as well as steeper changes, replicating the dynamic behavior of throttle adjustments in urban traffic.

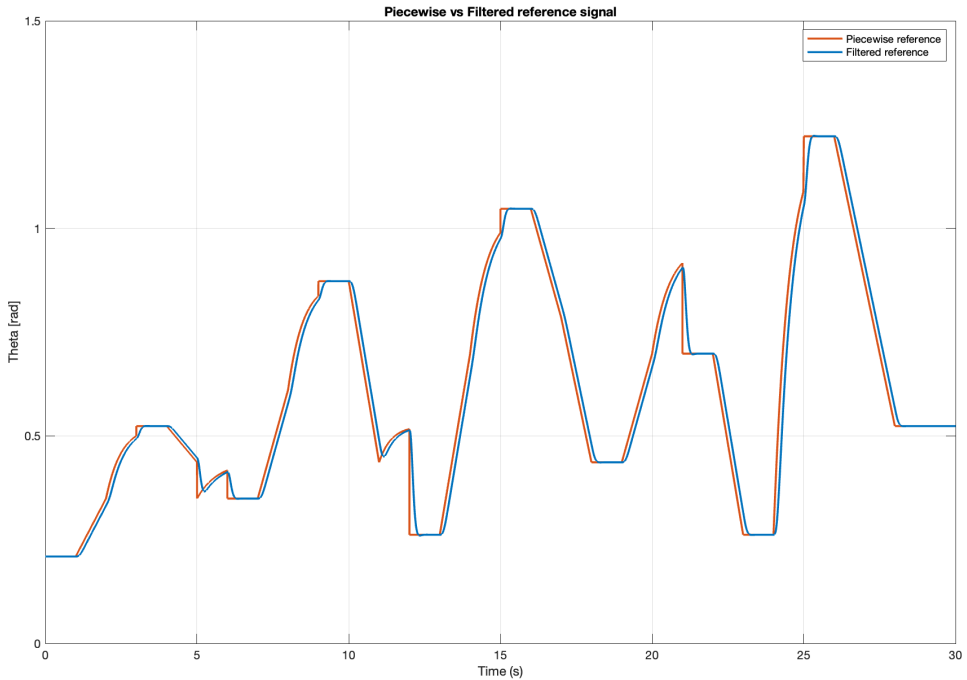


Figure 4.25: Pre and post-filtering reference signal

The reference signal is defined as follows:

$$\mathbf{r}(t) = \begin{cases} 0.2094 & t < 1\text{ s} \\ 0.2094 + \frac{0.3491 - 0.2094}{1}(t - 1) & 1\text{ s} \leq t < 2\text{ s} \\ 0.3491 + (0.5236 - 0.3491) \cdot (1 - e^{-2(t-2)}) & 2\text{ s} \leq t < 3\text{ s} \\ 0.5236 & 3\text{ s} \leq t < 4\text{ s} \\ 0.5236 - \frac{0.5236 - 0.4363}{1}(t - 4) & 4\text{ s} \leq t < 5\text{ s} \\ 0.4363 - (0.4363 - 0.3491) \cdot e^{-1.5(t-5)} & 5\text{ s} \leq t < 6\text{ s} \\ 0.3491 & 6\text{ s} \leq t < 7\text{ s} \\ 0.3491 + \frac{0.6109 - 0.3491}{1}(t - 7) & 7\text{ s} \leq t < 8\text{ s} \\ 0.6109 + (0.8727 - 0.6109) \cdot (1 - e^{-2(t-8)}) & 8\text{ s} \leq t < 9\text{ s} \\ 0.8727 & 9\text{ s} \leq t < 10\text{ s} \\ 0.8727 - \frac{0.8727 - 0.4363}{1}(t - 10) & 10\text{ s} \leq t < 11\text{ s} \\ 0.5236 - (0.5236 - 0.4363) \cdot e^{-2.5(t-11)} & 11\text{ s} \leq t < 12\text{ s} \\ 0.2618 & 12\text{ s} \leq t < 13\text{ s} \\ 0.2618 + \frac{0.6981 - 0.2618}{1}(t - 13) & 13\text{ s} \leq t < 14\text{ s} \\ 0.6981 + (1.0472 - 0.6981) \cdot (1 - e^{-1.8(t-14)}) & 14\text{ s} \leq t < 15\text{ s} \\ 1.0472 & 15\text{ s} \leq t < 16\text{ s} \\ 1.0472 - \frac{1.0472 - 0.7854}{1}(t - 16) & 16\text{ s} \leq t < 17\text{ s} \\ 0.7854 - \frac{0.7854 - 0.4363}{1}(t - 17) & 17\text{ s} \leq t < 18\text{ s} \\ 0.4363 & 18\text{ s} \leq t < 19\text{ s} \\ 0.4363 + \frac{0.6981 - 0.4363}{1}(t - 19) & 19\text{ s} \leq t < 20\text{ s} \\ 0.9599 - (0.9599 - 0.6981) \cdot e^{-1.8(t-20)} & 20\text{ s} \leq t < 21\text{ s} \\ 0.6981 & 21\text{ s} \leq t < 22\text{ s} \\ 0.6981 - \frac{0.6981 - 0.2618}{1}(t - 22) & 22\text{ s} \leq t < 23\text{ s} \\ 0.2618 & 23\text{ s} \leq t < 24\text{ s} \\ 0.2618 + (1.2217 - 0.2618) \cdot (1 - e^{-2(t-24)}) & 24\text{ s} \leq t < 25\text{ s} \\ 1.2217 & 25\text{ s} \leq t < 26\text{ s} \\ 1.2217 - \frac{1.2217 - 0.5236}{2}(t - 26) & 26\text{ s} \leq t < 28\text{ s} \\ 0.5236 & 28\text{ s} \leq t < 30\text{ s} \\ 0.5236 & t \geq 30\text{ s} \end{cases}$$

Each interval is described as follows:

- Interval $t < 1\text{ s}$: stabilization at 0.2094 rad .

The throttle remains constant at a low opening level (12°), simulating an initial stabilization phase.

- Interval $1 \text{ s} \leq t < 2 \text{ s}$: linear increase from 0.2094 rad to 0.3491 rad .
The throttle gradually opens, simulating a moderate acceleration.
- Interval $2 \text{ s} \leq t < 3 \text{ s}$: exponential rise from 0.3491 rad to 0.5236 rad .
This represents a sharper increase in throttle opening, reflecting a more sudden demand.
- Interval $3 \text{ s} \leq t < 4 \text{ s}$: stabilization at 0.5236 rad .
The throttle remains constant at 30° , maintaining a steady phase.
- Interval $4 \text{ s} \leq t < 5 \text{ s}$: linear decrease from 0.5236 rad to 0.4363 rad .
The throttle gradually closes, simulating a controlled deceleration.
- Interval $5 \text{ s} \leq t < 6 \text{ s}$: exponential decrease to 0.3491 rad .
The throttle continues to close smoothly, reflecting a further deceleration phase.
- Interval $6 \text{ s} \leq t < 7 \text{ s}$: stabilization at 0.3491 rad .
The throttle remains constant at 20° , representing a cruising phase.
- Interval $7 \text{ s} \leq t < 8 \text{ s}$: linear increase from 0.3491 rad to 0.6109 rad .
The throttle opens gradually, simulating a moderate acceleration.
- Interval $8 \text{ s} \leq t < 9 \text{ s}$: exponential rise from 0.6109 rad to 0.8727 rad .
The throttle opens more sharply, simulating a strong acceleration.
- Interval $9 \text{ s} \leq t < 10 \text{ s}$: stabilization at 0.8727 rad .
The throttle remains constant at 50° , maintaining a higher steady demand phase.
- Interval $10 \text{ s} \leq t < 11 \text{ s}$: linear decrease from 0.8727 rad to 0.4363 rad .
The throttle closes gradually, simulating a controlled deceleration.
- Interval $11 \text{ s} \leq t < 12 \text{ s}$: exponential decrease from 0.5236 rad to 0.2618 rad .
The throttle closes more steeply, reflecting a stronger deceleration.
- Interval $12 \text{ s} \leq t < 13 \text{ s}$: stabilization at 0.2618 rad .
The throttle remains constant at 15° , simulating a low cruising phase.
- Interval $13 \text{ s} \leq t < 14 \text{ s}$: linear increase from 0.2618 rad to 0.6981 rad .
The throttle opens gradually, representing a moderate acceleration.

- Interval $14 \text{ s} \leq t < 15 \text{ s}$: exponential rise from 0.6981 rad to 1.0472 rad .
The throttle opens more sharply, reflecting a strong acceleration.
- Interval $15 \text{ s} \leq t < 16 \text{ s}$: stabilization at 1.0472 rad .
The throttle remains constant at 60° for a steady high-demand phase.
- Interval $16 \text{ s} \leq t < 17 \text{ s}$: linear decrease from 1.0472 rad to 0.7854 rad .
The throttle closes gradually, simulating a controlled deceleration.
- Interval $17 \text{ s} \leq t < 18 \text{ s}$: linear decrease from 0.7854 rad to 0.4363 rad .
The throttle closes more steeply, reflecting a stronger deceleration.
- Interval $18 \text{ s} \leq t < 19 \text{ s}$: stabilization at 0.4363 rad .
The throttle remains constant at 25° , representing a steady cruising phase.
- Interval $19 \text{ s} \leq t < 20 \text{ s}$: linear increase from 0.4363 rad to 0.6981 rad .
The throttle opens gradually, simulating moderate acceleration.
- Interval $20 \text{ s} \leq t < 21 \text{ s}$: exponential decrease from 0.6981 rad to 0.5236 rad .
The throttle closes gradually, reflecting a smooth deceleration.
- Interval $21 \text{ s} \leq t < 22 \text{ s}$: stabilization at 0.6981 rad .
The throttle remains constant at 40° , maintaining a steady phase.
- Interval $22 \text{ s} \leq t < 23 \text{ s}$: linear decrease from 0.6981 rad to 0.2618 rad .
The throttle closes gradually, simulating a controlled deceleration.
- Interval $23 \text{ s} \leq t < 24 \text{ s}$: stabilization at 0.2618 rad .
The throttle remains constant at 15° , representing a cruising phase at low demand.
- Interval $24 \text{ s} \leq t < 25 \text{ s}$: exponential increase from 0.2618 rad to 1.2217 rad .
The throttle opens sharply, reflecting a strong acceleration demand.
- Interval $25 \text{ s} \leq t < 26 \text{ s}$: stabilization at 1.2217 rad .
The throttle remains constant at 70° for a steady high-demand phase.
- Interval $26 \text{ s} \leq t < 28 \text{ s}$: linear decrease from 1.2217 rad to 0.5236 rad .
The throttle closes gradually, simulating a controlled deceleration.
- Interval $t \geq 30 \text{ s}$: stabilization at 0.5236 rad .
At the end the throttle remains in a moderate steady phase at 30° .

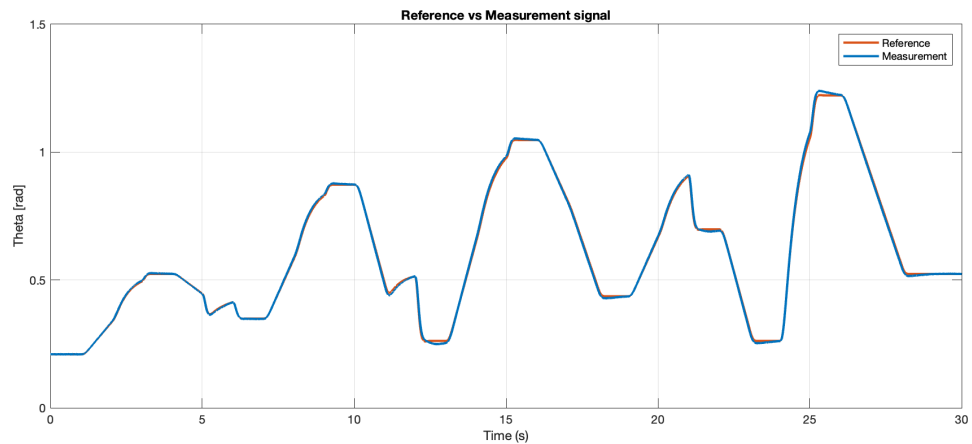


Figure 4.26: Reference vs Measurement

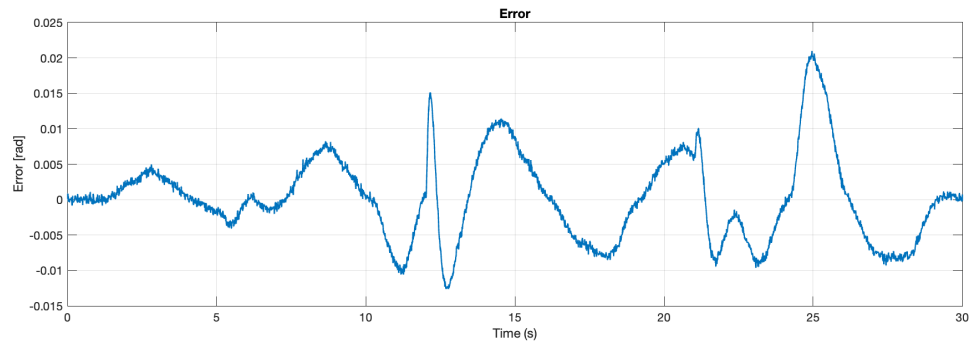
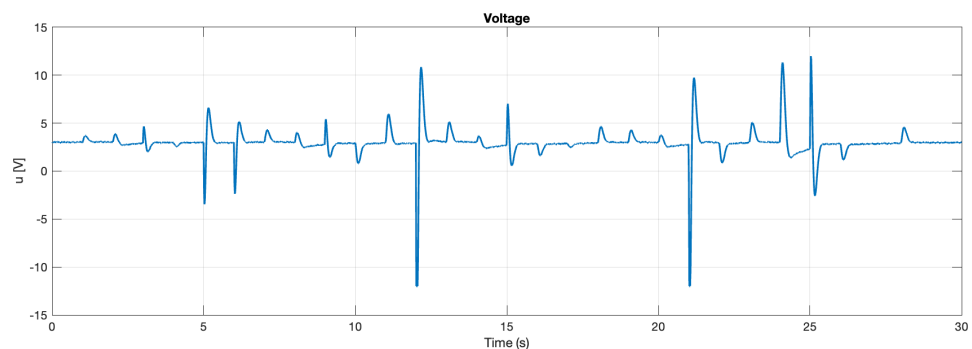


Figure 4.27: Error signal



The parameters set for the stabilizer, integral action and observer allow to track in a good way also this signal that is the most complex one.

Even though this result could be accepted, another tuning process can be performed in order to guarantee an even better tracking of the reference. In particular, it can be seen that reducing more $\varepsilon_{4,\max}$, the maximum allowable error embedded in the matrix \mathbf{Q} associated with the integral action, allows to steer the error to zero also in the most critical condition, which is usually represented by an aggressive variation of throttle opening in few milliseconds.

In this way, updating the values of \mathbf{K}_S and \mathbf{K}_I enables to reduce the overshoot problem seen using the previous tuning parameters.

The updated matrix \mathbf{Q} with $\varepsilon_{4,\max} = 0.001 \text{ rad}$ becomes:

$$\mathbf{Q} = \begin{bmatrix} 0.3086 & 0 & 0 & 0 \\ 0 & 100 & 0 & 0 \\ 0 & 0 & 25 & 0 \\ 0 & 0 & 0 & 250000 \end{bmatrix} \quad (4.1)$$

The updated \mathbf{K}_S and \mathbf{K}_I are the following:

$$\mathbf{K}_S = [-6.0452 \quad -1.3872 \times 10^3 \quad -1.5475 \times 10^2]$$

$$\mathbf{K}_I = [-6.1379 \times 10^3]$$

All the results obtained from the updated simulation are presented in the figures below.

With these new values, the tracking performance is improved, particularly in areas with deep valleys where the signal previously struggled to accurately follow the reference. The system struggles in these zones because the control voltage reaches the limit of the -12 VDC rail, leaving no headroom for further adjustment. As a result, the controller is unable to provide the necessary voltage to track the reference signal in a perfect way.

This behavior can be also observed in the updated case, by looking at the voltage peaks in figure 4.31, but shows significant improvement, characterized by greater responsiveness. By comparing the segments between 12 s and 13 s , and between 21 s and 22 s in figures 4.26 and 4.29, it becomes evident that in the latter, the measurement signal exhibits a quicker change in slope when the reference signal becomes constant.

Another perspective is provided by examining the error, which, as shown in figure 4.30, remains between 0.004 rad and -0.004 rad , except for two small peaks that do not exceed 0.01 rad .

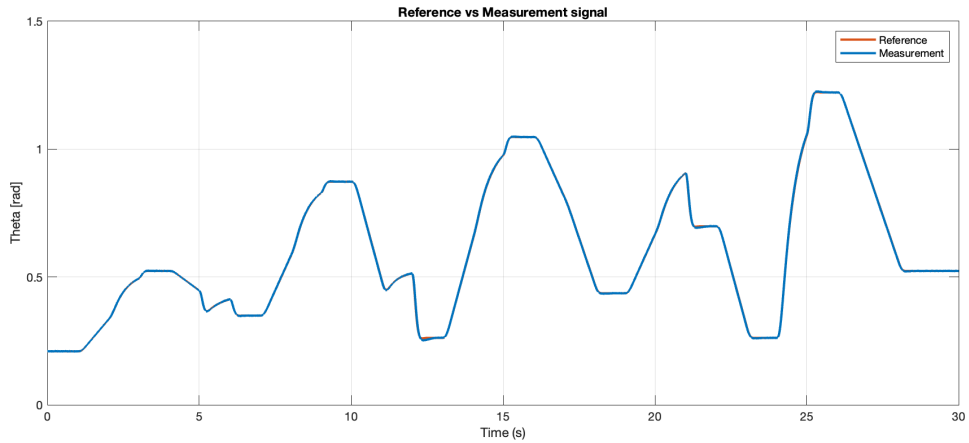


Figure 4.29: Reference vs Measurement

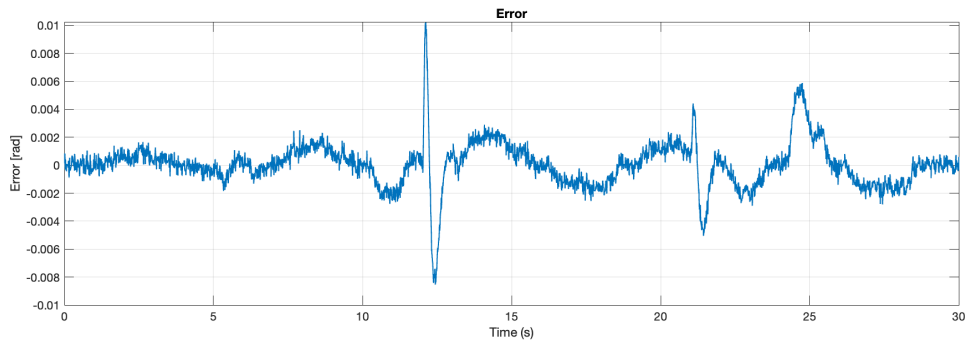
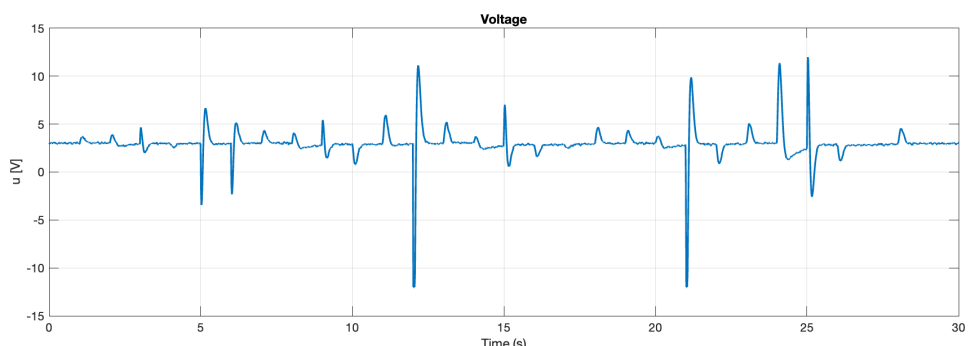


Figure 4.30: Error signal



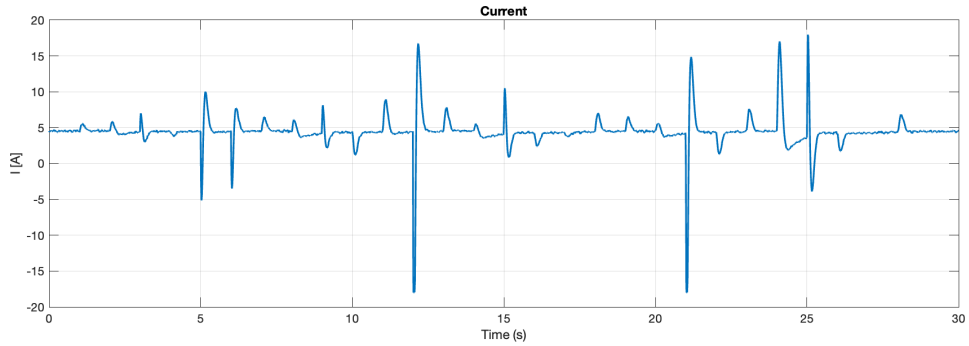


Figure 4.32: Current signal

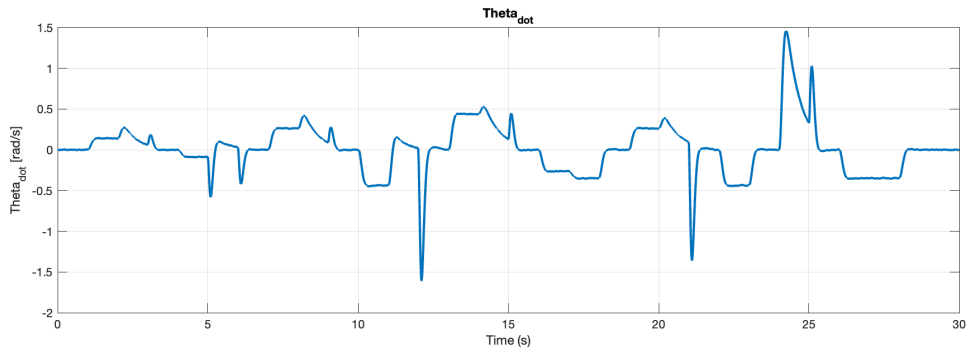


Figure 4.33: $\dot{\theta}$ signal

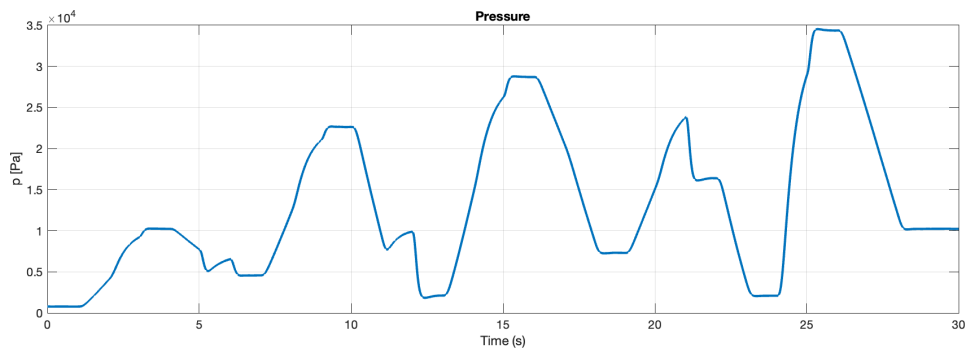


Figure 4.34: Pressure signal

For this specific case, the updated values allow the control system to outperform the previous configuration, effectively validating the new tuned values of \mathbf{K}_S and \mathbf{K}_I .

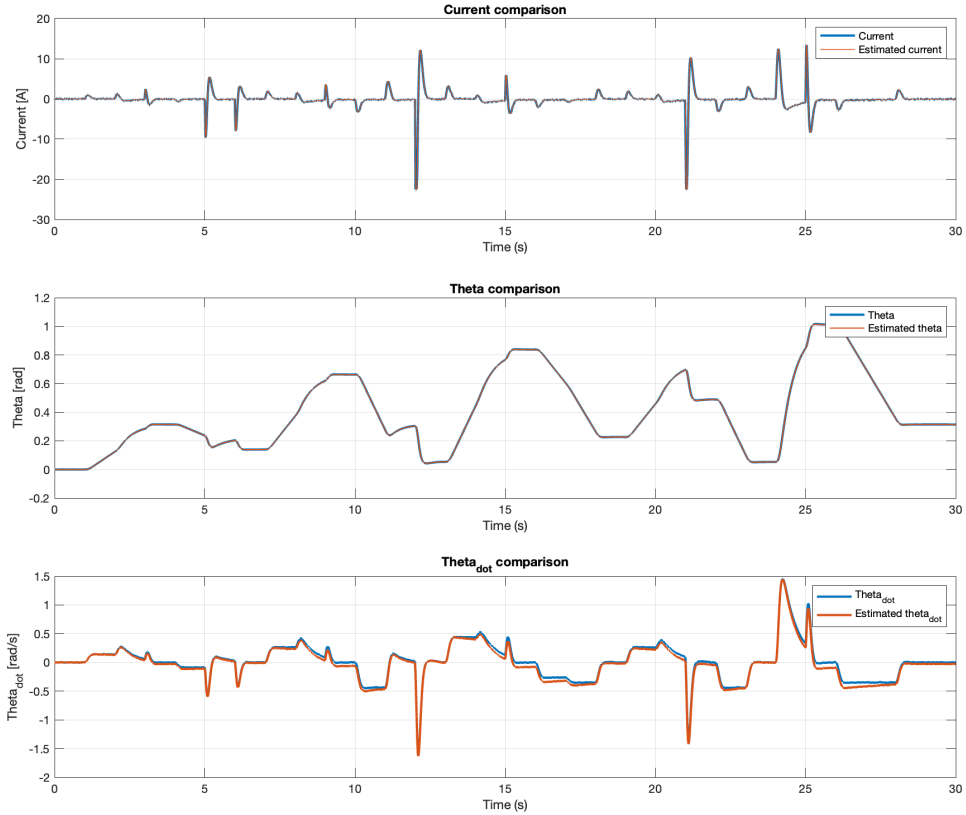


Figure 4.35: States vs Estimated states comparison

In the next paragraph, these new control parameters are tested on two of the previous reference signals to validate the effectiveness of this tuning from a broader perspective.

4.5.1 Validation of the Updated Tuning Strategy

The tracking signals from the previous sections, which require high responsiveness and accuracy during fast and steep transitions, are used for this validation test.

The control system is now expected to achieve even better tracking than before. This improvement can be observed in the figures below, where the updated results are presented. For the sake of brevity, only the comparison between the desired signal and the measurement one is reported, along with the relative measurement error.

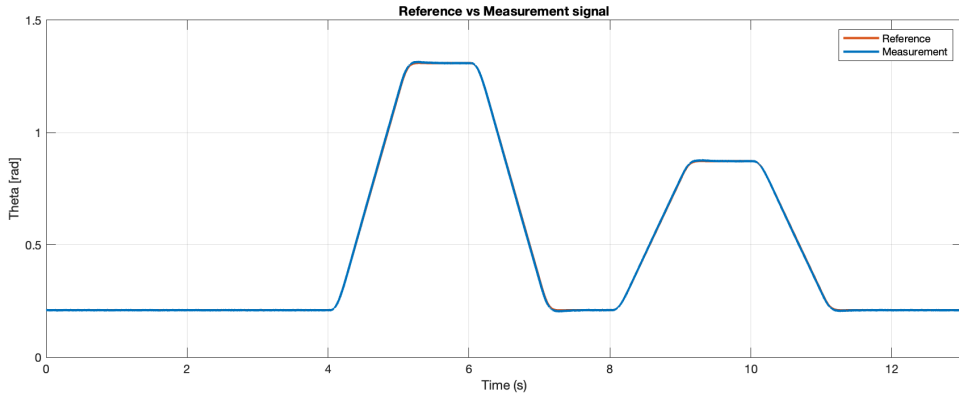


Figure 4.36: Updated tracking for the signal with fast transitions

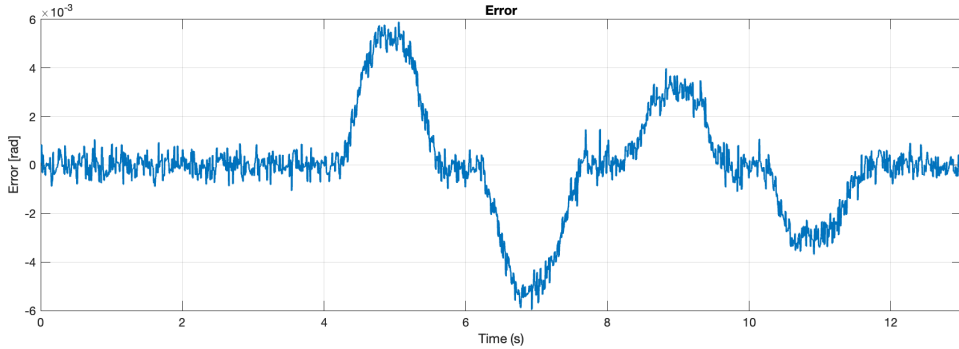


Figure 4.37: Updated error for the signal with fast transitions

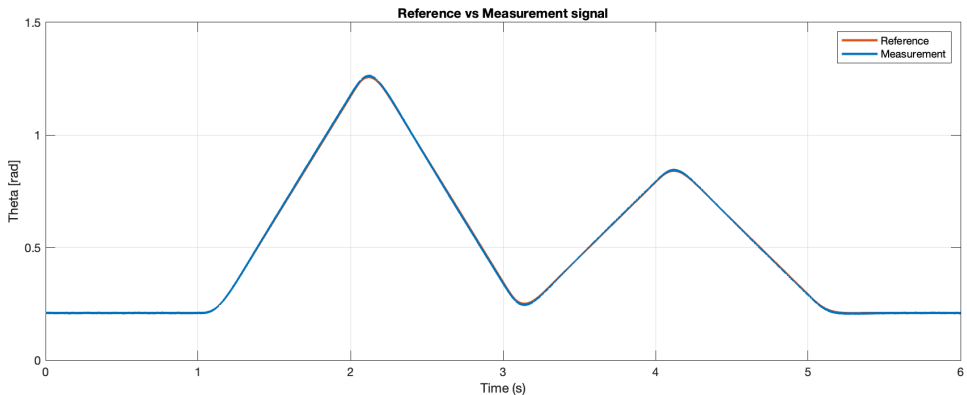


Figure 4.38: Updated tracking for the signal with peaks and cusps

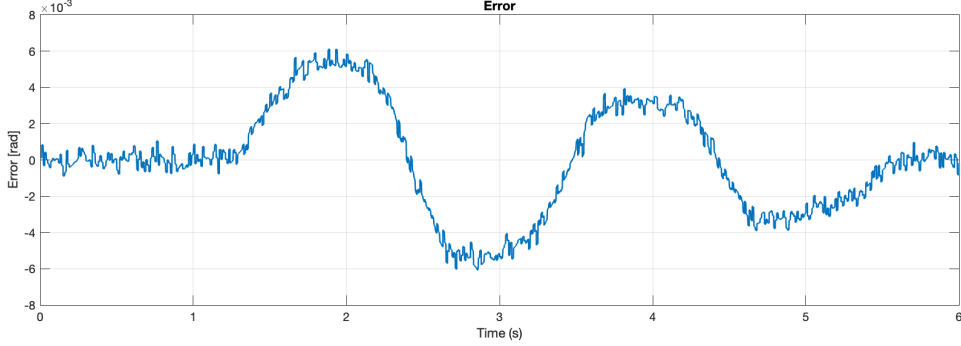


Figure 4.39: Updated error for the signal with peaks and cusps

In the first test, the tracking error is reduced from a value of 0.03 rad to a maximum of $6 \times 10^{-3} \text{ rad}$. In the second test, the tracking error is reduced from a value of 0.025 rad to a maximum of $6 \times 10^{-3} \text{ rad}$.

This is sufficient to validate the updated control strategy, which will also be applied to the subsequent scenarios presented.

4.6 Highway Entrance Maneuver

The following reference signal, $\mathbf{r}(t)$, represents the throttle valve behavior during a highway entrance maneuver.

This signal has been carefully designed by considering the typical structure of Italian highway entrances, which often include distinct sections.

Typically, the maneuver begins on an urban or suburban road that transitions into a turn leading towards the highway. This turn is generally characterized by a wide, uphill curve that gradually aligns the vehicle with the highway trajectory.

Finally, the merging lane provides the transition to fully integrate into the highway flow.

Each segment of the reference signal corresponds to these specific sections of the route, capturing the dynamic requirements of each stage of the maneuver.

The signal is defined as follows:

$$\mathbf{r}(t) = \begin{cases} 0.2094 & t < 4 \text{ s} \\ 0.2094 + 0.0349(t - 4) & 4 \text{ s} \leq t < 8 \text{ s} \\ 0.3491 + 0.9599(1 - e^{-(t-8)}) & t \geq 8 \text{ s} \end{cases}$$

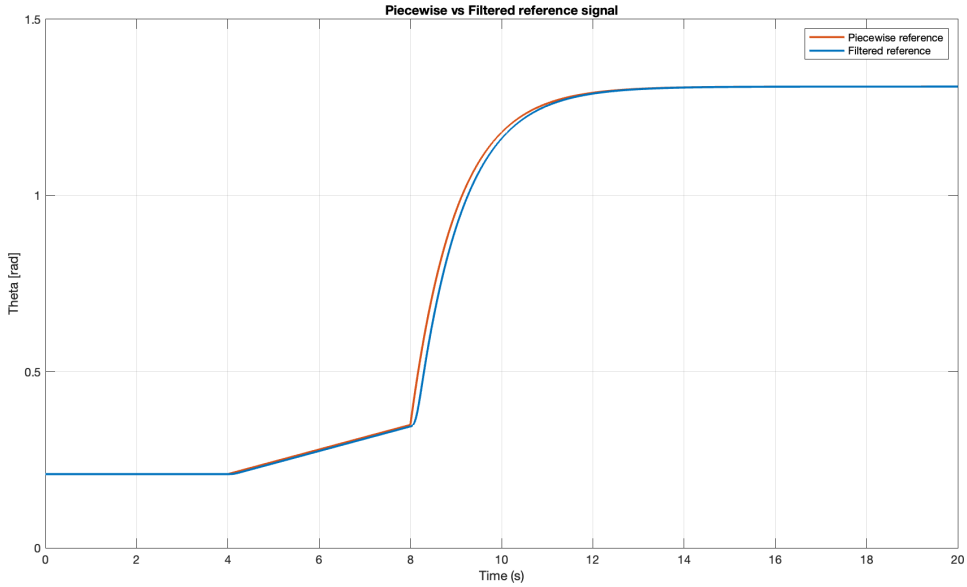


Figure 4.40: Pre and post-filtering reference signal

Each interval is described as follows:

- Interval $t < 4\text{ s}$: stabilization at 0.2094 rad .
During this phase, the reference signal remains constant at the value of 0.2094 rad (12°), representing a cruising speed before entering the ramp.
- Interval $4\text{ s} \leq t < 8\text{ s}$: linear increase from 0.2094 rad to 0.3491 rad .
Over this interval, the reference signal increases linearly by $0.0349\frac{\text{rad}}{\text{s}}$, reaching 0.3491 rad (20°) at $t = 8\text{ s}$. This represents the moderate acceleration required while traveling along the uphill ramp.
- Interval $t \geq 8\text{ s}$: exponential increase from 0.3491 rad to 1.3089 rad .
In this phase, the reference signal follows an exponential curve, gradually increasing from 0.3491 rad (20°) and asymptotically approaching 1.3089 rad (75°). This represents the merging phase, where the throttle is opened more significantly to match highway speeds and to fully integrate into the highway flow.

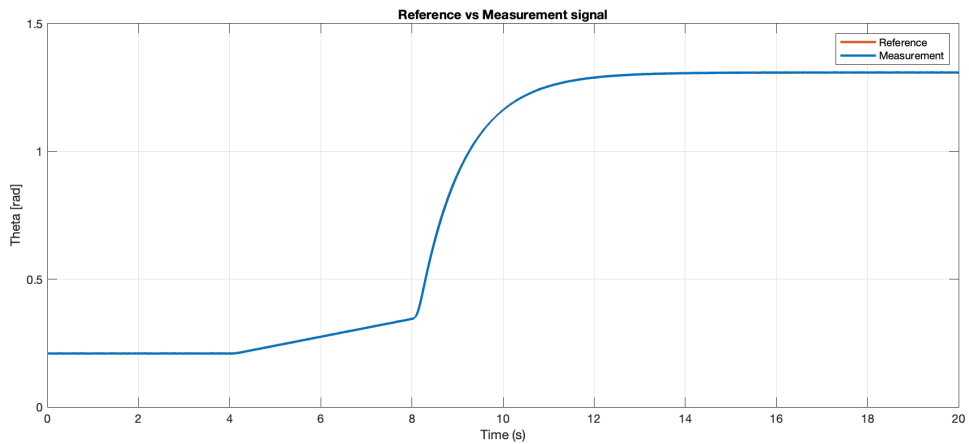


Figure 4.41: Reference vs Measurement

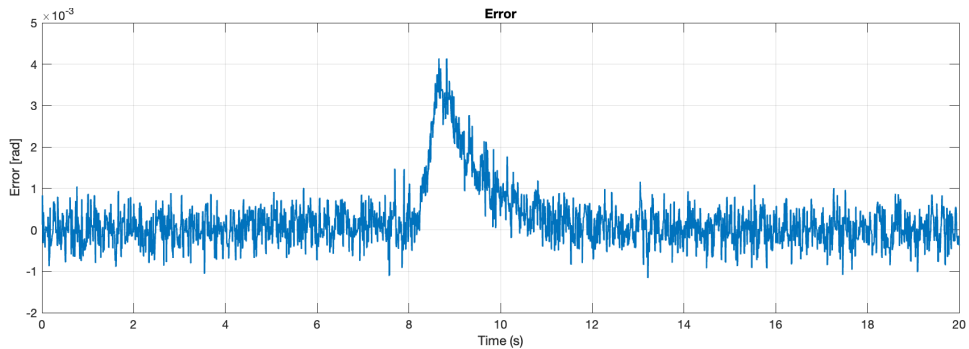


Figure 4.42: Error signal

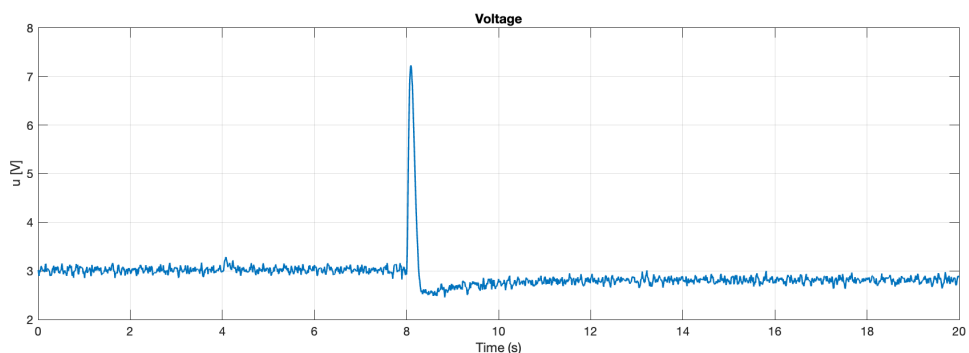


Figure 4.43: Control signal

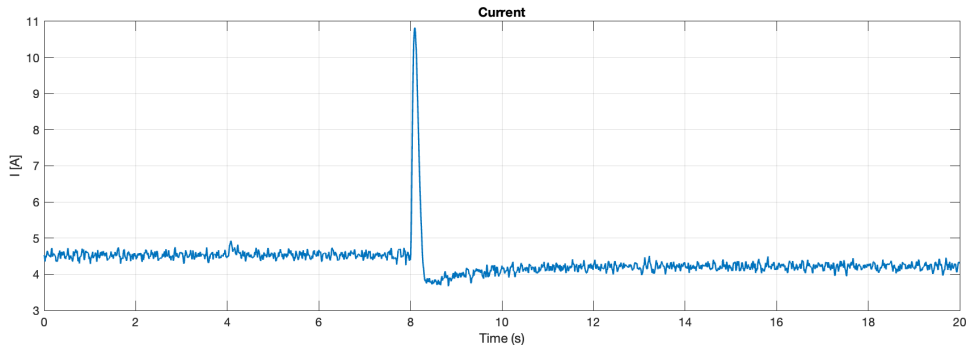


Figure 4.44: Current signal

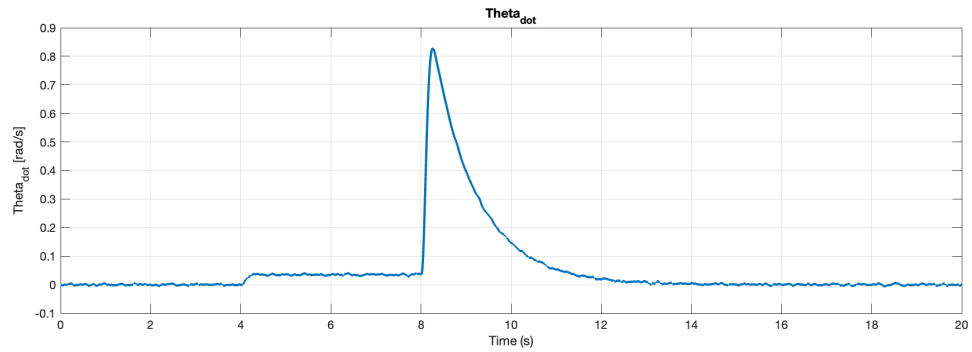


Figure 4.45: $\dot{\theta}$ signal

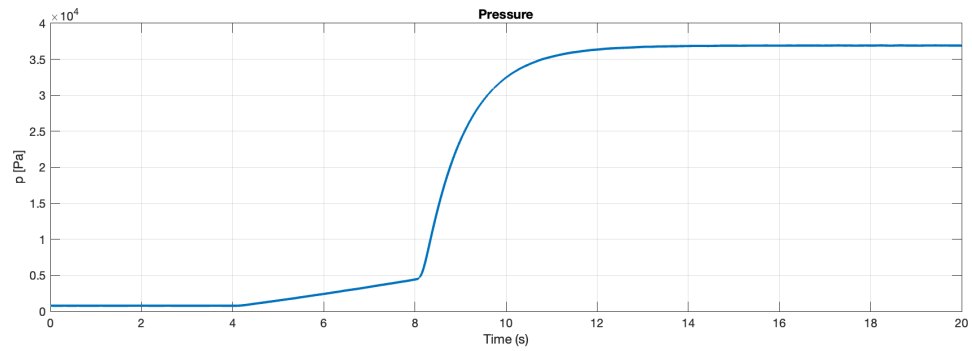


Figure 4.46: Pressure signal

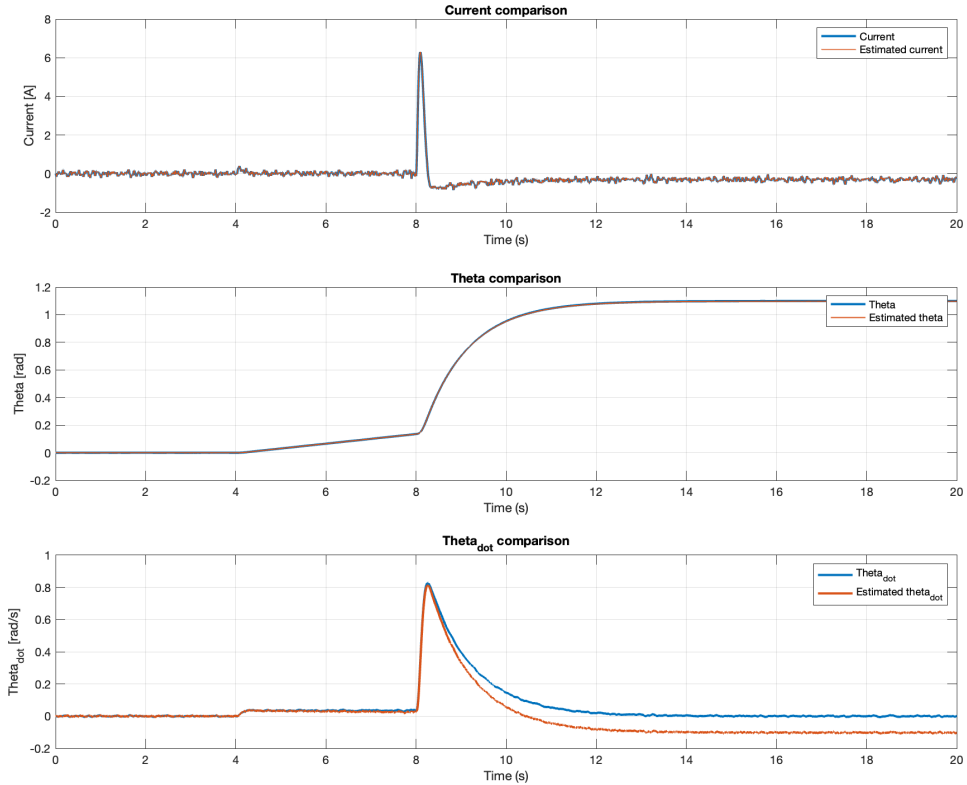


Figure 4.47: States vs Estimated states comparison

4.7 Overtaking Maneuver

The following reference signal $\mathbf{r}(t)$ represents the throttle valve behavior during a typical overtaking maneuver. It is designed to simulate the opening and closing of the throttle valve in a controlled manner, reflecting the dynamic demands of such a scenario. The signal includes periods of stabilization, acceleration, and deceleration, as detailed below:

$$\mathbf{r}(t) = \begin{cases} 0.2094 + (\frac{0.4363 - 0.2094}{2})t & 0 \leq t < 2 \text{ s} \\ 0.4363 + (1.2217 - 0.4363)(1 - e^{-3(t-2)}) & 2 \text{ s} \leq t < 4 \text{ s} \\ 1.2217 & 4 \text{ s} \leq t < 6 \text{ s} \\ 1.2217 - \frac{1.2217 - 0.5236}{2}(t - 6) & 6 \text{ s} \leq t < 8 \text{ s} \\ 0.5236 & 8 \text{ s} \leq t < 10 \text{ s} \end{cases}$$

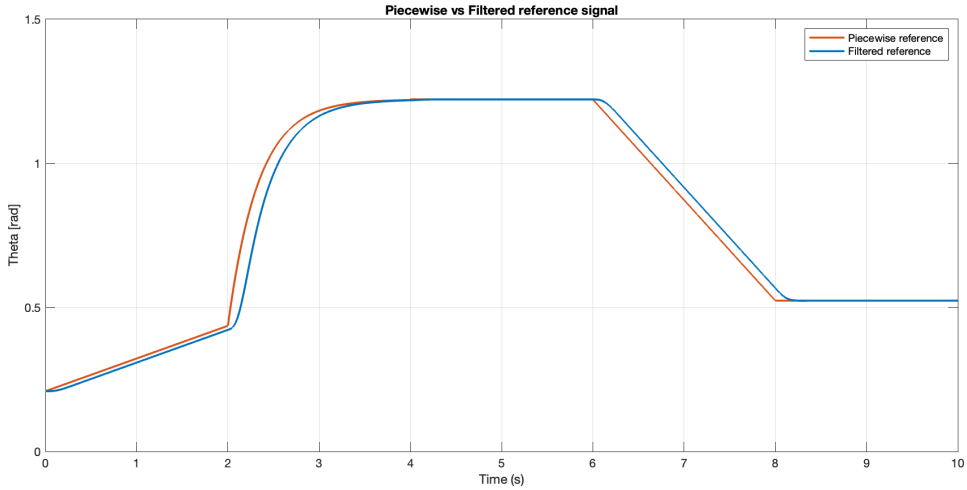


Figure 4.48: Pre and post-filtering reference signal

Each interval is described as follows:

- Interval $0 \leq t < 2 \text{ s}$: linear increase from 0.2094 rad to 0.4363 rad .
During this time, the reference signal increases linearly from 0.2094 rad (12°) to 0.4363 rad (25°), simulating a light acceleration phase to prepare for the overtaking maneuver.
- Interval $2 \text{ s} \leq t < 4 \text{ s}$: exponential rise from 0.4363 rad to 1.2217 rad .
The reference signal rises steeply from 0.4363 rad (25°) to 1.2217 rad (70°), representing a strong acceleration to initiate the overtaking.
- Interval $4 \text{ s} \leq t < 6 \text{ s}$: stabilization at 1.2217 rad .
During these 2 seconds, the reference signal is constant at 1.2217 rad (70°), maintaining the throttle valve at its maximum opening.
- Interval $6 \text{ s} \leq t < 8 \text{ s}$: linear decrease from 1.2217 rad to 0.5236 rad .
Over the 2 seconds of this interval, the reference signal decreases linearly from 1.2217 rad (70°) to 0.5236 rad (30°), simulating the gradual release of the accelerator after overtaking.
- Interval $8 \text{ s} \leq t < 10 \text{ s}$: stabilization at 0.5236 rad .
The reference signal remains constant at 0.5236 rad (30°), representing a lower throttle opening as the vehicle resumes normal speed.

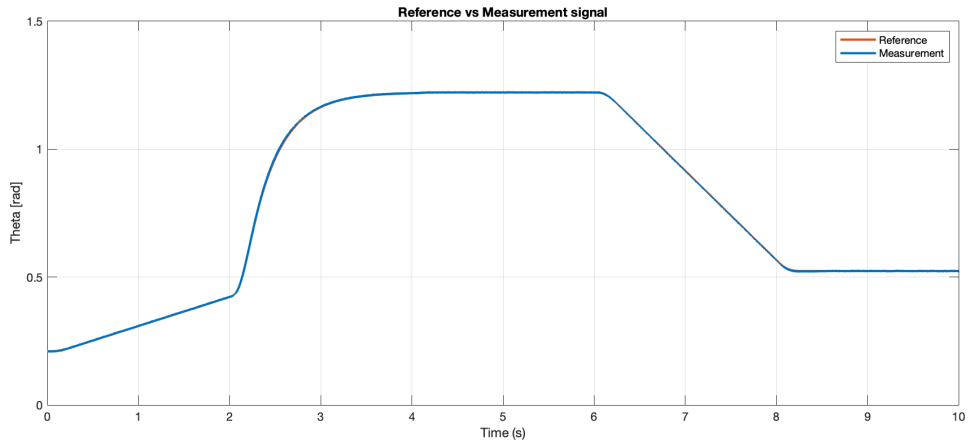


Figure 4.49: Reference vs Measurement

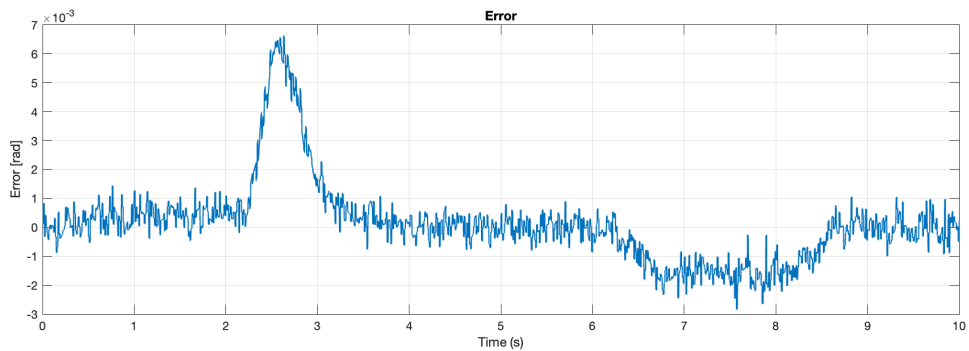
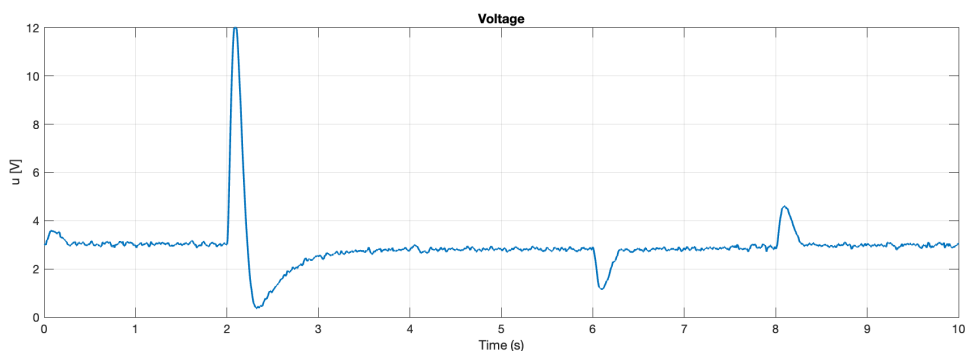


Figure 4.50: Error signal



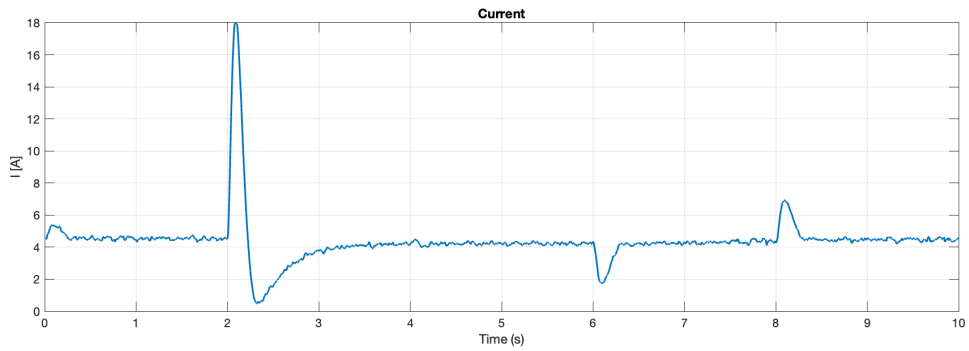


Figure 4.52: Current signal

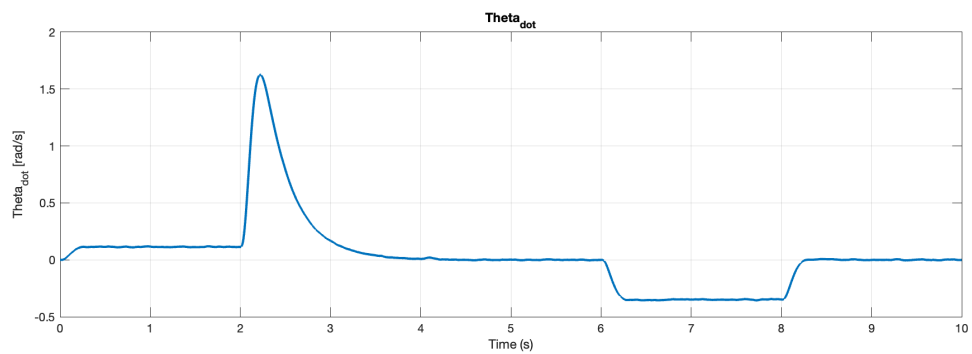


Figure 4.53: $\dot{\theta}$ signal

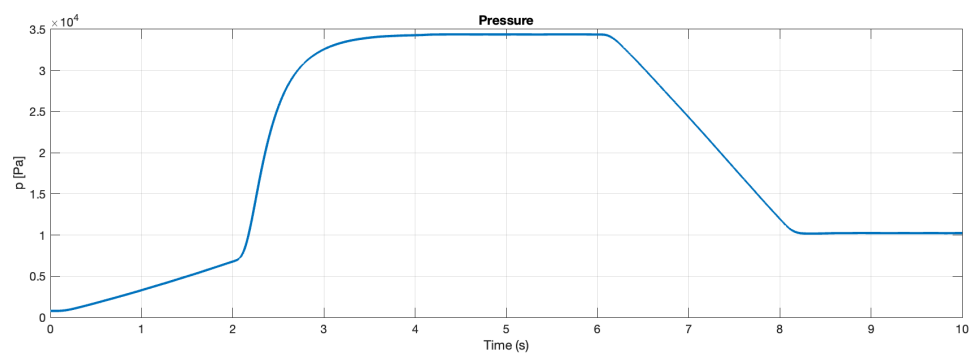


Figure 4.54: Pressure signal

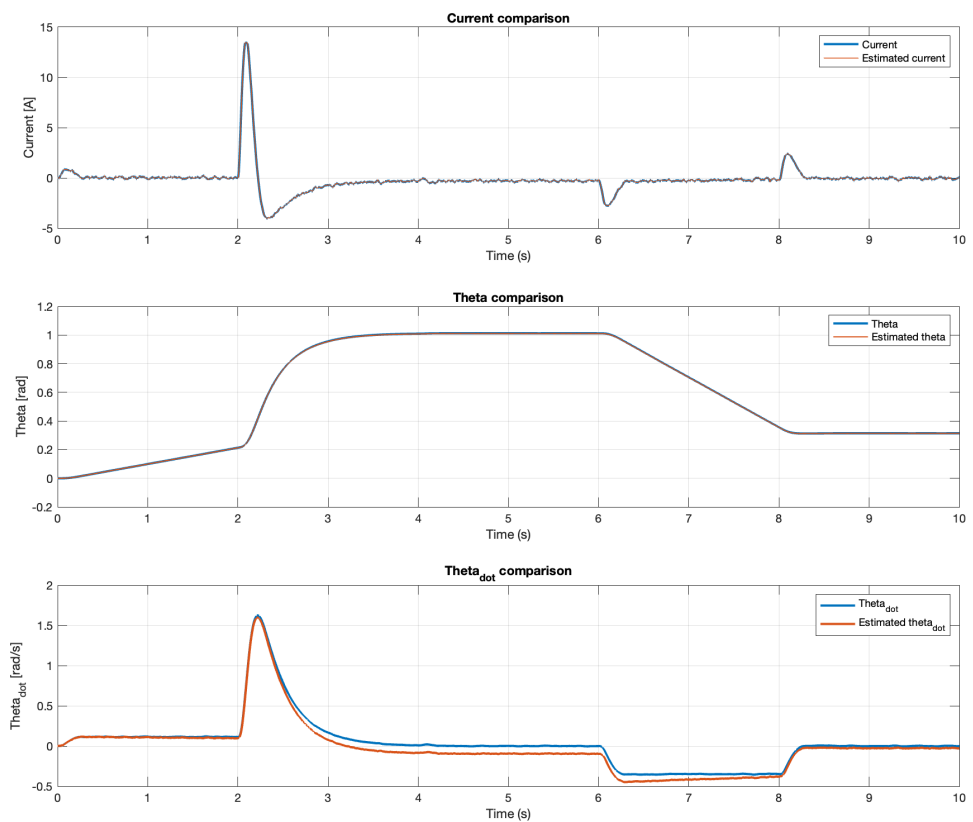


Figure 4.55: States vs Estimated states comparison

Chapter 5

APPLICATION

5.1 Simulink blocks description

In this section, both the non-linear and linear components of our simulator are analyzed, outlining the layout decisions and providing a brief description of each block.

5.2 Non-linear Plant

Figure 5.1 depicts the nonlinear plant in a closed-loop configuration. The model is implemented in Simulink using three MATLAB functions:

- **f**: This function represents the state evolution of the system. It takes as inputs the exogenous disturbances \mathbf{w} , which are managed through three distinct components: disturbance, noise, and reference. Additionally, the actual control law \mathbf{u} and the rotational speed of the engine (denoted as `regime`) are also inputs. The function outputs the state dynamics $\dot{\mathbf{x}}$, which is then integrated and fed back to the function as an input for the next time step.
- **h**: This function returns the output measurements when provided with the state, control law, and exogenous inputs. It models how the state of the system maps to the corresponding output measurements.
- **E**: This function calculates the error \mathbf{e} between the reference value and the current position of the throttle valve angle, denoted as θ . It represents the discrepancy between the desired and actual throttle valve positions.

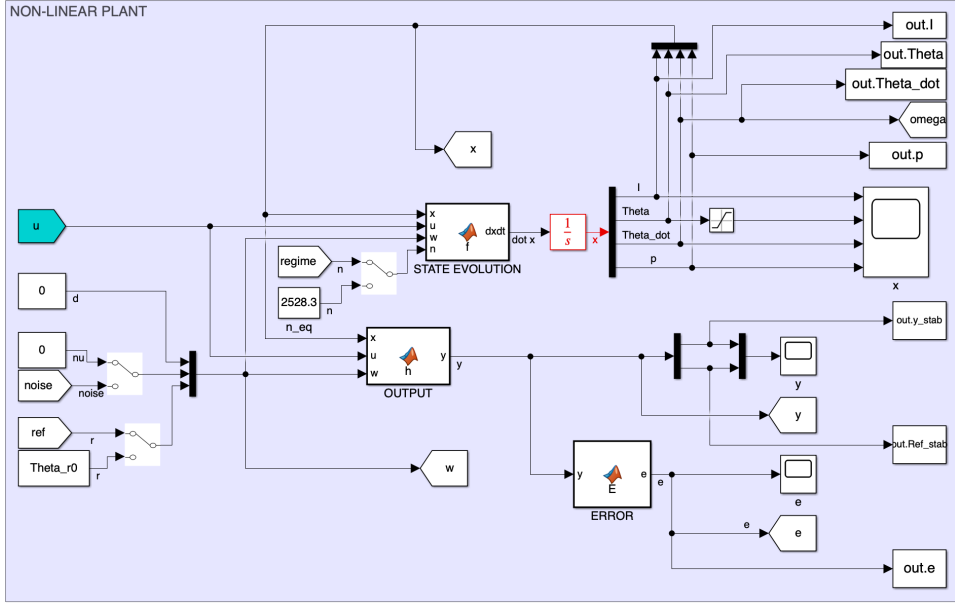


Figure 5.1: Non-linear plant

Several blocks in the model are configured to output real-time simulation data to the workspace. These blocks capture key variables, such as state, control law, and error, throughout the simulation. The exported data enables post-simulation analysis and visualization, offering insights into system performance and aiding in control tuning and error evaluation.



Figure 5.2: **regime** function

Finally, a MATLAB function was introduced in order to set the rotational speed of the engine as dependant to the reference position, thus outputting the ‘regime’ vector, which serves as an input for the non linear plant.

5.3 Reference and Feed-forward block

The reference paths have been designed as piecewise linear functions, composed of stabilization parts and ramping bits. However, as stated by the formal definition of the control problem, the reference \mathbf{r} and all its derivatives must be continuous and bounded. Therefore a low-pass filtering is applied. The now filtered reference and its derivatives served as inputs for the construction of the feed-forward control, which were implemented as two outputs (\mathbf{u}_{FF1} and ζ_r) of the block.

The input to the reference subsystem is a clock, which is crucial for defining the reference correctly.

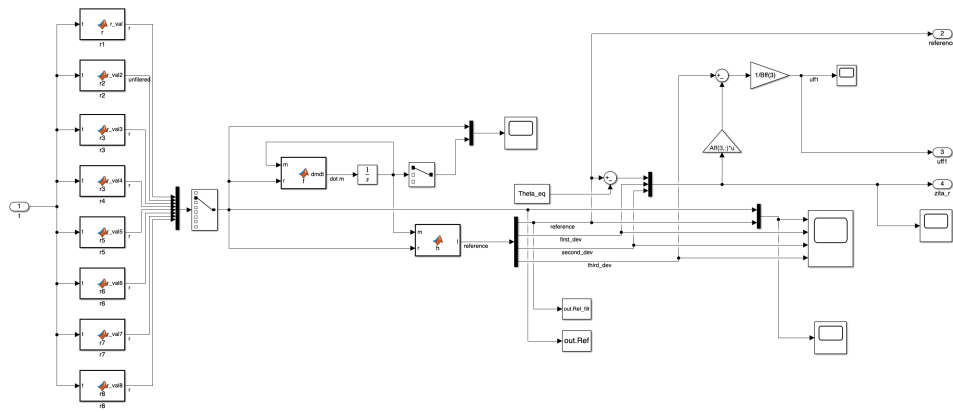


Figure 5.3: Reference block

Additionally, the inclusion of a 'selector' allows for selecting which reference to follow each time a simulation is started. Each reference is built through a MATLAB function

5.4 Control block for non-linear system

The control law \mathbf{u} is defined as the sum of $\tilde{\mathbf{u}}$ from the State Feedback, $\tilde{\mathbf{u}}$ from Integral Action, the control action demanded by the feed-forward, and the equilibrium \mathbf{u}^* . Doing so, the non-linear control vector that serves as input for the non-linear plant is obtained.

All the components that appear in figure 5.4 come from the subsystems that are going to be shown in the next subsections, with the exception of the feed-forward contributions that have already been indicated in the previous section.

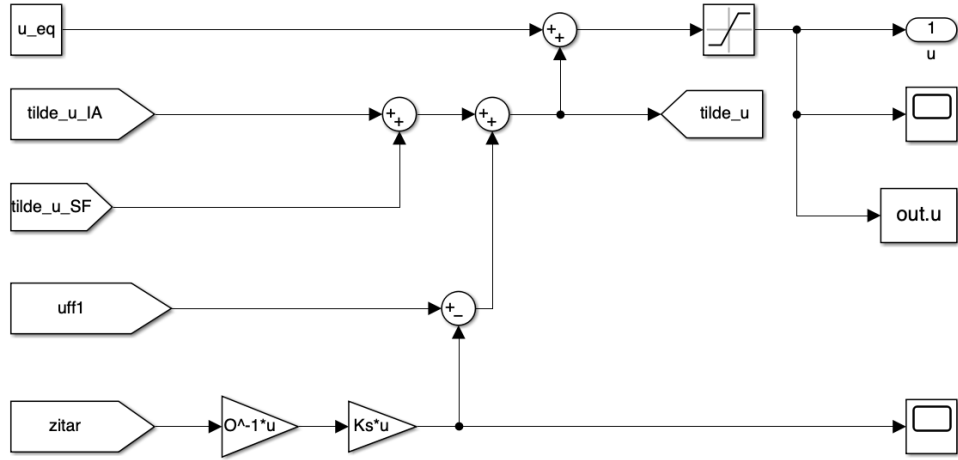


Figure 5.4: Control for non-linear system

5.4.1 Integral Action and State Feedback for non-linear

These 2 subsystems give in output 2 control contributions proportional to the estimated \hat{x} and to the integral of the error η through the \mathbf{K}_S and \mathbf{K}_I coefficients.

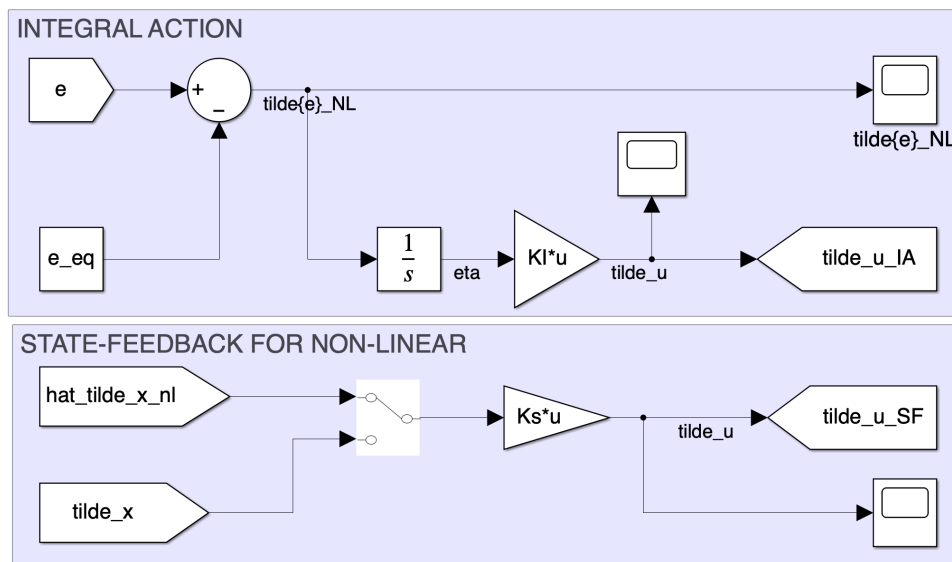


Figure 5.5: Integral action and state feedback for non-linear system

5.4.2 Observer for non-linear system

The \tilde{x} used during the simulation was the one estimated by the observer block.

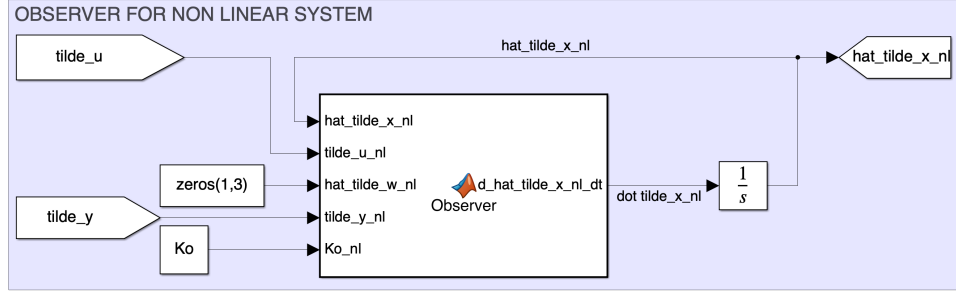


Figure 5.6: Observer for non-linear system

All the quantities involved, both in input and output, have been thoroughly discussed in the development of the control system. The equations within the MATLAB function are those elaborated earlier in the section dedicated to the observer and its optimal control.

5.5 Linear Plant

The linear plant conceptually works the same, introducing the same inputs and being provided with the same outputs. However, by definition, all input coordinates are linearized, therefore we wanted to concentrate our study close around the equilibrium point.

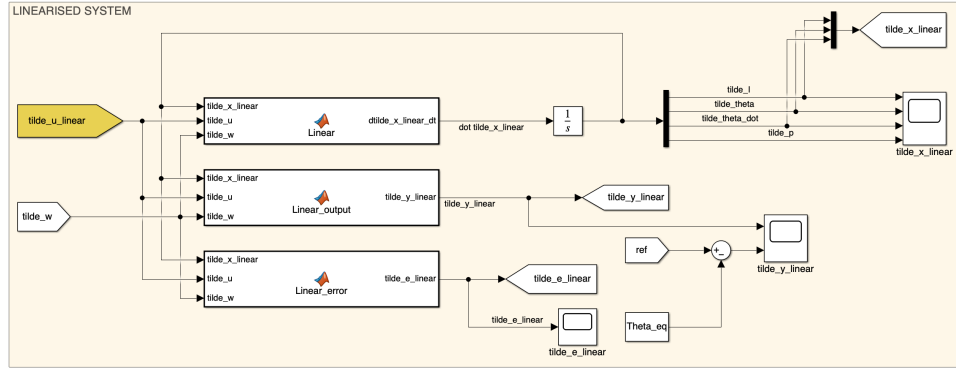


Figure 5.7: Linearised plant

5.6 Control block for linear system

Naturally, in order to achieve the same control implementation from the state feedback, the integral action and the observer, these subsystems must be provided with the linearized coordinates from the linear plant.

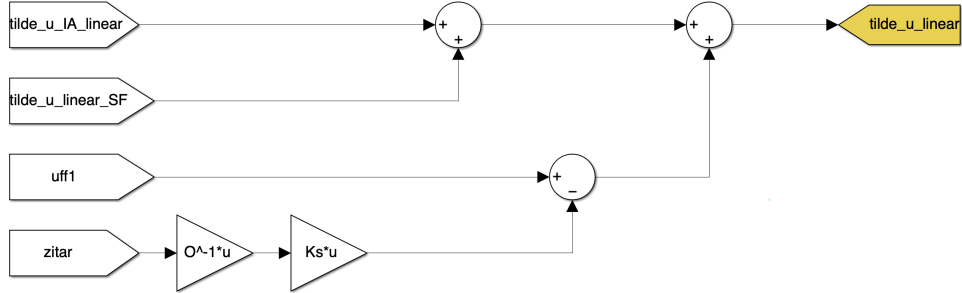


Figure 5.8: Control block for linear system

The contributions of this control law come from the following subsystems.

5.6.1 State Feedback and Integral Action for linear system

The blocks are built in the exact same way as the ones of the non-linear plant but, as mentioned, the input quantities are the linearized ones.

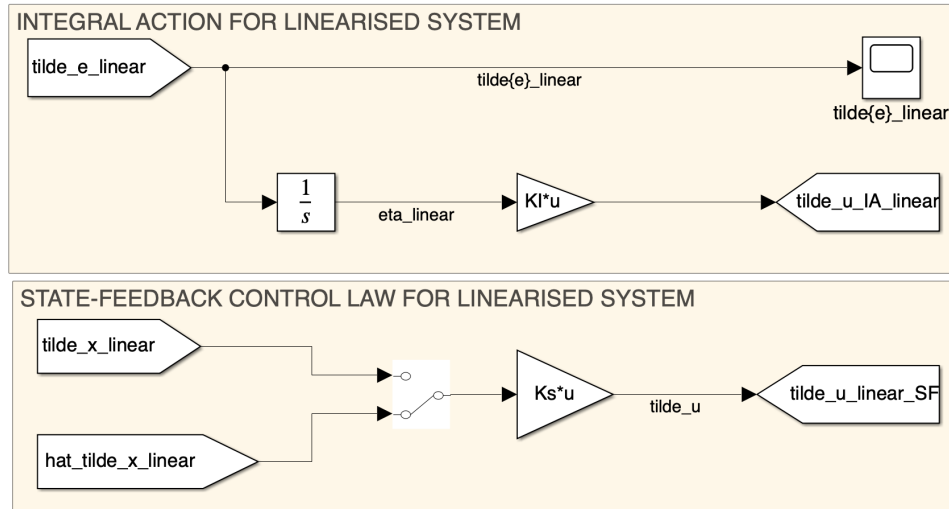


Figure 5.9: Integral action and state feedback for linear system

5.6.2 Observer for linear system

What said for the integral action and for the state feedback is valid also for the observer. The block is the same of the one for the non-linear system but the input quantities are the linearised ones.

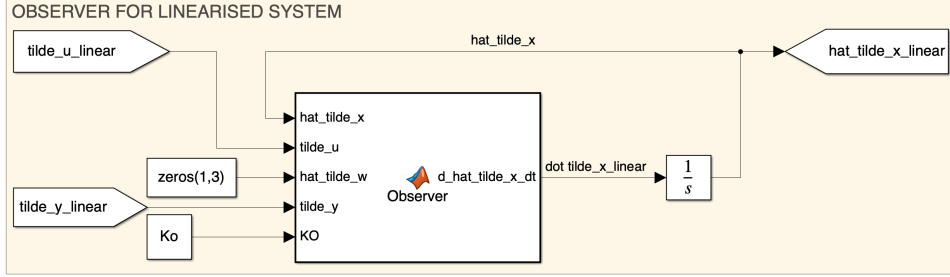


Figure 5.10: Observer for linear system

5.7 Measurement block

In this area, all scopes useful for verifying the correctness of calculations were included, facilitating comparisons between the linear and nonlinear plant to accurately analyze the model's behavior.

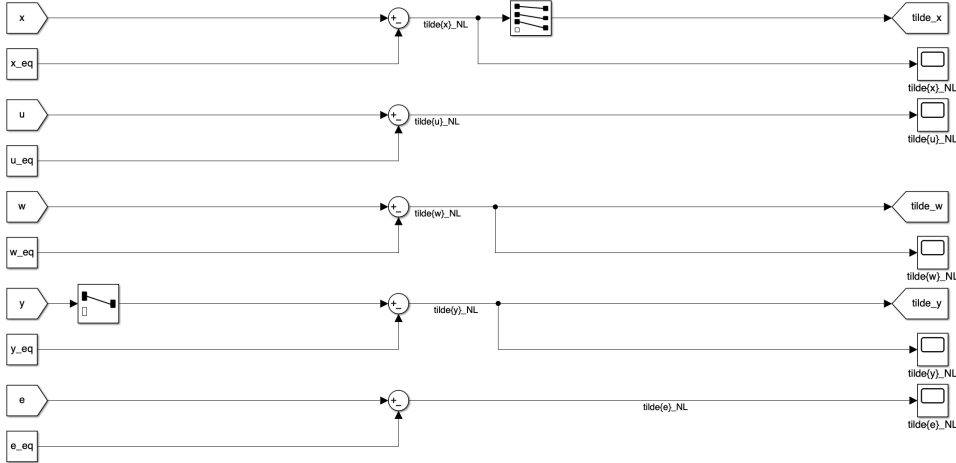


Figure 5.11: Measurement block

The state estimation scope, for instance, played a crucial role in moni-

toring the observer's performance and, consequently, the effectiveness of the state feedback control.

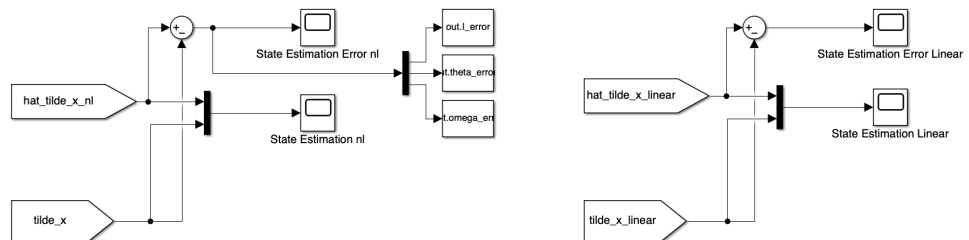


Figure 5.12: Estimation scope

Chapter 6

Conclusions and Further Improvements

6.1 General Improvements

In this comprehensive study, an approach to solve the problem of the throttle valve actuator control was presented. The results expected from the simulation environment were achieved, in accordance with the theory studied during the course.

In particular, the different cases of study, analyzing the response of our system when performing tests with reference signals representing real driving scenarios, validate our work as it demonstrates the abilities of a robust control strategy.

During the building of the final model, great focus was placed on the tuning for the optimal control of the observer, integral action, and state feedback. Indeed, the dynamics of the desired closed-loop system response have to be chosen properly, especially in the case of an engine throttle valve. A dynamic with too much lag can impact the engine emissions, as it fails to track the desired position for extended periods. On the other hand, a response that is too fast in the closed-loop system can quickly wear down the actuator gear system and DC motor.

The introduction of noise, which affects state estimation, contributes to elevating our simulation as close as possible to a real scenario. However, despite being relatively straightforward, the electronic throttle valve is a highly nonlinear system due to several factors:

- the presence of friction;

- the addition of the Limp Home Spring;
- voltage fluctuations in automobile batteries;
- disturbance torques induced on the throttle plate by in-line pressure variations.

This non-linear behavior adds a degree of complexity that limits the representation of an absolutely real-life accurate model when using classical control methods.

The Mean Value Model was employed to analyze the air intake process, but the simplifications and limitations imposed by this approach have a certain effect on the overall performance of the electronic throttle valve in practice.

- In our simulation environment, the temperature and pressure values within the intake manifold are assumed to be equal to ambient conditions.
- Inaccuracies are introduced in the whole range of the throttle angles, causing a prediction of downstream pressure significantly lower than typical experimental values in the same conditions.

To obtain more reliable calculations of the torque generated by the pressure difference between upstream and downstream of the valve, additional studies should investigate the implementation of improved and more accurate models throughout the entire operating window.

Alternatively, the most complete way to estimate the air intake process would involve Computational Fluid Dynamics (CFD) simulations. CFD solves the governing equations of fluid flow (Navier-Stokes) and provides precise insights into behavior around the throttle valve. This would require detailed modeling of the valve geometry and the boundary conditions of the problem, but it would yield high precision in capturing non-linear dynamics.

To conclude, our control system simulation could be made even more complex, but also more accurate, by considering every friction phenomenon within the throttle valve actuator. Friction generates another torque component that always opposes the body's motion.

In electronic throttle valves, where the coefficient of kinetic friction is less than the coefficient of static friction, there is a trend of intermittent jerking rather than smooth motion, known as the slip-stick phenomenon. Furthermore, elastic deformations and relatively large manufacturing tolerances between the valve components are significant contributors to this

behavior, causing a relevant impact on the performance of the control system.

6.2 Improvement of the Rotational Speed

In order to characterize the pressure in the intake manifold, a mean value model has been used. One of the key parameters in the model is the rotational velocity that, in chapter 2, has been elaborated in function of the angular position of the throttle valve.

$$n = 1900 + 3000 \cdot \theta \quad (6.1)$$

This relation between θ and n can be considered appropriate, but, in order to replicate as accurately as possible real-case scenarios, a more complex equation can be written [1][5].

$$\dot{n}_{up} = -\frac{\mathbf{P}_b}{n_{up}I} + \frac{H_u \eta_b}{n_{up}I} \dot{\mathbf{m}}_f \quad (6.2)$$

where:

- $\mathbf{T}_b(t)$ is the braking torque;
- η_b is the braking efficiency;
- I is the total moment of inertia loading the engine;
- H_u is the lower heating value of the fuel;
- $\dot{\mathbf{m}}_f$ is the fuel mass flow rate.

$$\mathbf{T}_b = c_0 + c_1 n_{up} + c_2 n_{up} \theta + c_3 \theta \quad (6.3)$$

$$\eta_b = c_4 \frac{\mathbf{T}_b T_{man} \lambda}{p + c_5 p_{amb}} \quad (6.4)$$

$$\dot{\mathbf{m}}_f = \frac{\dot{\mathbf{m}}}{AFR} \quad (6.5)$$

In equation (6.4), T_{man} is the temperature in the manifold, measurable through a temperature sensor, and λ is set to 1, the typical value for gasoline applications.

In equation (6.5), $\dot{\mathbf{m}}(t)$ is the air flow rate and AFR is the air-fuel ratio equal to 14.7 for gasoline.

The reason why this equation couldn't be used is due to the fact that the coefficients appearing in it must be retrieved through an interpolation starting from a set of experimental values coming from the test cell [1][5].

The updated formulation of the rotational speed evolution can be implemented in MATLAB and Simulink to replace the previous model.

Initially, the updated and previous rotational speed profiles should be plotted together to highlight the significant discrepancies between the two cases. Subsequently, all relevant signals, including plant signals, control inputs, estimation errors, and output errors, should be analyzed and compared to the results presented in earlier chapters.

Key differences must be emphasized to illustrate how the updated model provides a more accurate and realistic representation of the system dynamics.

6.3 Improvement of the Volumetric Efficiency

As in the case of the rotational speed, also for the volumetric efficiency η_f a more complex and accurate equation [5] could be used:

$$\eta_v = c_6 \left[\frac{r}{r-1} - \frac{1}{k(r-1)} \left(\frac{p_{amb}}{p} + (k-1) \right) \right] \quad (6.6)$$

where k is the specific heat ratio, and r is the compression ratio.

Also for this purpose, some experimental values are needed, but are not available as the absence of a test cell prevents the possibility of retrieving the correct coefficient c_6 in function of the working conditions.

6.4 Conclusions

From all the analysis carried out during this chapter, it is evident how the possibility to perform several physical tests on a test bench would lead to better performance of the control system.

The other main limitation turned out to be the estimation of the pressure inside the intake manifold. From this point of view, CFD analysis would lead to a better estimation as a result of a deeper understanding of the complex and turbulent dynamics of the system.

Bibliography

- [1] F Acquati et al. “An intake manifold model for spark ignition engines”. In: *IFAC Proceedings Volumes* 29.1 (1996), pp. 7945–7950.
- [2] Amjad J Humaidi and Akram H Hameed. “Design and comparative study of advanced adaptive control schemes for position control of electronic throttle valve”. In: *Information* 10.2 (2019), p. 65.
- [3] Nicola Mimmo. *Analysis and Design of Control Laws for Advanced Driver-Assistance Systems: Theory and Applications*. Springer, 2024.
- [4] Mimmo Nicola. “Notes from the course ”Automatic control””. In: 2024.
- [5] C Siviero et al. “Analysis & validation of mean value models for SI IC-Engines”. In: *Advances in Automotive Control 1995*. Elsevier, 1995, pp. 1–6.